



Cite this: DOI: 10.1039/d5mh01794g

## Materials for thermochemical energy storage and conversion: attributes for low-temperature applications

Steven Kiyabu, <sup>†</sup><sup>a</sup> Aleksandr Shkatulov, <sup>†</sup><sup>bc</sup> Alauddin Ahmed, <sup>a</sup> Samuel M. Greene, <sup>d</sup> Hendrik P. Huinink <sup>\*c</sup> and Donald J. Siegel <sup>\*de</sup>

The development of systems that can efficiently store and manage thermal energy – *i.e.*, heat – would improve the efficiencies of numerous processes throughout multiple sectors of the global economy. Nevertheless, the development of these thermal storage devices remains at a relatively early stage. To engage more researchers in the development of these devices and to accelerate their commercialization, this review presents an introduction to the properties of thermal storage materials that absorb and release heat through thermochemical reactions. Thermochemical materials typically exhibit the largest energy densities among all approaches to material-based heat storage. Nevertheless, they suffer from limited reaction rates and poor cycle life. An additional challenge is the multiscale nature of the energy storage process, which ranges from atomistic interactions that govern the storage of heat through alteration of chemical bonds, to mesoscale processes that control the transport of mass and heat. Following an overview of general concepts related to thermal energy storage, emphasis is placed on describing properties relevant for low-temperature applications. These applications include domestic heat storage/amplification (hot water heating), adsorptive cooling (air conditioning), and heat-moisture recuperation. Subsequently, detailed introductions are provided to the mechanisms and materials relevant for the three primary approaches to low-temperature thermochemical storage, including: (i) absorption in solids (hydrates, ammoniates, and methanolates); (ii) adsorption in porous hosts (zeolites, metal–organic frameworks); and (iii) dilution in liquids. For each category, advantages and shortcomings of benchmark and emerging materials are discussed. Finally, challenges and opportunities are highlighted for research aimed at developing optimal materials for thermochemical energy storage.

Received 22nd September 2025,  
Accepted 22nd October 2025

DOI: 10.1039/d5mh01794g

[rsc.li/materials-horizons](http://rsc.li/materials-horizons)



### Wider impact

Heat is a central component of the world's energy ecosystem. Examples of heat's prevalence include combustion engines, which convert heat into mechanical work, while heat from solar energy, geothermal wells, and the burning of fossil fuels is used to condition the air and water in homes, offices, and factories. In the U.S., approximately 10% of the energy consumed can be traced to residential heating and cooling alone. More generally, energy generation and use exhibit inefficiencies associated with large thermal losses – 66% of the energy produced in the U.S. in 2023 did no useful work and was lost to the environment as heat. Hence, technologies that capture, manage, and re-use heat have the potential to yield significant improvements in energy efficiency and expedite decarbonization. Thermal energy storage (TES) is one such technology. TES is predicted to reduce energy costs by 5–15% and peak electrical power demand by 13–33% globally. Despite these benefits, the development of TES systems remains in its infancy due to deficiencies in the underlying storage materials. This review introduces materials and mechanisms for low-temperature TES, emphasizing those that store heat using thermochemical reactions. Benefits, challenges, and high-priority research directions for thermochemical TES materials are described in detail.

<sup>a</sup> Mechanical Engineering Department, University of Michigan, Ann Arbor, MI 48109, USA

<sup>b</sup> Iberian Centre for Research in Energy Storage, CIIE, Polígono 13, Parcela 31, “El Cuartillo”, Cáceres, 10004, Spain

<sup>c</sup> Eindhoven Institute for Renewable Energy Systems, Eindhoven University of Technology, P.O. Box 513, 5600 MB Eindhoven, The Netherlands. E-mail: h.p.huinink@tue.nl

<sup>d</sup> Oden Institute for Computational Engineering and Sciences, University of Texas at Austin, Austin, TX, 78712, USA. E-mail: donald.siegel@austin.utexas.edu

<sup>e</sup> Walker Department of Mechanical Engineering and Texas Materials Institute, University of Texas at Austin, Austin, TX, 78712, USA

<sup>†</sup> These authors contributed equally.

## Introduction

Heat is a central component of the world's energy ecosystem. One example of heat's ubiquity is the production of heat in fossil-fuel-based combustion engines. The subsequent conversion of this heat into mechanical work is the basis for many of the transportation devices and industrial machinery that have been in use since the 19th century. In addition, heat from solar energy, geothermal wells, and combustion is used to condition the air and water in homes, offices, and factories.

Given its prevalence in our society, managing the flow and use of heat presents an opportunity for improving energy efficiency. For example, over two thirds of the energy produced in the United States – approximately 62 quadrillion BTUs – does no useful work, and is ultimately lost to the surroundings as heat.<sup>1</sup> This fraction of lost energy is typical of countries



**Steven Kiyabu**

*Dr Steven Kiyabu graduated with his PhD in Mechanical Engineering and Scientific Computing from the University of Michigan in 2022, where he researched the thermodynamic and heat storage properties of salt hydrates using computational and machine learning techniques. He now is a research scientist at AeroVironment, Inc., supporting research at the Air Force Research Laboratory. His research currently focuses on mechanical reservoir computing.*

worldwide.<sup>2,3</sup> While the second law of thermodynamics limits the conversion of heat into work, the magnitude of these losses suggests that the capture, storage, and/or re-use of only a small fraction of this “lost” thermal energy would be beneficial. Furthermore, since the production of heat often occurs through the combustion of fossil fuels, strategies that maximize the use of the generated heat have the potential to reduce carbon emissions.

One technology for effective heat management is thermal energy storage (TES), *i.e.*, the storage of heat. Several studies have estimated the potential benefits of TES systems, and the results are promising. For example, in the European Union TES has been projected to achieve a 7.5% overall energy savings.<sup>4</sup> Globally, TES is expected to reduce energy costs (by 5–15%) and peak electrical power demand (by 13–33%).<sup>5</sup> TES is also one of the few technologies that can provide significant value in decarbonizing multiple use sectors.<sup>6</sup> For example, TES has



**Aleksandr Shkatulov**

*Dr Aleksandr Shkatulov is a Senior Researcher at the Iberian Centre for Energy Storage Research (Cáceres, Spain). He previously held a Marie Curie Individual Fellowship at the German Aerospace Center and a postdoctoral position at Eindhoven University of Technology (Netherlands). His research focuses on advanced materials for thermochemical energy storage, sorptive heat pumps, advanced thermal cycles, and sustainable energy systems. Dr Shkatulov has*

*authored 25 peer-reviewed publications and one book chapter and has contributed to several European projects including HEAT INSYDE and 4TunaTES. His work bridges materials chemistry, energy conversion, and system integration for next-generation thermal storage technologies.*



**Alauddin Ahmed**

*Dr Alauddin Ahmed is a Research Faculty member in Mechanical Engineering at the University of Michigan. His work spans energy storage and integrates computational materials science with AI methods—including interpretable machine learning, causal inference, large language models, and digital twins. He studies nanoporous materials (metal-organic and covalent-organic frameworks) alongside energetic materials, electrolytes, dielectric fluids, and nanoparticles. He has advanced the discovery and design of high-performing materials for hydrogen, methane, and thermal storage by combining high-throughput computing with AI methods.*

*learning methods. He is a Rhodes Scholar, a Schmidt Science Fellow, and a recipient of the DOE Office of Science Graduate Student Research Fellowship.*



**Samuel M. Greene**

*Dr Samuel M. Greene is currently a postdoctoral fellow in the Oden Institute for Computational Engineering and Sciences at the University of Texas at Austin. He will be starting as an Assistant Professor of Mechanical Engineering at the University of Colorado Boulder in Fall 2026. His research focuses on the atomic-scale modeling of materials for energy storage and carbon capture, including solid electrolytes and MOFs, as well as on the development of new machine*



the projected potential to reduce carbon emissions by approximately 25% through the decarbonization of the energy grid.<sup>7,8</sup>

TES has the potential to be applied in many contexts and for multiple applications:

### Buildings

Applications of TES in buildings can improve the performance of heating, ventilation, and air conditioning (HVAC) systems.<sup>9–11</sup> Approximately 21% of the energy consumed in the U.S. can be traced to residential applications,<sup>12</sup> 48% of which is devoted to heating and cooling.<sup>13</sup> Because approximately 75% of all waste heat generated is below 100 °C (a temperature suitable for use in buildings), there is a high reuse potential for this lower-temperature heat in domestic heating applications. Improvements to HVAC made possible by TES will translate to higher efficiencies, lower operating costs, and reduced CO<sub>2</sub> emissions through reduced consumption of the fossil fuels used to generate the electricity that powers HVAC devices.

### Preservation of perishables

TES systems offer an increase in thermal inertia, which is measured by the responsiveness of a system's temperature to the supply or withdrawal of heat. As thermal inertia increases, a greater amount of heat is required to change the system's temperature. This feature of thermal energy storage systems has been exploited to preserve food and other perishables by maintaining them at low temperatures. A common example is the use of ice as a phase-change material, but containers with even greater thermal inertia have been developed. For example, the Greenbox Thermal Management System has been used to keep vaccines and other temperature-sensitive medical supplies cool during long periods of transportation.<sup>14</sup>

### Electronics

TES can be deployed to protect sensitive electronics.<sup>15,16</sup> As electricity flows through a circuit, the resistance of the circuit results in



Hendrik P. Huinink

*Hendrik P. Huinink is full professor physics of energy storage and leads the group Transport in Permeable Media (TPM) within the Applied Physics and Science Education (APSE) department of the Eindhoven University. He is an expert in thermochemical energy storage (TCES) based on salt hydrates and hydration processes. He focuses on developing and understanding materials for TCES from molecular up to the particle bed scales.*

energy loss through heat. This heat can physically damage fragile components in a circuit. As such, either cooling or a heat sink (a TES system) can aid in maintaining acceptable temperatures.

### Vehicles

TES can be used in vehicles to condition the temperature of engines.<sup>17–19</sup> When a vehicle starts from cold conditions, several minutes of operation are needed before a steady operating temperature is achieved. When cold, the engine operates less efficiently, consumes more fuel, and the exhaust gases from the engine are lower in temperature, resulting in a less effective catalytic converter. A TES system can aid in pre-heating the engine by capturing waste heat from prior operation, thereby reducing the inefficiencies associated with cold start. Further benefits can be derived by using TES as a thermal sink to reduce overheating under high tractive efforts.<sup>20</sup>

### Thermal batteries

A thermal battery, *i.e.* a system that captures and stores heat for later use, is a generalization of the cold-start TES application discussed above. Thermal batteries have been proposed to capture waste heat from industrial processes, operating in the range of 100–300 °C.<sup>21–24</sup> This captured heat is then used for electricity production, thus increasing the overall efficiency of the cogeneration scheme. TES can also be used in conjunction with solar energy generation.<sup>25,26</sup> The availability of solar energy fluctuates due to weather conditions and according to daily and seasonal cycles. By storing excess solar energy, a TES-enabled solar plant can provide output that is less dependent on the instantaneous solar conditions to meet time-varying energy demand.

The examples mentioned above illustrate that TES systems can take a variety of forms. Nevertheless, at their core all these systems share the common trait of employing a material that stores thermal energy. These materials store heat in one of three ways: as sensible heat, as latent heat, or as thermochemical heat.



Donald J. Siegel

*Donald J. Siegel is Professor and Chair of the Walker Department of Mechanical Engineering at the University of Texas at Austin, where he is a Temple Foundation Endowed Professor and holds a Cockrell Family Chair for Departmental Leadership. He is a member of the Oden Institute for Computational Engineering and Sciences and the Texas Materials Institute. Siegel is a computational materials scientist whose research targets the development of energy storage materials and lightweight alloys. He is a recipient of a Career Award from the U.S. National Science Foundation and a Gilbreth Lectureship from the National Academy of Engineering.*



## Sensible heat storage

All materials store sensible heat within the kinetic energy of atomic vibrations. The amount of heat stored is indicated macroscopically by the temperature. Materials with higher specific heat capacities store more sensible heat for a given temperature increase; therefore, these materials tend to store heat with higher energy densities. Liquid water, with its high specific heat capacity, is a common medium for sensible heat storage. Other materials such as alcohols, plastics, concrete, molten salts, and metals have also seen use in sensible heat storage systems.<sup>9</sup>

Sensible heat storage is the simplest form of TES. It has the advantage of being reversible, so long as changes to the operating temperature – which can trigger phase transformations – are avoided. However, sensible heat storage is characterized by low energy densities (Fig. 1). Thus, it is not suitable for applications where lightweight and/or compact TES systems are required. Furthermore, sensible heat storing materials will lose stored energy if the system is not well insulated. This limits its use in applications that target long-duration storage.

## Latent heat storage

Another method of TES exploits the latent heat of a phase transformation. To implement this approach, the so-called phase change materials (PCMs) are used.<sup>9,27</sup> A common example is an ice cube that keeps a drink cool. Here, heat transferred from the surroundings is absorbed by the ice as the

(endothermic) latent heat of melting. These phase changes occur at a specific temperature, which dictates the temperature at which the material will store or release heat. PCMs have 2–6 times greater energy densities than sensible heat-storing materials.<sup>28</sup> However, the change in the material during phase change can lead to practical issues, such as melting/solidification temperature hysteresis and volume change.

## Thermochemical energy storage

Lastly, thermochemical materials store heat by undergoing a reversible chemical reaction or sorption process. A typical thermochemical energy storage (TCES) reaction takes the form:



In the forward endothermic reaction, material *A* decomposes into material *B* and working fluid *C* while simultaneously absorbing heat *Q*. Unlike PCMs and sensible heat storing materials, thermochemical heat storing materials do not discharge energy over time as the energy is stored in the form of the chemical potential of the products, as long as they remain physically separated. When *B* and *C* are recombined and react, the reverse exothermic reaction occurs, re-forming *A* and releasing the stored heat. In the case of a sorption-based thermochemical process, *B* represents the sorbent, *C* is the sorbate, and *A* is the sorbate-sorbent complex. TCES materials have the largest energy densities of all TES materials, reflecting the large amount of energy that can be stored by a chemical reaction. However, the chemical reaction also poses some complexities. For example, it is common for these materials to experience irreversibility due to side reactions as well as slow kinetics due to limitations in mass and/or heat transfer.<sup>29,30</sup>

Fig. 1 shows a “temperature ladder” for various TES materials,<sup>31–40</sup> as well as temperature ranges<sup>9,17,21,31,41</sup> for various TES applications. Although they exhibit more practical complexity, thermochemical heat storage materials offer significantly higher energy densities on the material level. Additionally, the temperature ladder shows a general correlation between the operating temperature of TES materials and their energy densities. One reason for this is that higher enthalpies of transformation,  $\Delta H$ , associated with the relevant chemical reaction or phase change, correlate both with higher thermodynamic equilibrium temperatures and energy densities. This correlation is useful for understanding the limits of energy density for a particular application, as materials are generally chosen based on the target operating temperature. In some cases, it is possible to use all three methods in one material, thus boosting energy storage density.<sup>42</sup>

Although Li-ion batteries have experienced significant cost reductions, the low efficiency of converting heat to electricity suggests that batteries are less efficient options for energy storage when the energy to be stored is in the form of heat. For example, modern thermoelectric devices convert heat to electricity with efficiencies in the range of 5 to 15%.<sup>43,44</sup>

The preceding discussion illustrates that the field of TES is broad, encompassing many different applications, materials, and system designs. The present review provides an overview of

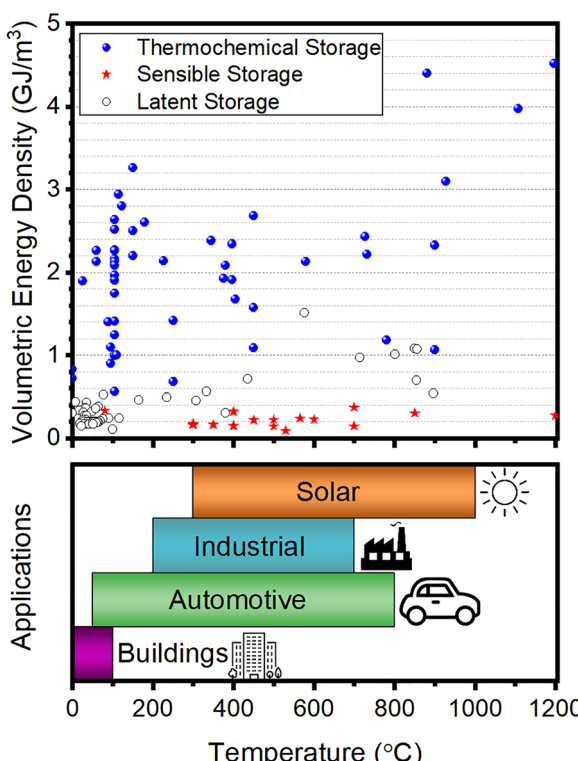


Fig. 1 Temperature ladder for thermal energy storage materials and their typical storage densities (top). The general temperature ranges for various thermal energy storage applications are also shown (bottom).



an important subset of the field, specifically focusing on thermochemical and sorptive heat storage materials that operate at low temperatures (*i.e.*, below  $\sim 100$  °C). Additionally, applications that operate in the low temperature region of interest, including TCES systems in buildings, are briefly discussed to illustrate the implications for material selection and characterization. The materials of interest include salt hydrates, porous media, and liquid absorption of gases. Key properties of these materials are discussed, including thermodynamic operating conditions, energy density, kinetic performance, stability, and several non-technical aspects. The review concludes with a discussion of current challenges and opportunities in the field.

## Materials performance criteria and example applications

### A. Criteria for materials selection

Several performance criteria exist for TCES systems (Fig. 2). These criteria can be loosely divided into those based on thermodynamic, dynamic, and 'other' characteristics. Thermodynamic criteria refer to the capacity and efficiency with which heat is stored (*e.g.*, COP, second-law efficiency). Dynamic criteria refer to the rate at which thermal energy is stored or released (power and cycle time). Other important characteristics include safety, cost, and energy density.

Since the properties of the TCES material strongly influence the performance of the resultant TCES system, the system

criteria illustrated in Fig. 2 can also be used to guide material selection. Additional application-specific requirements (*e.g.* low toxicity for domestic usage) or system design constraints (open/closed, fixed or moving bed) should also be accounted for when selecting suitable TCES materials.<sup>45–48</sup> This selection task is further complicated by the presence of design trade-offs (*e.g.* storage density vs. temperature lift<sup>49,50</sup>) and limited understanding of the relative importance of the various materials attributes in determining system performance.

Table 1 summarizes performance targets associated with several key properties of thermochemical energy storage systems and materials, as proposed by the U.S. Department of Energy (DOE) and the European Technology and Innovation Platform on Renewable Heating and Cooling (RHC-ETIP).<sup>51,52</sup> The target for energy density at the system level, 200 and 220 kWh m<sup>-3</sup>, respectively, is similar for both the DOE and RHC-ETIP. Translating this system-level target to an energy density at the material level requires knowledge of the volume occupied by the non-active components of the storage device. These components will vary depending on the system design (open *vs.* closed), and may include heat exchangers, evaporators, storage vessels, *etc.* Hence, to account for the volumes of the non-active components, a target for the energy density of the storage material should exceed that for the system. N'Tsoukpo compared the system-level and materials-level energy densities of several prototype thermal storage systems.<sup>53</sup> Their analysis found that in most cases the system-level energy densities were significantly smaller than that of the active material. In the best cases, the system energy density was 30% to 50% of the materials-only value. Assuming that these (best case) systems represent what can be achieved through system design optimizations, then a reasonable target for the materials-level energy density would be two to three times the system-level target, or 400–600 kWh m<sup>-3</sup>.

Below, important materials selection criteria are described for applications including domestic heating, cooling, heat-moisture recuperation in buildings, and water harvesting.

**Thermodynamic criteria.** The thermodynamic properties of a TCES system refer to the amount and quality of thermal energy processed.

**First-law efficiency.** The first-law efficiency or the Coefficient of Performance (COP) of a TCES system is defined as follows:

$$\text{COP} = \frac{|Q_{\text{useful}}|}{Q_{\text{input}}}, \quad (2)$$

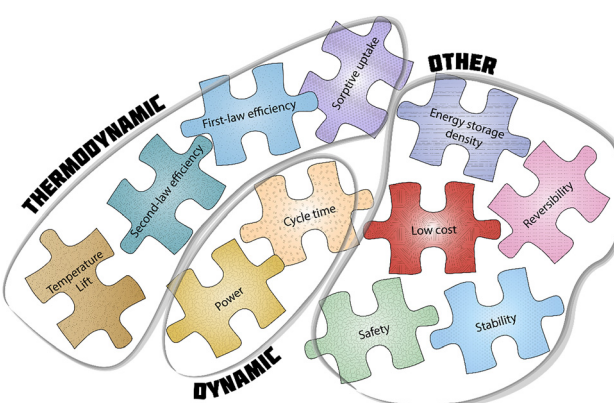


Fig. 2 Examples of thermodynamic, dynamic, and other selection criteria relevant for thermochemical heat storage systems.

Table 1 Performance targets for domestic thermochemical energy storage

Property	Target	Comments
System-level energy density	200 kWh m <sup>-3</sup> <sup>49</sup> 220 kWh m <sup>-3</sup> <sup>52</sup>	Based on U.S. DOE and RHC-ETIP
Materials-level energy density	400–600 kWh m <sup>-3</sup>	Assumes system energy density is 30%–50% of materials energy density <sup>53</sup>
Cost of composite storage material	< \$15 per kWh <sup>49</sup>	Includes active material and materials that facilitate heat/mass transport
Thermal conductivity	> 1.0 W m <sup>-1</sup> K <sup>-1</sup> <sup>49</sup>	For composite storage material
Capacity retention and cycle life	> 90%, 7500 cycles or 20 years <sup>49</sup> 25 years <sup>52</sup>	
Subcooling/supercooling	< 2 °C <sup>49</sup>	Low temperature hysteresis desired for charging/discharging



where  $Q_{\text{useful}}$  is the amount (or flow) of useful heat from a system, and  $Q_{\text{input}}$  is the total amount (or flow) of heat that drives a cycle under consideration. For thermal energy storage, a larger COP implies that a greater amount of useful heat can be recovered upon discharging relative to the lower-grade heat supplied to the system upon charging. A high COP can be achieved by minimizing thermal losses incurred during charging or discharging, for example by minimizing hysteresis and improving the system's kinetics. For water as the working fluid, the COP for TCES systems is usually less than 1.<sup>54,55</sup> For thermally-driven TCES applications where the input energy  $Q_{\text{input}}$  is available "for free" from, for instance, a solar concentrator or a PV panel, the COP is often not a highly-relevant quantity.

*Temperature lift.* Temperature lift,  $\text{TL}_{\text{eq}}$ , is another parameter that is meaningful for heat storage systems. Thermodynamic temperature lift may be defined as:

$$\text{TL}_{\text{eq}} = T_{\text{release(eq)}} - T_0 \quad (3)$$

Here,  $T_{\text{release(eq)}}$  is the equilibrium temperature for the heat release process and  $T_0$  is the ambient temperature, which is equal to the temperature of the working fluid.

*Second-law efficiency.* The second-law efficiency (or exergy efficiency) describes the usefulness of the heat recovered upon charging and discharging a TCES system.<sup>56</sup> The exergy,  $A$ , of a heat transfer process is defined in terms of the Carnot factor as:

$$A = \left(1 - \frac{T_0}{T}\right)Q, \quad (4)$$

where  $T_0$  is the ambient temperature,  $T$  is the temperature at which heat is transferred, and  $Q$  is the amount of heat transferred. By analogy with eqn (2), one can introduce the exergy efficiency,  $\Psi$ , of a system:

$$\Psi = \frac{|A_{\text{useful}}|}{A_{\text{input}}}$$

where  $A_{\text{useful}}$  is the amount (or flow) of useful exergy from a system, and  $A_{\text{input}}$  is the total input amount (or flow) of exergy. Exergy quantifies the usefulness of heat by quantifying how much work could be extracted from 1 J of heat supplied to an ideal machine operating with Carnot efficiency. For instance, a material releasing "useful" heat at 299 K with  $T_0 = 298$  K will not be suitable for TCES as the number of "useful" Joules (exergy) extracted will be low, even if  $Q_{\text{useful}}$  is large. For a similar reason, low values of temperature lift for TCES systems yield low values of exergy efficiency. For many solid-state transformations, a substantial metastability is observed (discussed below), which results in sluggish kinetics for heat storage and/or release close to equilibrium.<sup>57</sup> Such metastability lowers the exergy efficiency, thus limiting the material's applicability for TCES. However, we note that despite low exergy efficiency for some TCES cycles they still may be appropriate for certain low-temperature applications where heat is used directly, *e.g.* space heating or drying.

**Dynamic criteria.** Heat must be absorbed or released at sufficient rates for a TCES system to be practically useful.

*Heating power.* Heating power,  $W$ , is the most straightforward way to quantify the rate of heat or cold storage/release:

$$W = \frac{dQ_{\text{useful}}}{dt} \quad (6)$$

The heating power is predominantly determined by the system design and by material properties such as the rate of heat/mass transfer within the material bed. For a bed of TCES particles, thermal conductivity, heat capacity, and the diffusion coefficient are important factors in achieving an optimal bed design.<sup>48</sup>

*Cooling power or SCP.* Cooling power or specific cooling power, SCP, is defined as the amount of heat absorbed by a system per unit time divided by either the mass of the material ( $m$ ):

$$\text{SCP} = -\frac{1}{m} \frac{dQ_{\text{useful}}}{dt} \quad (7)$$

or by its volume ( $V$ ):

$$\text{SCP} = -\frac{1}{V} \frac{dQ_{\text{useful}}}{dt} \quad (8)$$

*Cycle time.* Cycle time is another important factor that affects material selection. For short-term cycles (*e.g.* daily storage) adsorption on a surface or absorption in a liquid is often preferable for TCES. On the other hand, for long-term storage, chemical reactions involving absorption in solid materials are preferred due to their lower tendency for heat losses.

*Dynamic temperature lift.* An alternative form of temperature lift, termed dynamic temperature lift,  $\text{TL}_{\text{dyn}}$ , is commonly used in studies dedicated to TCES prototypes. In this case the temperature lift is defined as the temperature reached during discharging,  $T_{\text{release}}$ , at the outlet (maximal or average) minus the initial temperature,  $T_{\text{inlet}}$ , of the heat transfer fluid (HTF):<sup>58</sup>

$$\text{TL}_{\text{dyn}} = \max(T_{\text{release}}) - T_{\text{inlet}} \quad (9)$$

**Other criteria.** Other aspects of TCES materials relevant for domestic applications include:

- Energy storage density (ESD, energy stored per unit volume of the material, bed, or the device) and specific energy (energy stored per unit mass)
- Amount of working fluid (or sorbate) exchanged during the cycle  $\Delta w$ , g g<sup>-1</sup> (for cooling, moisture recuperation, water harvesting)
- Presence/absence of side reactions (*i.e.*, chemical degradation)
- Reversibility of reaction or sorption/desorption
- Mechanical properties (compressibility, volume change, flowability – for moving beds)
- Cost (per unit of processed energy)
- Toxicity (high LD<sub>50</sub>, mg kg<sup>-1</sup>)
- Flammability



The above criteria point to challenges associated with the use of several materials for domestic applications, for instance, those based on ammonia or methanol (due to toxicity and flammability) or those involving compounds of expensive metals.<sup>39,45–47,59</sup> While the costs of new technologies that rely on the sourcing of materials that are not in wide use can initially be high (such as for the TCES systems discussed here), rapid cost reductions have been demonstrated in related technologies by exploiting economies of scale. For example, the cost of Li-ion batteries has decreased by approximately 97% over the past three decades.<sup>60</sup> We anticipate that similar cost reductions can be achieved for the materials relevant for TCES.

## B. Example applications for TCES

**Domestic heat storage.** A thermochemical energy storage system for domestic applications may be considered a thermally-driven heat pump based on endothermic decomposition (or desorption) and exothermic synthesis (or sorption) reactions.<sup>47</sup> Fig. 3 shows an ideal thermodynamic cycle of a domestic TCES system, which consists of two isobars and two isosteres. During storage or charging (process 3 → 4) the material is decomposed at  $(T_{\text{storage}}, P_{\text{dec}})$  while the resultant gas is condensed at  $T_{\text{cond}}$  in the condenser (or ejected to the surroundings for an open system). Once the decomposition is complete (4), the heat is stored in the form of chemical potential which is constant across isosteres (2–3 and 1–4 in Fig. 3). In a domestic storage cycle, heat is released at  $T_{\text{release}} < T_{\text{storage}}$  during synthesis by evaporating the working fluid at  $(P_{\text{syn}}, T_{\text{evap}})$  while bringing it in contact with the charged thermochemical material. The cooling effect in the evaporator is produced simultaneously with useful heating.

The most popular closed TCES systems exchange only heat with the surroundings. These consist of an adsorber–desorber for decomposition/synthesis of the TCES materials and an evaporator–condenser for the evaporation/condensation of a working fluid. In contrast, open systems exchange the working fluid with the environment and do not require a separate vessel for condensation.

For both open and closed systems the adsorber–desorber subsystem often consists of a packed bed of an active storage

material with an integrated heat exchanger.<sup>61</sup> Alternatively, one can decouple decomposition–synthesis and storage by allowing them to occur separately in a heat exchanger and a storage tank, respectively. However, this approach requires the transport of the storage material from the storage vessel to the heat exchanger; such systems are referred to as moving bed systems. Each system design has advantages and drawbacks; helpful reviews of these topics can be found elsewhere.<sup>30,62</sup>

For domestic heat storage, the boundary temperatures and pressures are defined by the available source(s) of heat to be stored and by the heating demand. Ideally, decomposition would be driven by a solar collector/PV panel with typical temperatures  $T_{\text{storage}} = 80\text{--}100\text{ }^{\circ}\text{C}$ , while the condensation of the working fluid (water) would occur at near ambient temperature,  $T_{\text{cond}} = 25\text{--}30\text{ }^{\circ}\text{C}$ .<sup>47</sup> The stored heat may be used for space heating ( $T_{\text{release}} = 30\text{--}45\text{ }^{\circ}\text{C}$ ) or for the production of hot water ( $T_{\text{release}} = 60\text{--}70\text{ }^{\circ}\text{C}$ ) by upgrading low-temperature heat taken from the environment (e.g. from geothermal wells or directly from air) at  $T_{\text{evap}} = 5\text{--}25\text{ }^{\circ}\text{C}$ . While these boundary conditions are typical for domestic applications (Table 2), more exotic examples include decomposition *via* an electric heater at  $T_{\text{storage}} > 300\text{ }^{\circ}\text{C}$ <sup>63</sup> or upgrading heat using a temperature difference between air ( $-40\text{--}25\text{ }^{\circ}\text{C}$ ) and water ( $2\text{--}3\text{ }^{\circ}\text{C}$ ) in colder climates for space heating.<sup>64</sup> In the latter case, the so-called “heat-from-cold” (HeCol) cycle differs from the one presented in Fig. 3 as the sorbent is regenerated *via* pressure rather than through a temperature difference.<sup>65,66</sup>

The criteria for material selection in domestic heating applications arise from space constraints for the TCES system, and from temperature requirements for hot tap water or space heating. Consequently, energy storage density (*i.e.* the amount of heat stored per cubic meter of the storage bed or device), temperature lift, power, and cyclability are the most relevant parameters. Material toxicity is also a concern as many governments impose restrictions on working fluids for refrigerants used in the domestic environment (e.g. ammonia or methanol). Unsurprisingly, material price per unit of stored energy is also an important criterion.<sup>67</sup> Additional system-specific requirements on the storage materials may be introduced – *e.g.* absence of side reactions with air or mechanical strength of the storage particles – for certain system designs (open/closed and fixed/moving bed).

Most existing domestic heat storage prototypes based on salt hydrates are closed systems that contain a packed bed. In these designs a heat exchanger is embedded within the bed, usually by means of metal plates or fins (Table 2). Only a few existing prototypes employ solid-state heat-storing reactions; most are based on solid-solution transitions, followed by dilution of the salt solution held by capillary forces in porous media. The deliquescence of the salt allows for the extraction of more heat in comparison with solid-state transformation, but at the expense of reduced temperature lift.<sup>49</sup>

TCES for domestic heat storage has not been widely adopted because the primary operating requirements are not yet fully met. For example, typical energy storage densities are 0.3–0.9 GJ per  $\text{m}^3$  of bed, and these values are further lowered by the

Fig. 3 The four-temperature thermodynamic cycle of a thermally-driven chemical heat pump for domestic TCES depicted in  $\ln P/P^{\circ}$  –  $(-1/T)$  coordinates with typical temperature values in the inset.



**Table 2** Examples of lab-scale prototypes of domestic TCES systems and their most relevant characteristics. Only prototypes releasing heat at  $T_{\text{release}} > 30^\circ\text{C}$  and having temperature lift > 10 °C are included

Heat release transition	Type	ESD <sub>mat</sub> /ESD <sub>bed</sub> , GJ m <sup>-3</sup>	Temperatures T <sub>evap</sub> /T <sub>release</sub> /T <sub>storage</sub> , °C	TL <sub>max</sub> , °C	Power, W kg <sup>-1</sup>	N <sub>cycles</sub>	Ref.
MgCl <sub>2</sub> ·2H <sub>2</sub> O + 4H <sub>2</sub> O ⇌ MgCl <sub>2</sub> ·6H <sub>2</sub> O	Packed bed, closed	2.0/0.5	10/50/130	54	—	—	339
K <sub>2</sub> CO <sub>3</sub> + 1.5H <sub>2</sub> O ⇌ K <sub>2</sub> CO <sub>3</sub> ·1.5H <sub>2</sub> O	Packed bed, closed	1.3/0.8	10/40/90	50	—	14	340
SrBr <sub>2</sub> ·H <sub>2</sub> O + 5H <sub>2</sub> O ⇌ SrBr <sub>2</sub> ·6H <sub>2</sub> O	Packed bed, closed	2.6/0.67	15/35/80	—	86.4 (avg)	—	341
LiCl + H <sub>2</sub> O ⇌ LiCl solution (vermiculite)	Packed bed, closed	—/1.0	10/35/90	12	2100 (peak)	14	342
LiBr + H <sub>2</sub> O ⇌ LiBr solution (silica)	Packed bed, closed	1.37/—	10/30/120	17	300 (peak)	10	343
K <sub>2</sub> CO <sub>3</sub> + H <sub>2</sub> O ⇌ K <sub>2</sub> CO <sub>3</sub> solution (vermiculite)	Packed bed, closed	—/0.9	25/40/120	15	450 (avg)	47	344
CaCl <sub>2</sub> ·2H <sub>2</sub> O + H <sub>2</sub> O ⇌ CaCl <sub>2</sub> solution (vermiculite)	Packed bed, open	—/0.36	20/57/80	36	106 (peak)	6	58

volume of the condenser, pipes, and other components. Unfortunately, energy storage densities at the system level are reported infrequently. For systems that undergo deliquescence, low temperature lift (<20 °C) remains a challenge, while low power is a common limitation for systems employing solid-solid heat-storing reactions. At present, there exists no “best” material or system design for TCES in domestic applications. Rather, every prototype strives to meet performance demands through a combination of design trade-offs. The necessity of these compromises reflects the absence of an ideal TCES material. Developing improved material(s) is one of the main challenges for accelerating the adoption of TCES.

**Cooling and air conditioning.** Sorptive cooling dates to the work of Michael Faraday, who used ammonia as an adsorbate and AgCl as a sorbent.<sup>68,69</sup> The thermodynamic cycle for cooling is similar to the cycle for domestic heating (Fig. 3), with two major differences: the useful effect (*i.e.* cooling) occurs during evaporation, and the boundary temperatures can vary depending on the purpose of the cooling.

Typical applications include air conditioning in buildings and in transport (cars, marine vessels), cooling of datacenters, and ice making for food preservation. For air conditioning,  $T_{\text{evap}} = 0\text{--}10^\circ\text{C}$ , while  $T_{\text{evap}} = -5\text{--}0^\circ\text{C}$  is used for ice making and deep freezing.<sup>70</sup> Depending on ambient conditions, the condensation temperature is typically 25–40 °C.  $T_{\text{storage}}$  and  $T_{\text{release}}$  are usually within similar ranges as for heat storage: 80–100 °C and 35–50 °C, respectively.

The two main criteria for material selection for a refrigeration cycle are the specific cooling power of a bed, SCP, (*i.e.*, how fast cold can be produced), and the amount of refrigerant exchanged in a cycle<sup>70</sup> (*i.e.*, the specific refrigerant uptake,  $\Delta w$ ), defined by:

$$\Delta w = w_{\text{rich}} - w_{\text{weak}} \quad (10)$$

where  $w_{\text{rich}}$  and  $w_{\text{weak}}$  are the maximum and minimum mass of sorbate, respectively, adsorbed or absorbed during a refrigeration cycle per mass of sorbent (Fig. 4). Other criteria include cyclability and cost.

The preference for high specific cooling power (SCP) limits the use of water as a refrigerant; the saturated vapor pressure of water at 0–10 °C is too low for fast vapor transport and, therefore, fast heat reallocation. (In principle, water may be used at  $T < 0^\circ\text{C}$  in the form of a salt solution<sup>71</sup>). For this reason, the most promising refrigerants are ammonia, methanol, ethanol, CO<sub>2</sub> and some fluorocarbons.<sup>72</sup> The need for high

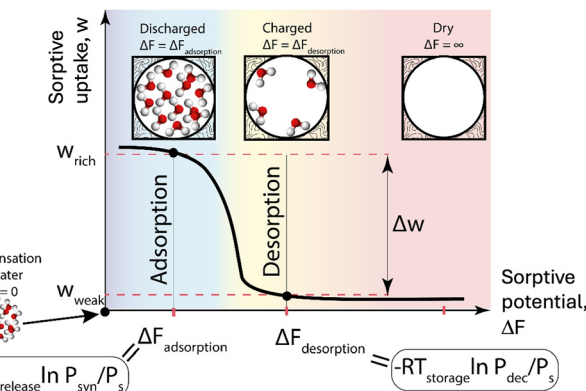


**Fig. 4** Representation of the four-temperature adsorptive/desorptive cycle for domestic heating and cooling in  $w$ ,  $-\Delta F$  coordinates.

SCP implies that the sorption process itself should be rapid. The two main sorption mechanisms employed in the TCES field are physical adsorption and absorption of the refrigerant by a salt solution (often in pores of a matrix). Typical SCPs for existing prototypes fall within the range of 300–1000 W kg<sup>-1</sup> (Table 3). There is a complex and not yet fully understood interplay of power, layer and heat exchanger geometry, and cycle time, leading to heuristic relations for optimization of such systems.<sup>73,74</sup>

The connections between adsorbate uptake, pressure, and temperature can be described in terms of the Polanyi sorption potential:<sup>75</sup>

$$\Delta F(T, P) = -RT \ln \left( \frac{P}{P_s} \right), \quad (11)$$

where  $R$  is the ideal gas constant and  $P_s$  is the saturated pressure of the sorbate at temperature  $T$ . For most physical

**Table 3** Examples of working pairs for sorptive cooling by salts, based on prototype studies

Sorbent	Refrigerant	SCP, W kg <sup>-1</sup>	$\Delta w, \text{g g}^{-1}$	Ref.
CaCl <sub>2</sub> in silica	H <sub>2</sub> O	—	0.75	345
CaCl <sub>2</sub> in zeolite + MWCNT	H <sub>2</sub> O	1111	0.5	346
MnCl <sub>2</sub> in expanded graphite	NH <sub>3</sub>	350	0.54	285
BaCl <sub>2</sub> in vermiculite	NH <sub>3</sub>	300–680	0.25	286 and 347
LiCl in silica	CH <sub>3</sub> OH	210–290	0.6	348



adsorbents and composites the sorption uptake curve is invariant with respect to sorption potential (Fig. 4). Once the boundary conditions of the cycle are fixed (Fig. 3), the Polanyi potentials required to trigger sorption and desorption can be defined (Fig. 4). An optimal sorbent will exchange a large amount of refrigerant between the two boundary potentials. Typical  $\Delta w$  values are 0.2–0.7 g g<sup>-1</sup> for adsorbents such as silica gel, zeolites, and salt composites retained within the pores of a host. Recently, several metal-organic frameworks (MOFs) with high water uptake (up to 2 g g<sup>-1</sup>, the highest uptake reported to date) were identified as promising for cooling.<sup>76–78</sup>

Thus, the main challenge for material science in sorptive cooling is the identification of sorbents that can exchange large quantities of adsorbate rapidly and repeatedly under  $T, P$  conditions appropriate for the cooling cycle.

**Heat and moisture recuperation in ventilation systems.** In cold climates, the share of heat loss from ventilation systems can reach ~50%. Hence, one promising niche application for TCES is sorptive recuperation of moisture and heat from ventilation. The operating principle for sorptive heat/moisture recuperation involves sorption of water from outgoing air at room temperature and relative humidity (RH) ~40–50%, followed by heat transfer to the ingoing air by means of a heat exchanger (Fig. 5). The ingoing air (which is heated in the heat exchanger) is moisturized *via* the sorbent bed to recuperate humidity. This process minimizes the freezing of air in the heat

exchanger and allows for the maintenance of comfortable relative humidity indoors.

Climate conditions and the desired indoor RH set the requirements for the sorbents used for heat and moisture recuperation:

- The water affinity of the sorbent must be large enough to ensure deep drying of the outlet air to the ambient dew point, to prevent ice formation at the bed outlet

- Water affinity must be low enough to ensure the release of water to humidify the inlet air to a comfortable RH (40–60%)

- Water uptake,  $\Delta w$ , must be maximized

These requirements can be formulated in terms of the sorption potential, as explained above for sorptive cooling. Currently, traditional adsorbents<sup>79</sup> (e.g. in form of desiccant wheels) and composite sorbents<sup>80</sup> are considered promising for this application.

**Other applications.** Other sorptive applications include water desalination<sup>81</sup> and water harvesting from air.<sup>82</sup> Performance requirements for these cases are typically formulated in terms of the amount of water harvested/produced per unit time. For the materials, this means a large uptake swing  $\Delta w$  between sorptive potentials (Fig. 4), which are in turn defined by climatic or ambient conditions such as temperature and relative humidity. Other requirements are low cost and cycling stability. Recent advances in MOF chemistry have led to the design of adsorbents suited for these applications.<sup>83</sup> Unlike zeolites or salts in porous matrices, these MOFs allow for milder regeneration temperatures and greater water uptake.<sup>84–86</sup>

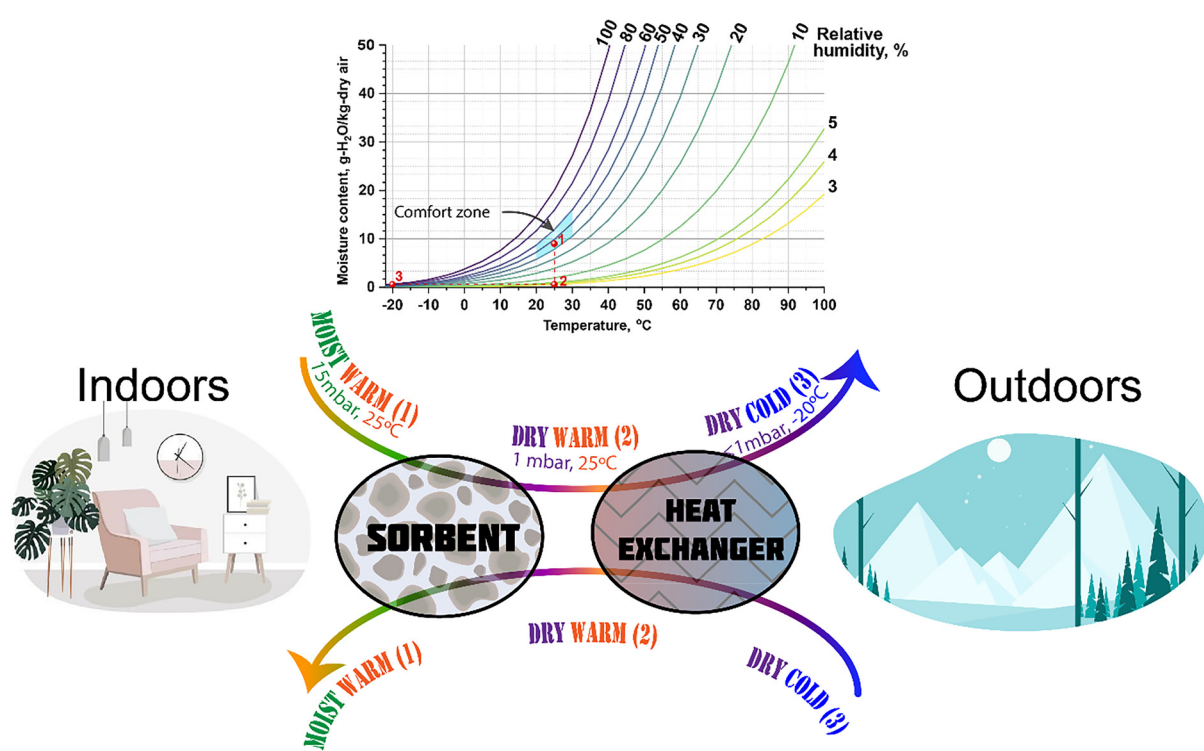


Fig. 5 Ventilation systems. The moist warm air (point 1 on the psychrometric chart) enters the layer of adsorbent to isothermally dry (point 2), then it exchanges the heat with the cold air at point 3 and is exhausted. Conversely, the outside cold air is heated up and moisturized by the sorbent. The indoor comfort zone is highlighted in blue on the psychrometric chart.

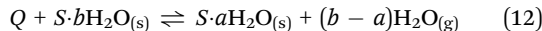


## Materials classes and their key attributes

### A. Overview of low-temperature thermochemical storage materials

There are three general classes of processes for low temperature thermochemical energy storage. In the first class, a solid chemically reacts with a gas through an absorption process, forming another solid. The most common materials used for this class are salt hydrates, although ammoniates and methanolates operate analogously. The second class consists of the adsorption of a gas within a porous host, such as silica gel, a zeolite, or a MOF. Finally, the third class involves the absorption of a gas by a liquid. The different material families corresponding to these three classes of processes have different properties, which are summarized in Table 4.

In the process, heat is stored in the endothermic decomposition of a more complex solid into another (compositionally simpler) solid and a gas. Heat is released during the reverse synthesis reaction. In the case of salt hydrates (*i.e.*, salts with water molecules incorporated into their crystal structure), the reaction is:

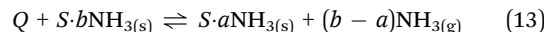


where  $Q$  is the heat of reaction,  $S \cdot b\text{H}_2\text{O}_{(s)}$  is a salt hydrate,  $S \cdot a\text{H}_2\text{O}_{(s)}$  is the dehydrated salt or hydrate (with  $b > a$ ), and  $\text{H}_2\text{O}_{(g)}$  is water vapor. The choice of water as the reactive fluid carries several benefits for low temperature TCES, including safety and abundance, as well as favorable thermodynamic properties that allow the (de)hydration reactions to be reversed at relatively low temperatures.

Of the low temperature TCES materials, hydrates tend to have the highest energy densities at the materials level, both theoretically<sup>87</sup> and experimentally.<sup>88</sup> However, many salt hydrates display complexities when implemented in practical systems. For example, some hydrates melt (*i.e.*, form concentrated aqueous salt solutions) rather than dehydrate (*i.e.*, release water vapor) when heated. Others deliquesce when the water vapor pressure is too large, *i.e.*, greater than the deliquescence relative humidity (DRH) of the material. Still others will experience side reactions, such as the well-known hydrolysis of lower hydrates of  $\text{MgCl}_2$ , which forms gaseous  $\text{HCl}$ .<sup>89</sup> All of these phenomena cause irreversibilities that reduce, upon cycling, the amount of active material that can store heat. Furthermore, the complexities of heat and mass transfer in salt hydrates can result in slow kinetics. In addition to these technical issues, some salts are impractical due to their high cost or toxicity. Despite these practical complications, salt hydrates remain a promising class of TCES materials. Much research is being done to characterize and understand their performance at the materials level, and recently some large-scale prototypes using salt hydrates have been built.<sup>63,90</sup>

Like hydrates, ammoniates are salts with ammonia molecules present within the crystal structure. Salt ammoniates were originally proposed decades ago for TCES, but only recently

have drawn serious attention.<sup>91–93</sup> The ammoniates are analogues of salt hydrates as they are defined by the reaction:



where the reactive fluid is ammonia rather than water. The use of ammonia poses a practical challenge for many applications as ammonia is toxic. Regardless, these materials may be of interest to a sub-set of applications where the toxicity issue can be managed. Recently, Müller *et al.* characterized many ammoniates according to their energy density.<sup>91</sup> The value recorded in Table 4 has been adjusted to maintain consistency with other entries in the table, where energy densities are reported in terms of the volume and/or mass of the more complex (hydrated or ammoniated) material. Here, it can be seen that ammoniates have comparable, although slightly smaller energy densities than hydrates. Similar to hydrates, ammoniates may experience irreversible side reactions, such as the formation of  $\text{NH}_4\text{Cl}$  in chloride salts.<sup>91</sup> They also require the use of pressurized vessels in system designs, which will increase cost and potentially impact energy densities. However, one potential advantage of ammoniates over hydrates is their faster charging/discharging rates due to higher pressures. This is demonstrated by the power value calculated from data reported by Yan *et al.* for the reaction of  $\text{MnCl}_2$  with ammonia.<sup>94</sup> Finally, since ammoniates have not drawn as much attention as salt hydrates, most ammoniate studies for TCES are on the laboratory scale.

A smaller family of TCES materials in the first class are salt methanolates, which store methanol molecules in the salt crystal structure. Their reaction is defined as:



The literature on methanolates for TCES is sparse. Given methanol's favorable properties for refrigeration they are mainly of interest for refrigeration applications.<sup>95</sup> From the data available in the literature, methanolates appear to exhibit similar (perhaps slightly smaller) energy and power densities compared to salt hydrates.<sup>96,97</sup> Methanolates tend to deliquesce easily, so porous matrices have been used to stabilize and exploit deliquescence.<sup>98–101</sup> The main drawback to their use is the flammability and toxicity of methanol.

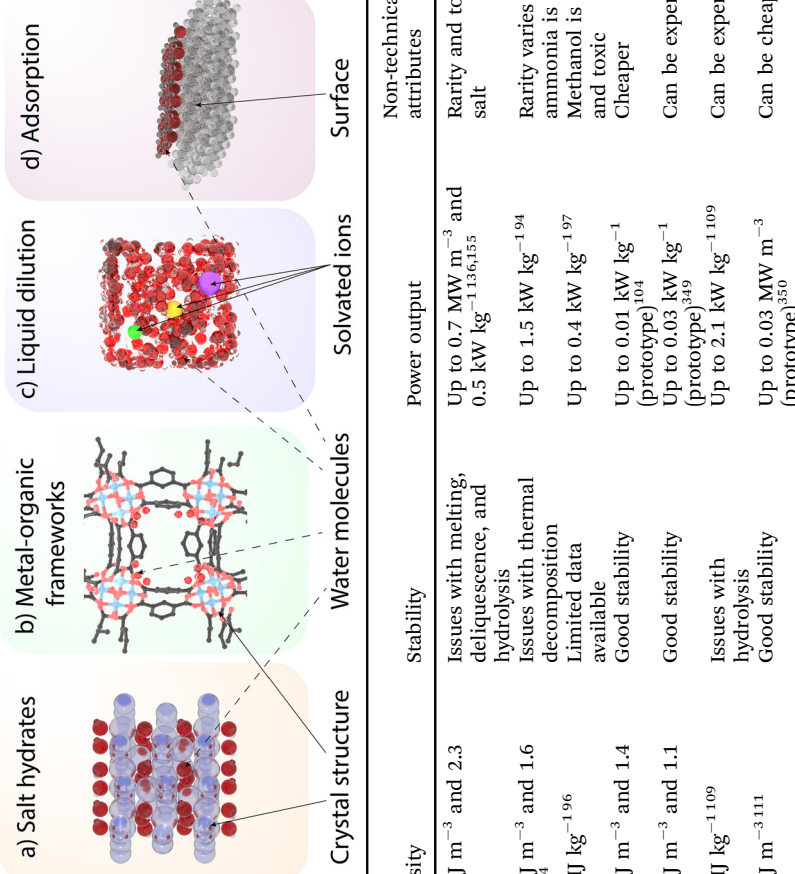
The second class of low temperature TCES materials are porous media. These materials adsorb a reactive gas onto the surfaces of their pores. In most cases, this gas is water, as water has many favorable properties mentioned previously. The different porous media display a range of pore sizes, classified as micropores (pore diameter  $< 2$  nm), mesopores (2–50 nm), or macropores ( $> 50$  nm).<sup>102</sup> An example of one of the most mature TCES storage materials is silica gel, which consists of mesoporous amorphous silicon dioxide. These pores readily absorb water from the environment, leading to its common use as a desiccant. Advantages of silica gel include its relatively low cost, widespread availability, and good cyclability.<sup>103</sup> As a result, it has been developed to commercial scale quicker than other thermochemical materials. However, its relatively low





**Table 4** Overview of low temperature thermochemical heat storing materials. The illustration shows a few examples of TCES materials, including (a) a crystal structure of a salt hydrate ( $\text{LiCl}\cdot\text{H}_2\text{O}$ , Class I), (b) a crystal structure of a MOF (CAU-10, Class II), (c) a cartoon depicting liquid dilution (Class III), and (d) surface adsorption (on quartz (001))

Class	Material	Energy density	Stability	Power output	Technology readiness level	
					Non-technical attributes	
I	Salt hydrates	Up to $3.8 \text{ GJ m}^{-3}$ and 2.3 $\text{MJ kg}^{-1,87}$	Issues with melting, deliquescence, and hydrolysis	Up to $0.7 \text{ MW m}^{-3}$ and $0.5 \text{ kW kg}^{-1,136,155}$	Rarity and toxicity vary by salt	Laboratory and prototype scale
I	Salt ammoniates	Up to $2.1 \text{ GJ m}^{-3}$ and 1.6 $\text{MJ kg}^{-1,91,94}$	Issues with thermal decomposition	Up to $1.5 \text{ kW kg}^{-1,94}$	Rarity varies by salt, ammonia is toxic	Laboratory scale
I	Salt methanolates	Up to $1.3 \text{ MJ kg}^{-1,96}$	Limited data available	Up to $0.4 \text{ kW kg}^{-1,97}$	Methanol is flammable and toxic	Laboratory scale
II	Silica gel	Up to $0.8 \text{ GJ m}^{-3}$ and 1.4 $\text{MJ kg}^{-1,34}$	Good stability	Up to $0.01 \text{ kW kg}^{-1}$ (prototype) <sup>104</sup>	Cheaper	Commercial scale
II	Zeolites	Up to $0.7 \text{ GJ m}^{-3}$ and 1.1 $\text{MJ kg}^{-1,34}$	Good stability	Up to $0.03 \text{ kW kg}^{-1}$ (prototype) <sup>349</sup>	Can be expensive	Commercial scale
II	MOFs	Up to $1.3 \text{ MJ kg}^{-1,109}$	Issues with hydrolysis	Up to $2.1 \text{ kW kg}^{-1,109}$	Can be expensive	Laboratory scale
III	Liquid dilution	Up to $1.4 \text{ GJ m}^{-3,111}$	Good stability	Up to $0.03 \text{ MW m}^{-3}$ (prototype) <sup>350</sup>	Can be cheaper	Commercial scale



energy density in the operational window of low-temperature TCES limits its potential in compact applications. The low power cited in Table 4 for this material is derived from a large-scale prototype involving 350 kg of silica gel.<sup>104</sup>

Zeolites represent another category of material that falls within the second class of TCES media. Zeolites are aluminosilicates that can adsorb water into their micropores. Like silica gel, zeolites have been developed to the commercial scale. They are stable but are costlier than silica gel. They possess slightly smaller gravimetric energy densities than silica gels due to their weight, but higher power densities at the prototype scale compared to silica gels. One characteristic of zeolites is their hydrophilicity, resulting in high desorption temperatures for water.<sup>103</sup> As such, depending on the maximum charging temperature available, the reversible capacity of zeolites at low temperatures (100 °C) can be limited.

Metal-organic frameworks (MOFs) represent another promising category of porous materials that are of interest for low temperature TCES. MOFs are porous, crystalline materials consisting of metal clusters connected by organic linkers. Well known for their extremely high surface areas, the size of the pores in MOFs can be tuned by substitution of linkers of varying length.<sup>105</sup> Given the many degrees of freedom in MOF structure and composition, the potential chemical space for MOFs is extremely large, which has attracted the interest of materials designers.<sup>106</sup> In addition to their cost, the main disadvantage of MOFs is that some MOFs decompose irreversibly in the presence of water, making reversible water capture and release an impossibility for those compositions.<sup>107</sup> However, several water-stable MOFs are known and show promise for TCES, such as MIL-101, CAU-10, NH<sub>2</sub>-MIL-125, MOF-801.<sup>86</sup> Recent efforts have focused on computationally predicting the water stability of MOFs.<sup>108</sup> Ehrenmann *et al.* characterized the water adsorption of MIL-101, for which energy density and power are reported in Table 4.<sup>109</sup> While the energy density of MOFs is similar to other types of materials, the main advantages are the high power density, which reflects the high degree of regular porosity found in MOFs, and the stepwise adsorption behavior, which, albeit, has been demonstrated only for a few MOFs.<sup>110</sup>

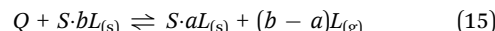
Finally, the third class of low temperature TCES materials operates *via* liquid absorption, in which a solute is reversibly evaporated from/absorbed into a solvent. Evaporation, which concentrates the solute (by desorbing the solvent), is endothermic, while the condensation of the solvent back into solution is exothermic. This approach tends to exhibit good stability and thus has reached commercial scale. Also, depending on the solute chosen, the material cost can be relatively inexpensive. Regarding its energy density and prototype-scale power density, its performance is average compared to other types of materials. Yu *et al.* proposed a three-phase sorption cycle using LiCl/H<sub>2</sub>O, where the liquid absorption accounted for 57% of the energy stored, translating to an energy storage density of 1.4 GJ m<sup>-3</sup> for heat storage.<sup>111</sup> Another remarkable solute is NaOH with potential storage density exceeding 1 GJ m<sup>-3</sup> and 20–25 °C temperature lift.<sup>50</sup> A trade-off between the energy

storage density and the temperature lift is the main reason why absorptive heat storage systems are not yet widespread.<sup>112</sup>

## B. Class I: salt hydrates, ammoniates, and methanolates

**Materials and scales.** Before going into details regarding the properties of salts and their interactions with vapor, it is helpful to have a basic understanding of how these materials will be deployed within a thermal energy storage device. In the core of the device will be a storage bed comprised of small particles of the storage material. Since a powder based on very small crystallites will have a poor permeability for water vapor, use of millimeter-sized particles is foreseen. The particles will be manufactured from a powder and themselves be porous in nature. This introduces several length scales as illustrated in Fig. 6, where a cartoon of a hydrating K<sub>2</sub>CO<sub>3</sub> particle is shown. The structure and processes occurring at these length scales have distinct contributions to properties like energy density, power, stability, *etc.*

**Phase equilibria.** Consider a salt that can change its loading with vapor according to the following reaction equilibrium.



Here, *S* represents a neutral ion pair in the salt. *L* is the gaseous compound that reacts with the salt: *i.e.* H<sub>2</sub>O (hydrates),<sup>46,47,114</sup> NH<sub>3</sub> (ammoniates),<sup>115–117</sup> CH<sub>3</sub>OH (methanolates),<sup>118</sup> C<sub>2</sub>H<sub>5</sub>OH (ethanolates),<sup>118</sup> *etc.* *Q* is the heat associated with the reaction. During reaction, the salt switches between two states of loading (the number of molecules *L* per neutral ion pair) *a* and *b* with *b* > *a*. Bonding of the gas to the salt is accompanied by a release of heat. Therefore, increasing the loading of *L* within the salt (*a* → *b*) takes place with the discharge of heat, while reducing the loading (*b* → *a*) charges the medium. Since the reaction involves a structural change of the crystalline lattice, the process behaves as a phase change. According to the Gibbs phase rule, such a transition occurs at a well-defined set of temperatures *T* and vapor pressures *p*, with *p* = *f*(*T*). From here forward we will focus the discussion on salt hydrates, *L* = H<sub>2</sub>O, but similar considerations apply to ammoniates, methanolates, *etc.* As needed, considerations unique to the ammoniates and methanolates will be discussed separately.

When the reaction shown in eqn (15) is in equilibrium,  $\Delta G_{rxn} = 0$ . It follows from this equilibrium condition that the

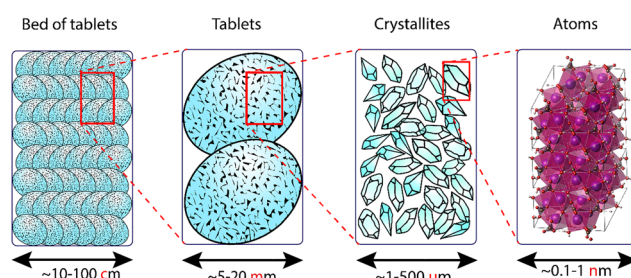


Fig. 6 The different length scales associated with the hydration of K<sub>2</sub>CO<sub>3</sub>. Reproduced from ref. 113 under the terms of the Creative Commons CC-BY license, copyright 2024.



equilibrium vapor pressure  $p_{\text{eq}}$  and  $T$  are related *via* the van 'Hoff equation.

$$p_{\text{eq}} = p^0 \exp \left[ \frac{\Delta H_{\text{ab}}^0 - T \Delta S_{\text{ab}}^0}{RT} \right] \quad (16)$$

where  $p^0$ ,  $\Delta H_{\text{ab}}^0$  and  $\Delta S_{\text{ab}}^0$  are the standard pressure (1 bar), the standard molar enthalpy of absorption (per mole vapor), and the standard molar entropy of absorption (per mole vapor), respectively. Further,  $R$  is the gas constant and  $T$  [K] is the absolute temperature. In the case of hydration reactions, the enthalpy and entropy are the molar enthalpy and entropy of hydration, respectively. Typical values for the enthalpy  $\Delta H_{\text{ab}}^0$  and entropy  $S_{\text{ab}}^0$  are 40–80 kJ mol<sup>-1</sup> and 140–160 J mol<sup>-1</sup> K, respectively.<sup>87,119</sup>

To illustrate the phase behavior of hydrates a water vapor pressure diagram for  $\text{MgCl}_2$  is shown in Fig. 7.  $\text{MgCl}_2$  can form multiple hydrate phases ( $n = 0, 1, 2, 4, 6, 8, 10, 12$ )<sup>120–124</sup> that are stable at different combinations of temperature and water vapor pressure. The most important of these are for  $n = 2, 4$  and  $6$ , which are shown in Fig. 7, with data taken from Derby *et al.*<sup>125</sup> and Carling.<sup>126</sup> The higher hydrates ( $n > 6$ ) are not stable at the given conditions. The lines for the lower hydrates  $n = 0$  and  $1$  (not shown) are below the line for the  $2 \rightarrow 4$  transition. At high vapor pressures the salt deliquesces: *i.e.* it absorbs water and liquefies (turns into solution). It is important to stress that a pressure–temperature diagram like Fig. 7 is an intrinsic property of the selected salt.

A driving force for the hydration reaction exists when the chemical potential for water in the vapor phase and water in the solid is unequal.

$$\Delta\mu = RT \ln(p/p_{\text{eq}}) \neq 0 \quad (17)$$

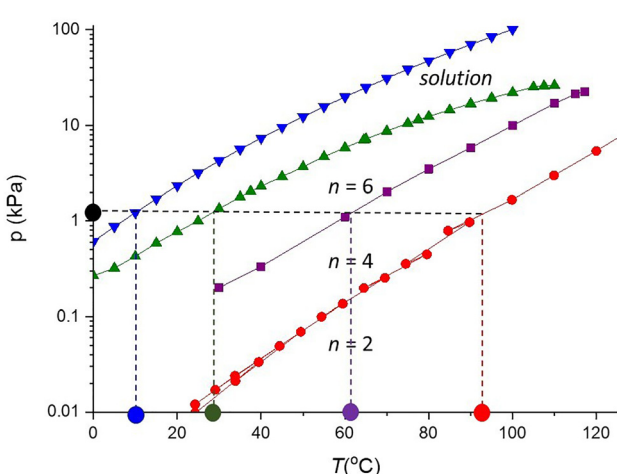


Fig. 7 Water vapor pressure–temperature lines for phase transitions of  $\text{MgCl}_2$  hydrates  $\text{MgCl}_2 \cdot n\text{H}_2\text{O}$ : deliquescence (green),  $n = 4 \rightarrow 6$  transition (purple), and  $n = 2 \rightarrow 4$  transition (red). The blue line/points refer to the  $P$ – $T$  combinations for saturated water vapor. The coloured dots on the abscissa indicate the theoretical output temperatures of the different phase transitions at water vapor generated at 10 °C (12 mbar). Data adapted from Derby *et al.*<sup>125</sup> and Carling.<sup>126</sup>

Specifically, the salt is hydrated (discharged) when  $p/p_{\text{eq}} > 1$  and dehydrated (charged) when  $p/p_{\text{eq}} < 1$ .

Diagrams like the one shown for  $\text{MgCl}_2$  in Fig. 7 are helpful because they demonstrate important aspects of the operation of salt hydrates. First, a strong coupling exists between the use conditions of a heat storage device and the optimal salt. As the phase lines are intrinsic features of the crystalline structure and composition of the salt, they cannot be easily adapted to accommodate the prescribed conditions. For discharge (heat generation) it is extremely important to know the conditions of the water vapor source that comes into contact with the salt. For example, Fig. 7 shows that when  $\text{MgCl}_2$  is reacted with saturated water vapor at 12 mbar/10 °C, the resulting reactions can theoretically deliver heat at several temperatures, corresponding to one deliquescence reaction and two distinct hydration reactions. When the  $2 \rightarrow 4$  transition occurs, heat at a temperature slightly above 90 °C is released. However, the temperature of the discharge will drop to lower values of ~60 °C at the  $4 \rightarrow 6$  transition. In cases where multiple hydration reactions occur for a given salt (*i.e.*, several hydrated phases are stable), the temperature of the generated heat will decrease as one progresses through transitions corresponding to the formation of phases with larger water content. Hence, the use conditions not only determine the kinetics, but also the available heat and thus the effective energy storage density.

The hydration reaction involves risks. At low temperatures, a salt may undergo deliquescence, which can harm the operation of the heat storage device. This complication can be circumvented by avoiding the low temperatures with a system control, or by stabilizing the material to minimize the impact of deliquescence. Despite these stabilization options, extremely deliquescent salts, like  $\text{LiCl} \cdot \text{H}_2\text{O}$  (DRH = 11.2%),<sup>127</sup>  $\text{LiBr} \cdot 2\text{H}_2\text{O}$  (DRH = 7.75%),<sup>127</sup> and  $\text{CaCl}_2 \cdot 2\text{H}_2\text{O}$  (DRH = 12.9%),<sup>128</sup> are not suitable candidates for heat storage based on salt hydration, as decreases in temperature will immediately lead to deliquescence. It should be noted though that exploiting deliquescence is one of the routes to mitigate these risks.<sup>111,344</sup> While it is possible to boost storage density by exploiting deliquescence, such systems operating with salt solutions require a porous medium to stabilize and, as noted earlier, often suffer from a poor trade-off between storage density and temperature lift.

**Temperature lift.** While equilibrium temperature lift (eqn (3)) is determined by the transition on the phase diagram dictated by the boundary conditions ( $T$ ,  $P(\text{H}_2\text{O})$ ) for heat storage and release, dynamic temperature lift (eqn (9)) is determined by the balance between mass transport and heat transport in a TCES material.<sup>129</sup> The rate of heat release is determined by the rate at which the sorbate reaches the reaction front and the reaction rate, while the rate of heat transport away from the reaction front is determined by diffusive and advective processes. The dynamic temperature lift is closely related to the power density. Mass transport, reaction kinetics, and heat transport are discussed in more detail below.

**Energy density.** Energy storage density (ESD) is a key property of an energy storage device. Of course, the system ESD is limited by the intrinsic ESD of the material itself: by embedding



the storage material in a system the resulting system ESD will be less than that of the material alone, due to the volume occupied by the system components. Similar arguments hold for specific energy. Given that system-related penalties are unavoidable, it is desirable to maximize the intrinsic ESD of the material. Since the molar enthalpy of hydration  $H_{ab}^0$  of an  $a \rightarrow b$  transition is a fixed number, the energy density on the crystal level  $u_c$  equals

$$u_c = \frac{N(b-a)H_{ab}^0}{V_{\max}} = \frac{(b-a)H_{ab}^0}{v_b} \quad (18)$$

where  $N$  [moles],  $V_{\max} = V_b$  [ $\text{m}^3$ ], and  $v_b$  [ $\text{m}^3$  per mole] are the moles of neutral ionic pairs, the maximal molar volume of the material (mostly  $V_b$ ), and the molar volume of neutral ion pair in phase  $b$ , respectively. Note this formula assumes that in the device only a single hydration reaction is accessible. Eqn (18) demonstrates that materials with large energy densities should exhibit an efficient packing of water molecules in combination with a large hydration enthalpy.

In cases where multiple reactions (involving different degrees of hydration of the salt) can be accessed the energy density may be expressed as:

$$u_c = \frac{N \sum_{ij} \Delta n_{ij} \Delta H_{ij}^0}{V_{\max}} \quad (19)$$

The summation  $ij$  runs over all possible hydration transitions and  $V_{\max}$  is the maximal molar volume, usually for the highest hydrate considered.  $H_{ij}^0$  and  $\Delta n_{ij}$  are the molar enthalpy and change in degree of hydration during the transition  $ij$ . The total change in hydration state is given  $\Delta n = \sum_{ij} \Delta n_{ij}$ .

Although eqn (18) and (19) provide an upper limit to the ESD, taking into consideration the discussion about the accessibility of phase lines and the use conditions, the system ESD is strongly dependent on the use conditions of the foreseen application. To illustrate this, Table 5 lists the values for the energy densities and output temperatures for use conditions relevant for the built environment (*i.e.*, assuming hydration at 12 mbar and 10 °C, and dehydration at 20 mbar).<sup>47</sup>

When the ambient temperature or relative humidity are not sufficient to deliver water vapor to the storage system at the required vapor pressure, energy may be required to generate additional vapor from liquid water.<sup>30</sup> Accounting for this energy reduces the effective ESD, assuming that this energy cannot be recovered upon discharging. Ideally, all the energy required to generate water vapor should be freely extracted from the environment. However, in some applications, such as in environments near 0 °C, this may not be possible.

There are many system-related factors influencing the system-level ESD.<sup>130</sup> These include bed porosity, internal storage of water, piping, auxiliary equipment, sensible heat losses during operation, *etc.* Here we limit the discussion to the impact of bed porosity and the internal storage of water.

Regarding porosity, the storage system should allow for easy access of water vapor to the salt. For that reason, the storage medium will likely be filled with discrete particles rather than

**Table 5** Overview of crystal-level properties of a selection of salts reported as promising TCES materials. The range of possible hydration states ( $n$ ), energy density for an open TCES system, decrease in molar volume upon dehydration, temperature delivered during hydration ( $T_{\text{release}}$ ), and deliquescence relative humidity are presented for each material. All values are calculated based on water vapor pressures of 12 and 20 mbar for hydration and dehydration, respectively. Data obtained from ref. 47

Salt	$n$ in Salt- $n\text{H}_2\text{O}$	Energy density [ $\text{GJ m}^{-3}$ ]	Volume decrease (%)	$T_{\text{release}}$ [°C]	DRH (%)
$\text{CaCl}_2$	0–2	1.54	35	63	13
$\text{K}_2\text{CO}_3$	0–1.5	1.30	22	59	43
$\text{MgCl}_2$	2–6	1.93	47	61	33
$\text{MgSO}_4$	1–7	2.27	63	24	90
$\text{Na}_2\text{S}$	0.5–5	2.79	60	66	> 34
$\text{SrBr}_2$	0–6	2.49	61	48	61
$\text{SrCl}_2$	0–6	2.99	62	28	73

with a salt monolith. Incomplete particle packing introduces porosity (typically 30–50%) into the storage bed, reducing the energy density proportionally.<sup>47</sup> Furthermore, the particles themselves may exhibit internal porosity which further reduces the ESD.<sup>131</sup> Regarding the internal storage of water,<sup>47,130</sup> in a closed system the water involved in the hydration reaction is not extracted from the environment and must be stored. As the amount of water to hydrate a salt can be large, the volume of the water storage vessel should be accounted for and can significantly reduce the ESD on the system level.

**Metastability.** Although the thermodynamics of a hydration reaction imply that hydration will occur when and dehydration at  $p/p_{\text{eq}} < 1$ , there can exist a zone around the equilibrium pressure–temperature line where the kinetics of the reaction are slow: this is referred to  $p/p_{\text{eq}} > 1$  as the metastable zone.<sup>57</sup> Some reactions suffer from large metastable zones, while others with narrow metastable zones demonstrate fast kinetics close to equilibrium. Metastable zones have been observed for many salts, including  $\text{LiOH}$ ,<sup>132</sup>  $\text{BaCl}_2$ ,<sup>133</sup>  $\text{K}_2\text{CO}_3$ ,<sup>57,134</sup>  $\text{Na}_2\text{S}$ ,<sup>135</sup>  $\text{MgCl}_2$ ,<sup>136</sup>  $\text{CuCl}_2$ ,<sup>57</sup>  $\text{SrBr}_2$ ,<sup>137</sup> and certain minerals.<sup>138</sup> In Fig. 8 the implications of a metastable zone for discharge are shown with the help of the phase diagram of  $\text{K}_2\text{CO}_3$ .<sup>57</sup> Upon discharge, when water vapor at 12 mbar is supplied the maximum temperature is about 10 °C lower (50 °C) than what is expected in equilibrium (60 °C). Sufficient power is extracted only outside of the metastable zone. Despite numerous reports of metastable behavior,<sup>57,88</sup> this phenomenon is still poorly understood.

The existence of a metastable zone with poor kinetics has been hypothesized to result from two rate-limiting mechanisms: deliquescence-recrystallization and nucleation. Deliquescence-recrystallization has been introduced to explain poor hydration kinetics of certain salts in regions of the phase diagram where the thermodynamics favor hydration. For example, the hydration rates of  $\text{Na}_2\text{SO}_4$  and  $\text{Mg}(\text{ClO}_4)_2$  dramatically increase when the water vapor pressure exceeds the point at which the original (lower hydrate phase) deliquesces.<sup>139,140</sup> The idea is that an  $a \rightarrow b$  hydration process follows two steps: deliquescence of the lower hydrate phase,  $a$ , followed by crystallization of the higher hydrate phase,  $b$ .



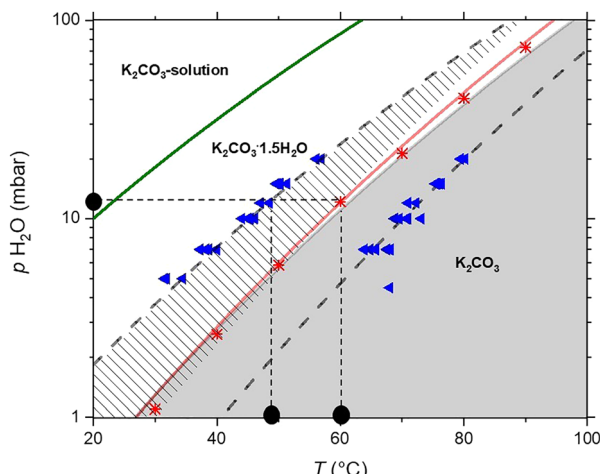


Fig. 8 Phase diagram of  $\text{K}_2\text{CO}_3$  illustrating its metastable zone. The red and green lines refer to the hydration transition and deliquescence line, respectively. The red and blue data points refer to measurements of the hydration–dehydration equilibrium and the metastable zone boundaries. Data adapted from ref. 57.

However, predictions for the deliquescence points of anhydrous  $\text{K}_2\text{CO}_3$  and  $\text{CuCl}_2$  demonstrated that this hydration mechanism could not explain metastability for these two salts.<sup>57</sup> In the same study it was shown that the hydration rate of these salts was slowed down due to sluggish nucleation of the hydrate phase. This explanation was proposed decades ago<sup>141</sup> for the dehydration of salts. When metastability is explained using classical nucleation theory (CNT), the boundaries of the metastable zones are the points where the critical nucleus size becomes on the order of a neutral ion pair and/or the free energy barrier for nucleation is comparable to the thermal energy:<sup>57</sup>  $\Delta G^\# / k_{\text{B}}T \sim 1$ .

As hydration–dehydration processes are solid–solid transitions involving significant modifications to the crystalline lattice, mobile intermediate phases could play a role in controlling the rate of the reaction. Therefore, CNT alone is likely insufficient to explain the origins of metastability. In the case of the hydration transition  $a \rightarrow b$  a natural source for ionic mobility could be the surfaces of the relevant crystalline phases. Studies on  $\text{NaCl}$  have reported the presence of water layers on the crystalline surface far below the deliquescence point of  $\text{NaCl}$  (DRH = 75%).<sup>142,143</sup> Furthermore, in these layers there is significant ionic mobility, implying local dissolution processes.<sup>144,145</sup> Some reports indicate that similar processes might occur on the surfaces of salt hydrates,<sup>146,147</sup> potentially facilitating the hydration process. It may be expected that the ion mobility on the surface of an ionic crystal will strongly increase with the applied water vapor pressure. In recent studies the existence of such a mobile layer has been proven with the help of electrical impedance spectroscopy.<sup>148</sup> Related to this, extreme deliquescent salts have successfully been used to decrease the metastable zone and/or increase the reaction rate.<sup>149–151</sup> These surface processes, in combination with a nucleation barrier, could contribute to the metastable zone.

Hence, the metastable boundary for hydration might not only be determined by the disappearance of a nucleation barrier, but also by the presence of sufficient water molecules at the surface allowing for increased ion mobility.

**Kinetics and power.** The power delivered by a salt hydrate-based storage system relies upon the rate of the underlying hydration–dehydration reaction. In the previous section metastability due to sluggish nucleation and surface effects were introduced as factors influencing these rates. Here, the kinetics of the material outside the metastable zone are discussed. Although many kinetic studies have been published,<sup>29,152,153</sup> the complexity of these reactions has limited the development of mechanistic insight: crystalline lattices must be restructured, water molecules must be incorporated (hydration) or extracted (dehydration) from the lattice, water molecules must migrate through solids, *etc.*

Based on Fig. 6 the hydration reaction can be thought of as consisting of two steps: (a) diffusion of water vapor through the particle's pore space to the reaction zone, and, (b) transformation of the crystal lattice during simultaneous insertion of water. While the first process occurs at length scales comparable to the particle diameter, the second process occurs at nanometer length scales. Below we briefly summarize the current understanding of these processes.

As an example of a solid–gas reaction,<sup>154</sup> the rate of a hydration–dehydration reaction  $X$  can be expressed as:

$$\frac{dX}{dt} = k(T)f(X)h(p/p_{\text{eq}}) \quad (20)$$

Here,  $k(T)$ ,  $f(X)$  and  $h(p/p_{\text{eq}})$  are, respectively: a temperature dependent reaction constant that can be coupled with an energy barrier, a function describing the reaction pathway, and a driving force term related to the water vapor pressure. Examples of studies using this model to fit the hydration kinetics of salts and salt composites are abundant.<sup>137,153,155,156</sup> What most studies overlook is that the equation is an attempt to decouple the reaction pathway  $f(X)$  from the driving force  $h(p/p_{\text{eq}})$  and the intrinsic rate  $k(T)$ . However, in the case of salt hydration, one might expect that the water vapor pressure can influence both the rate and the reaction pathway. For example, (and as discussed above), with increasing water vapor pressure the amount of adsorbed water at the surface of an ionic solid increases<sup>142,143,157</sup> and can enhance surface (reaction) mobility.<sup>158</sup> Transition State Theory<sup>159</sup> gives the best justification for using eqn (20) for local hydration/dehydration processes and the most rigorous derivation of the functional relationship of  $h(p/p_{\text{eq}})$ ,<sup>156</sup> but fails in describing many kinetic aspects of salt hydration.<sup>160</sup> Presently, the model is mainly useful for parameterizing the kinetics of salt hydration on a powder level as input for models to describe the kinetics of porous salt particles.

In larger salt particles, the diffusion of water vapor to the reaction zones can impact the reaction rate. The relative importance of this diffusion process can be estimated with the second Damköhler number,  $\text{Da}_{\text{II}} = (k_{\text{R}}L^2)/D$ , where  $k_{\text{R}}$ ,  $L$ , and  $D$  are the reaction rate, size of the particle, and the diffusion



constant in the particle, respectively. For millimeter size  $K_2CO_3$  particles  $D_{aII} > 1$  and diffusion thus limits the reaction rate and power output of the particle,<sup>131</sup> allowing modelling with the Shrinking Core Model.<sup>161</sup> The following equation holds for the conversion rate in 1D:<sup>131</sup>

$$\frac{dX}{dt} = \frac{M_a D}{(b-a)\rho_a(1-\phi_a)L^2 RT} \left( \frac{1}{X} \right) (p - p_{eq}) \quad (21)$$

In this model  $\rho_a$ ,  $\phi_a$ , and  $M_a$  are the density, porosity, and molar mass of the starting phase. Note that eqn (20) can be mapped onto eqn (21) with the substitution  $h = p - p_{eq}$  and  $f = X^{-1}$ . Eqn (21) demonstrates the key factors for understanding and improving the power of TCES particles. Firstly, the power decreases with the extent of the reaction:  $dX/dt \propto X^{-1}$ . Secondly, the power can be increased by reducing the particle dimensions:  $dX/dt \propto L^{-2}$ . Based on these findings, models for the hydration of particle beds have been developed.<sup>162,163</sup>

**Degradation.** Robustness with respect to degradation of the storage material is also important for the (long-term) performance of a storage device. Three considerations related to degradation are important: first, side reactions during materials manufacturing and use are generally undesirable and should be avoided, as they can compromise energy density and can lead to safety concerns. Second, humid conditions should be avoided during production as deliquescence can hinder the performance of the salt. Third, volume expansion of the salt should not block access of water vapor as this leads to a drop in power output. These three aspects are described in more detail below.

First, in selecting salt hydrates, assessing chemical stability under use conditions is a necessary step. Several examples can be found in the literature that emphasize this point.  $Na_2S$  has been considered as a storage material due to its high energy density.<sup>164,165</sup> Unfortunately, it readily reacts with  $CO_2$  and forms  $Na_2CO_3$  with emission of  $H_2S$ .<sup>136,166</sup> These reactions make  $Na_2S$  particle manufacturing a cumbersome process, restricts its use to pure water vapor conditions, and involves a safety risk due to the toxicity of  $H_2S$ . Similarly,  $MgCl_2$  is still a widely studied material in the field of thermochemical energy storage,<sup>153,167–169</sup> despite the fact it is prone to hydrolysis reactions leading to  $HCl$  formation<sup>170–172</sup> even at relatively low temperatures.<sup>136</sup> Similar hydrolysis reactions are known for other halides like  $CuCl_2$ ,<sup>173,174</sup>  $MgBr_2$ ,<sup>175</sup> and carnallite  $KMgCl_3$ .<sup>176,177</sup> Further, metal ions that are prone to oxidation by air (*e.g.*,  $Fe^{2+}$ ,  $Cr^{2+}$ ,  $Mn^{2+}$ ,  $I^-$ ) should be avoided.<sup>47</sup> Less stable anions (*i.e.*,  $ClO_4^-$ ,  $NO_3^-$ ) should also be treated with care.<sup>46,47</sup>

Second, deliquescence presents a challenge for hygroscopic salt hydrates. A salt or salt hydrate's tendency to deliquesce is characterized by the deliquescence relative humidity (DRH). When the RH of the environment exceeds the material's DRH, the material will deliquesce, *i.e.*, it will spontaneously absorb water from the atmosphere and dissolve within it, forming a liquid solution. Hygroscopic salts/hydrates are characterized by a low DRH. Generally, deliquescence results in reduced cyclability and reaction kinetics due to agglomeration when

liquefied.<sup>178</sup> While this tends to hold true for many salt hydrates, some mixed salt hydrates have demonstrated good cyclability when deliquesced.<sup>179</sup> Furthermore, while hygroscopic salts require more care regarding their stability with respect to deliquescence, these salts also tend to have faster hydration kinetics (below the DRH of the hydrated phase) due to the mobility of the resulting wetting layer.<sup>57</sup>

Third, the volume expansion of the heat storage material is a source of performance degradation in TCES systems. When a salt hydrates and dehydrates, it undergoes considerable volume expansion and contraction.<sup>180</sup> According to the Thermodynamic Difference Rules,<sup>181</sup> the relative volume expansion during hydration from  $a \rightarrow b$  can be approximated as:

$$\frac{\Delta V}{V_0} \approx (b-a) \frac{v_w}{v_a}, \quad (22)$$

where  $\Delta V$  is the volume change,  $V_0$  is the volume of the dehydrated phase,  $v_w$  is the average specific volume of water in a salt hydrate (similar to the specific volume of ice), and  $v_a$  is the specific volume of the dehydrated phase.

Fig. 9 presents the relative volume expansion for selected salt hydration reactions.<sup>47</sup> A trade-off exists with respect to volume expansion. When a salt undergoes a large volume expansion, many water molecules are typically absorbed in the hydrate (eqn (22)). As shown in eqn (18) and (19), a large difference ( $b - a$ ) results in a larger energy storage density. However, a large volume expansion poses greater risk to the mechanical stability of the salt hydrate. Large volume expansion/contraction can create voids and cracks in the material as it is repeatedly hydrated and dehydrated, resulting in mechanical wear on the system. The material in a TCES reactor will expand over cycling, leading to a porosity reduction of the

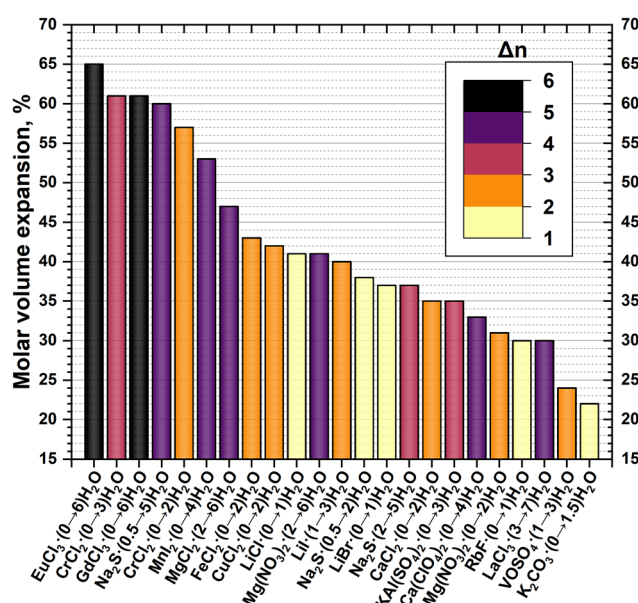


Fig. 9 Relative volume expansion during hydration for representative salt hydrates. The numbers in parentheses indicate the range of hydration states ( $n$  in  $Salt \cdot n H_2O$ ) accessed during the hydration reaction.  $\Delta n$  is the number of water molecules absorbed. Data adapted from ref. 47.



bed.<sup>182</sup> This leads to a reduction of the permeability of the bed, which compromises the working of the TCES reactor.<sup>183</sup> Furthermore, these voids can affect the kinetics of the reaction. Negatively, the voids reduce the contact area with heat exchanging elements, resulting in lower heat transfer. Positively, the voids increase the porosity of the material, increasing local mass transfer on a particle scale.

One of the major challenges with salt hydrates is to make them stable upon cycling. There are several approaches reported in the literature: encapsulation, matrix stabilization and impregnation of porous media. A review of this topic is beyond the scope of this paper and for this we refer to the recent literature.<sup>184</sup> Prolonging the cyclability of salt hydrate particles is of utmost importance to make salt hydrates viable for the application. It is the opinion of the authors that a breakthrough at this point has not been achieved so far.

**Synthetic salts.** In recent years there have been several attempts to synthesize new salt hydrates. Especially the sulphate based Tutton salts seem to be a versatile class of materials as the composition of these materials can be changed, which allows for targeted design of the phase diagram of these salts.<sup>185–187</sup> Sulphate based Tutton salts have a chemical formula  $M_2M'(\text{SO}_4)_2(\text{H}_2\text{O})_6$ , where  $M^+$  and  $M'^{2+}$  are two different cations. Just like with the regular sulphate and phosphate salts, the major challenge with these salts is in the reversibility of the hydration/dehydration reaction.

**Thermal properties.** The power output of a TCES device depends on the rates of mass and heat transfer during the chemical reaction. Thus, high thermal conductivity is desirable within the heat storage medium to allow for rapid heat transfer. Unfortunately, many TCES materials exhibit low thermal conductivities. Thermal conductivities for salt hydrates fall within the range of  $0.3\text{--}1.3\text{ W m}^{-1}\text{ K}^{-1}$ .<sup>188–191</sup> This is much smaller than that of metallic conductors such as Al and Cu, whose values are roughly  $200\text{--}400\text{ W m}^{-1}\text{ K}^{-1}$ . Thermal conductivity tends to increase with the hydrate number,<sup>191</sup> indicating a greater thermal limitation in the dehydrated phase. The use of composite materials, such as a salt hydrate embedded in expanded graphite, has been used to increase the thermal conductivity of the material.<sup>192,193</sup> This approach incurs a trade-off between thermal conductivity and energy storage density, as the energy storage density of the overall material decreases as more of the thermal conductivity enhancing material is used. Thus, TCES system designs must strike a balance between energy storage density and power density.

**Scarcity, cost, and toxicity.** Non-technical aspects such as scarcity, cost, and toxicity can impact the practicality of a TCES material. The importance of these factors can be illustrated with a simple calculation focusing on the built environment in Europe. In 2019 the population of the EU was about 513 million<sup>194</sup> people living in approximately 223 million households.<sup>195</sup> Let us assume that each of these households owns a 2 GJ thermal storage unit, and that the typical energy density at the materials level is  $u_c = 1\text{ GJ m}^{-3}$ , with a materials density of  $1000\text{ kg m}^{-3}$ . For this scenario approximately 400 million metric tons of storage material is required. Although

this is a simple estimate, it demonstrates that significant demand for TCES materials may be expected. This increase in demand mimics the dramatic increase in the supply of raw materials required for widespread adoption of more mature energy technologies (PV, wind turbines, and batteries).<sup>196</sup>

Although the price of a given salt on the bulk market serves as one indicator of scarcity,<sup>47</sup> this approach is not predictive of future demand and associated costs.<sup>196</sup> An analysis that accounts for known resources, mining capacities, and production capacities for synthetic salts would be more useful in assessing scarcity. Although elements such as K, Na, and Ca are abundant, limiting factors for using salts containing these elements are the mining capacities for specific minerals or the production capacities in the case of synthetic salts (*i.e.*  $\text{K}_2\text{CO}_3$  and  $\text{Na}_2\text{S}$ ). Furthermore, many salts under investigation contain minerals that should be treated with care in view of resources and mining production. Fig. 10 illustrates resource and mining data from the U.S. Geological Survey for elements frequently considered in studies of TCES materials.<sup>197</sup> These materials quantities are compared to the 400 million ton estimate for widespread use of thermal energy storage in Europe.

First, let us consider the data presented in Fig. 10 for lithium. Although lithium salts are promising for thermochemical energy storage,<sup>198</sup> lithium already plays a key role in the electrification of energy systems due to its use in Li-ion batteries. While the abundance of lithium is high (estimated mining resources in 2020 were 86 million tons<sup>197</sup>), its use as a key ingredient for both electrical and thermal energy storage devices presents challenges. Considering the production capabilities of Li, Fig. 10 shows that in 2020 the global annual mining production was about 82 000 tons.<sup>197</sup> This is orders of magnitude lower than is expected to be needed for global implementation of Li-based thermal energy storage systems. In view of the growing demand for Li-ion batteries (which is expected to cause a 40-fold increase in Li supply by 2040<sup>199</sup>) and the emerging strain this has induced on the global market, it is fair to ask whether TCES should also employ Li-based media.

Salts based on rare earth metals should also be treated with care. In light of the available resources and the present mining production volumes, Fig. 10, the use of lanthanum (*i.e.*  $\text{LaCl}_3$ <sup>39</sup> and  $\text{La}_2(\text{SO}_4)_3$ ,<sup>200</sup> yttrium (*i.e.*  $\text{Y}_2(\text{SO}_4)_3$ )<sup>201</sup> and vanadium containing salts are of questionable long-term viability. Similar reasoning can be applied to sulphate salts based on elements such as Sc, Yb, Y, Dy, Ga and In.<sup>201</sup> On the other hand, strontium-containing salts deserve attention in view of their substantial annual mining production.  $\text{SrBr}_2$  and  $\text{SrCl}_2$  are considered promising as they have suitable thermodynamic properties.<sup>39,137,202</sup> However, mining and production capacities will need to be increased for these salts to become practical ingredients in future heat storage systems.

As discussed above, costs can be high to source materials that are not in wide use. One may expect these higher costs to apply to materials needed for new technologies such as the TCES materials discussed here. Nevertheless, rapid cost reductions have been demonstrated in related technologies by



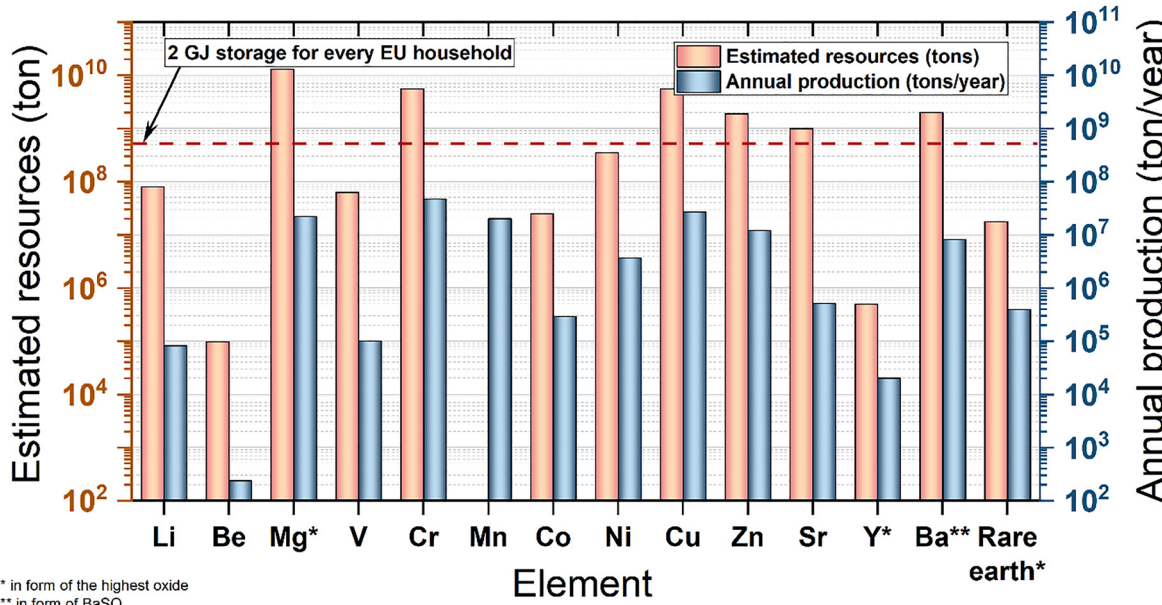


Fig. 10 Estimated resources (left axis) and global annual mining production (right axis) in 2023–2024 for elements that frequently appear in studies of thermochemical energy storage. The dashed red lines mark the 400 million tons of material needed for a use scenario in which all EU-households operate a 2 GJ thermal storage unit. Data is from the U.S. Geological Survey.<sup>197</sup>

exploiting economies of scale. For example, the cost of Li-ion batteries has decreased by approximately 97% over the past three decades.<sup>60</sup> We anticipate that similar cost reductions can be achieved for the materials relevant for TCES.

Toxicity is another important factor for salt hydrates.<sup>39,47,203</sup> A screening study of 125 salts focusing on safety issues highlighted that 80 salts exhibit challenges due to toxicity.<sup>39</sup> For similar reasons, an assessment of medium-temperature heat storage applications urged caution in the use of compounds containing ions like  $\text{Cr}^{6+}$ ,  $\text{Co}^{2+/3+}$  and  $\text{Ni}^{2+/4+}$ .<sup>203</sup> An assessment of 563 hydration reactions (later extended to 1073 reactions<sup>48</sup>) for the built environment (hot tap water and space heating) generated a list of 25 candidates with suitable thermodynamic properties (energy density and discharge temperatures). In this case salts such as  $\text{GdCl}_3$ ,  $\text{NiCl}_2$ ,  $\text{Na}_2\text{S}$ ,  $\text{MnI}_2$ ,  $\text{VOSO}_4$  and  $\text{CuCl}_2$  were excluded due to toxicity considerations.<sup>47</sup> Hence, substances such as  $\text{CrF}_3$  and  $\text{CuBr}_2$ , identified as promising based on their hydration enthalpies,<sup>87</sup> warrant additional care in their manufacture and use due to toxicity considerations.

The above considerations suggest two conclusions: first, investments in mining and production capabilities are needed to facilitate global adoption of salt hydrate heat batteries. Secondly, more detailed knowledge of the non-technical features of these materials will be helpful to material scientists in the selection of appropriate materials.

**Computational discovery of salt hydrates.** Computational modelling has also been employed to investigate materials for TCES. In a trio of studies,<sup>87,204,205</sup> Kiyabu *et al.* used Density Functional Theory calculations to predict the energy densities and turning temperatures of salt hydrates and hydroxides. In the first study,<sup>87</sup> 265 hydration reactions were examined for all the halide hydrates and hydroxides present within the

Inorganic Crystal Structure Database (ICSD). Promising reactions having high gravimetric and volumetric energy densities were identified and categorized according to their operating temperatures. Of these,  $\text{CrF}_3 \cdot 9\text{H}_2\text{O}$  was highlighted as a promising under-explored material for moderate-temperature TCES applications ( $T \sim 200$  °C). Using this database of calculated properties, property-performance relationships were examined across the hydrates and hydroxides using a Pearson correlation matrix. In the hydroxides these analyses identified the ionicity of the cation-hydroxide bond as a good predictor of the enthalpy of reaction. However, similar (linear) correlations did not emerge in the hydrates, suggesting that more flexible models were needed to predict the thermodynamics in this class of materials.

Kiyabu *et al.* subsequently expanded their screening of TCES materials to include a larger collection of hypothetical salt hydrates, including 5292 metal halides<sup>204</sup> and 7012 salts containing chalcogenides and complex anions.<sup>205</sup> From these datasets, the hydrates of several salts, including  $\text{CaF}_2$ ,  $\text{VF}_2$ ,  $\text{CoF}_3$ ,  $\text{Li}_2\text{S}$ ,  $\text{Ca}(\text{OH})_2$ , and  $\text{Li}_2\text{CO}_3$  were identified as potentially new TCES materials with class-leading energy densities and operating temperatures suitable for use in domestic heating and intermediate-temperature applications. Fig. 11 illustrates energy densities for the subset of the screened metal halides that were predicted to be stable with respect to competing phases at all stages of their respective hydration/dehydration reactions. The performance of these materials was projected to the system level by parameterizing an operating model<sup>90,165,206</sup> of a solar thermal TES system with data from the new hydrates. Finally, machine learning models were developed to predict salt hydrate thermodynamics and identify design guidelines for maximizing energy density. These models demonstrate that

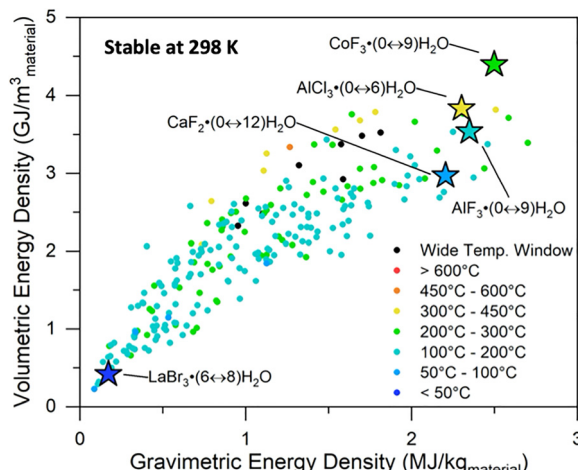


**Fig. 11** Volumetric energy density, gravimetric energy density, and temperature category for 238 TCES reactions involving new hypothetical salt hydrates. Promising reactions in distinct temperature categories are shown as stars. All of these hydrates, as well as all intermediate phases present during (de)hydration, are predicted to sit on the convex hull, and thus to be stable with respect to the formation of other phases at 298 K. Adapted from ref. 204 with permission from the American Chemical Society, copyright 2022.

salts composed of cations that exhibit small electronegativities and molar masses (e.g.,  $\text{Na}^+$  and  $\text{K}^+$ ) yield increased energy densities *via* increased  $\Delta H$  of hydration. For complex anion hydrates, the identity of the anion was also found to be a significant predictor of  $\Delta H$ : a greater elemental fraction of nonmetals was found to correlate with a greater  $\Delta H$ .

### C. Class II: porous media/sorption

Porous solid adsorbents constitute a well-established class of thermal energy storage materials that have been considered for use in heat pumps and chillers. Prominent examples of this

class include activated carbon, silica gel, zeolites, activated alumina oxide, covalent organic frameworks (COFs), and metal organic frameworks (MOFs). These materials store heat by exploiting the heat of adsorption of the working fluid vapor. Recent developments have demonstrated remarkable performance improvements, with advanced COF materials achieving thermal conductivities exceeding  $15 \text{ W m}^{-1} \text{ K}^{-1}$ <sup>207</sup> while novel MOF-salt composites have reached ammonia storage capacities of  $48.3 \text{ mmol g}^{-1}$ .<sup>208</sup> The working fluid can be condensed during the storage/release cycle (e.g. water, ethanol, methanol, ammonia); alternatively, non-condensable gases are used, the most common of which are  $\text{CO}_2$  and  $\text{H}_2$ .

A combination of material-level (*i.e.*, chemical composition, textural/crystallographic, thermodynamic, and kinetic) and system-level (*i.e.*, packing density, vapor transport, thermal conductivity, *etc.*) properties determine the performance of an adsorption-based TCES system (Fig. 12). In general, textural and crystallographic properties such as specific surface area, pore volume, pore size and distribution, and single crystal density determine the amount of working fluid adsorbed by the porous host at a certain sorption potential (Fig. 4). Hence, the structure of the adsorbent strongly influences the capacity for heat storage. On the other hand, the operating temperature window is partly determined by the enthalpy of adsorption and its dependency on sorption uptake, which itself is strongly influenced by the composition of the adsorbent/adsorbate pair through the nature of the bonds formed between host and guest atoms.

**Criteria for selecting adsorbents.** The selection of porous adsorbents for TCES is guided by the operating conditions of the intended application. As described below, the application places constraints upon the adsorbent's operating temperature range, storage capacity, and its kinetics.

**Adsorbent-adsorbate working pair.** The selection of the working fluid is a critical design factor of an adsorbent-based TCES system. The selection criteria for a suitable working fluid

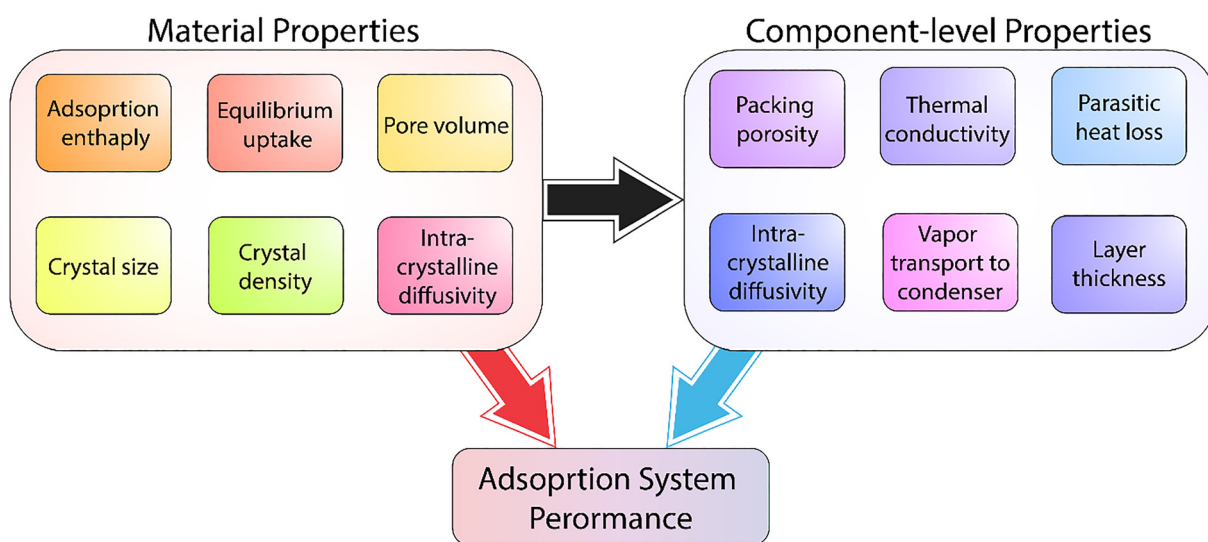


**Fig. 12** Performance and efficiency of porous materials-based TCES systems depends on both material-level and system-level property optimizations. Reproduced from ref. 229 with permission from the American Chemical Society, copyright 2019.



include: a high enthalpy of evaporation, condensability under operating conditions, moderate vapor pressure, and being pollution free, non-toxic, and non-corrosive to the system components.<sup>209</sup> Water is a popular choice of working fluid due to its abundance, low cost, and non-toxic nature. Water is currently used commercially with zeolites and silica gel adsorbents.<sup>209,210</sup> However, water is not suitable for subzero temperature applications due to ice formation and freezing issues. Ethanol and methanol have been adopted as alternatives in MOF-based systems to overcome this limitation. Recent simulations and experiments demonstrated high working capacities and COPs in ethanol/MAF-6 systems.<sup>211</sup> Advanced composite working pairs have emerged that significantly outperform traditional systems. For instance, vermiculite/LiCl systems demonstrate superior thermal performance with COPs of 0.75 for cooling and 1.51 for heating, alongside specific cooling performance of 5760.7 kJ kg<sup>-1</sup>.<sup>212</sup> Zeolite-based composites, 13X/MgSO<sub>4</sub>-LiCl, have also shown substantial improvements, exhibiting higher energy density than pure zeolite 13X and achieving heat storage capacities of 458.3 kJ kg<sup>-1</sup>.<sup>213</sup> Hydrogen<sup>214</sup> and classical freons<sup>215</sup> are also used as working fluids in specific systems.

The selection criteria for adsorbents are governed by thermodynamic boundary temperatures and equilibrium vapor pressures for adsorption and desorption.

**Adsorption isotherms.** The adsorption isotherm quantifies the capacity of a given adsorbent to uptake a working fluid as a function of pressure at a constant temperature, Fig. 13. So-called “S-shaped” or stepwise isotherms are desirable for achieving high working capacity and second-law efficiency.<sup>70</sup> The International Union of Pure and Applied Chemistry (IUPAC) classifies this family of isotherms as Type V.<sup>216</sup> The stepwise adsorption typical of a Type V isotherm facilitates the storage of a large quantity of energy within a relatively small change in pressure.<sup>209,217,218</sup> Recent experiments comparing water adsorption isotherms across Zeolite-Y, activated carbon,

silica gel, and AQSOA™ variants confirm the significance of isotherm steepness and step pressure. For example, AQSOA-Z01 and -Z02 demonstrate sharper S-shaped isotherms at  $P/P_0 \approx 0.15-0.35$ , enabling better utilization of low-temperature driving heat.<sup>219</sup> New MOFs such as KMF-1 and KMF-2 are engineered to produce Type V water isotherms centered at relative pressures  $\sim 0.13-0.2$ , with corresponding volumetric energy densities up to 330 kWh m<sup>-3</sup>.<sup>220</sup> Recent data show MOFs like MIL-125(Ti)-NH<sub>2</sub> exhibit Type V isotherms with high water uptake at relative pressures of 0.1–0.4, ideal for cooling and heating applications.<sup>221</sup> For water-based TCES systems, the hydrophilicity or hydrophobicity of the adsorbent governs the shape of the adsorption isotherm: hydrophobic adsorbents often exhibit Type V isotherms. In addition, the volumetric capacity (*i.e.*, the mass of working fluid adsorbed per unit volume of adsorbent), is related to the crystal density and influences the size of the TCES system.

**Heat of adsorption.** The isosteric heat of adsorption (IHA) is a measure of the strength of interaction between molecules of the working fluid and the adsorbent at a fixed adsorption uptake.<sup>222,223</sup> In computational studies, this quantity is commonly referred to as the differential enthalpy of adsorption, and is typically derived from Monte Carlo simulations. This interaction determines the hydrophilicity or hydrophobicity of the adsorbent and the regeneration temperature. Recent work suggests that the ideal IHA range for water adsorbents lies between 45–60 kJ mol<sup>-1</sup>, balancing high working capacity with low-temperature desorption.<sup>224</sup> For example, KMF-2 achieves an IHA of 40.7 kJ mol<sup>-1</sup> and can be regenerated at 70 °C, enabling integration with solar or waste heat sources. A more exothermic IHA leads to a greater amount of energy stored per adsorbate molecule and to a higher regeneration temperature. In addition to the composition of the working fluid and adsorbent, the IHA depends on the size, shape, and polarity of the adsorbate molecules, and on the amount of the working fluid adsorbed (*i.e.*, uptake). IHAs are known to be more exothermic for the adsorption of polar working fluids (*e.g.*, water, ethanol, ammonia) at coordinatively unsaturated metal sites in MOFs. For example, MIL-100(Fe) and MIL-125-NH<sub>2</sub> achieve IHAs supporting energy densities of  $\sim 875$  MJ m<sup>-3</sup> and  $\sim 1100$  MJ m<sup>-3</sup>, respectively,<sup>221</sup> making them promising candidates for compact thermal storage systems. Thus, the IHA defines the first-law efficiency and the COP. The optimal IHA depends on the application and operating conditions of the TCES system. It should also be noted that, due to the divariance of the adsorption equilibrium, the IHA is often presented as a function of the adsorption uptake.

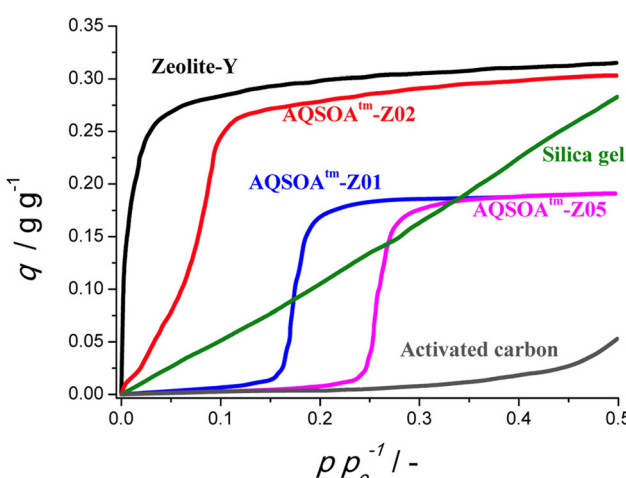


Fig. 13 Adsorption isotherms for water in common commercially available adsorbents. Reproduced from ref. 209 with permission from the American Chemical Society, copyright 2015.

**Regeneration temperature.** The temperature at which the adsorbed working fluid molecules are desorbed from the porous host determines the second-law efficiency and cyclability of a TCES system. Ideally, a low (<100 °C) regeneration temperature is preferable for domestic, solar, and industrial waste heat-based TCES systems.<sup>225</sup>



**Heat and mass transport.** The performance of an adsorbent-based TCES system also depends on the rates at which heat and mass can be transported through the sorbent bed. These properties depend upon *intra*-crystalline and *inter*-crystalline diffusivities (Fig. 12).<sup>85,209,226</sup> Fick's law<sup>85,227</sup> is often used to estimate intracrystalline diffusion – *i.e.*, vapor diffusion within single crystals of porous materials – of the working fluid vapor, which in turn allows for modelling of sorption kinetics within porous media using the linear driving force model.<sup>85,226,228</sup> Due to their crystallinity (and thus lower tortuosity), MOFs are anticipated to exhibit advantages in mass transport compared to non-crystalline hosts such as activated carbons and zeolites. In contrast, intercrystalline diffusion – *i.e.*, vapor diffusion through the interstitial regions between crystallites or particles of the adsorbent – depends on the size, shape, and packing densities of the adsorbent crystals/particles.<sup>229,230</sup>

One transport-related challenge associated with the use of porous TCES materials such as MOFs is their low thermal conductivity.<sup>231–233</sup> Hence improving the rate of heat transport through the storage bed may require the addition of thermally conductive additives,<sup>234–236</sup> which can degrade the effective energy density and possibly slow down the mass transport. However, recent progress in materials design has demonstrated progress in overcoming this limitation. For example, three-dimensional COFs have demonstrated thermal conductivities exceeding  $15 \text{ W m}^{-1} \text{ K}^{-1}$ , which is the unique performance for 3D polymers.<sup>237</sup> These improvements stem from the optimized structural parameters, particularly small pore sizes around 0.63 nm, four-connected nodes, and material densities above  $1.0 \text{ g cm}^{-3}$ .<sup>238</sup> In addition, interpenetrated COFs enhance performance through phonon hardening mechanisms, achieving

up to 6-fold thermal conductivity improvements.<sup>207</sup> Achieving optimal performance in an adsorption-based TCES system thus depends on both materials-level and system-level design considerations.

**Discovery of promising adsorbents.** In 2017, Boman *et al.*<sup>239</sup> assessed 110 and 81 adsorbent/adsorbate working pairs for cooling and heating applications, respectively. They identified several MOF-ethanol pairs that outperformed other pairs for heating applications, and additional activated carbon-ethanol pairs suitable for cooling applications (Fig. 14).<sup>239</sup> MOF-water-alcohol pairs were identified as strong candidates for both cooling and heating applications (Fig. 14).<sup>239,240</sup> In 2021, Liu *et al.*<sup>241</sup> reported a screening study of 231 experimentally measured water adsorption isotherms for 6 different classes of porous adsorbents. These included MOFs, carbons, zeolites, silicic materials, composites, and other adsorbents. Isotherm data were collected from the NIST/ARPA-E Database of Novel and Emerging Adsorbent Materials.<sup>242</sup> The 231 systems were assessed according to two metrics: the coefficient of performance for cooling/heating ( $\text{COP}_C/\text{COP}_H$ ) and the specific cooling/heating effects (SCE/SHE). Fig. 15 shows the distribution of different classes of porous materials according to their  $\text{COP}_C/\text{SCE}$  (Fig. 15a) and  $\text{COP}_H/\text{SHE}$  (Fig. 15b). Liu *et al.*<sup>241</sup> found that MOFs and zeolites outperform other porous adsorbents based on the  $\text{COP}_C/\text{COP}_H$  and SCE/SHE metrics. The best adsorbents were found to exhibit Type V isotherms with step positions at relative pressures of 0.1–0.4 and 0–0.2 for cooling and heating applications, respectively.

Computational screening for porous materials for water adsorption remains an area ripe for development. The absence of validated interatomic potentials for adsorbent-water

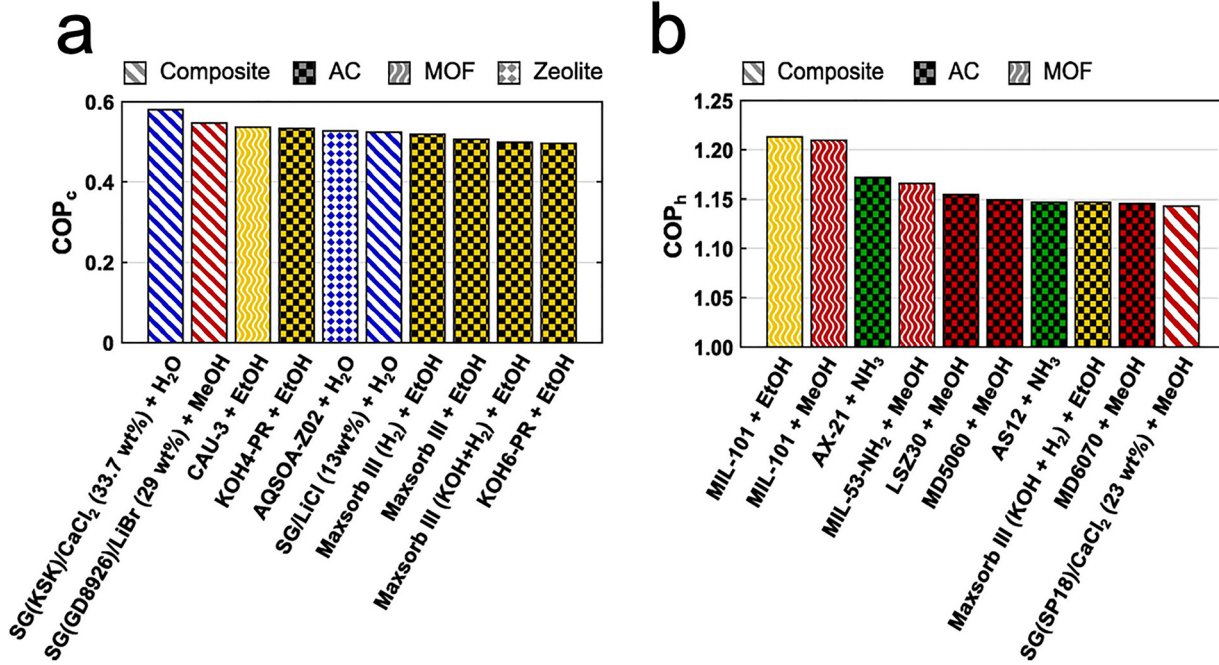


Fig. 14 Top 10 adsorbent–adsorbate working pairs for (a) cooling and (b) heating applications identified based on screening. Reproduced from ref. 239 with permission from Elsevier, copyright 2017.



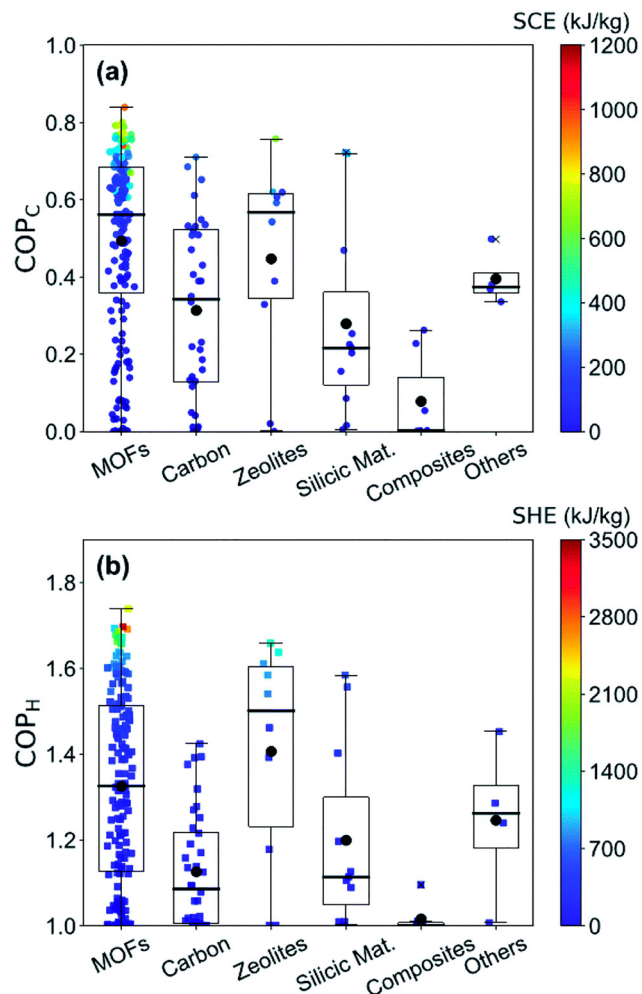


Fig. 15 Coefficients of performance (COP) for cooling (a) and heating (b) for different classes of adsorbent materials. Specific cooling/heating effects (SCE/SHE) indicate the amount of useful energy for cooling/heating, corresponding to  $Q_{\text{useful}}$  in eqn (2).  $\text{COP}_C$  and SCE were obtained at  $T_{\text{evap}} = 283 \text{ K}$ ,  $T_{\text{con}} = T_{\text{ads}} = 303 \text{ K}$ ,  $T_{\text{des}} = 368 \text{ K}$ , and  $\text{COP}_H$  and SHE were obtained at  $T_{\text{ev}} = 288 \text{ K}$ ,  $T_{\text{con}} = T_{\text{ads}} = 318 \text{ K}$ ,  $T_{\text{des}} = 413 \text{ K}$ . Reproduced from ref. 241 with permission from the Royal Society of Chemistry, copyright 2021.

interactions<sup>243</sup> and a lack of consensus regarding atomic charges for adsorbent atoms<sup>244,245</sup> have both contributed to the limited application of simulation in accelerating materials discovery. Nevertheless, significant computational advances have emerged through large-scale screening studies. High-throughput molecular dynamics investigations have evaluated over 10 000 hypothetical MOFs for thermal conductivity,

revealing that optimal performance requires material densities above  $1.0 \text{ g cm}^{-3}$ , pore sizes below  $10 \text{ \AA}$ , and four-connected metal nodes.<sup>246</sup> These computational capabilities are supported by expanded databases, with the CoRE MOF Database containing over 40 000 experimentally reported structures,<sup>247</sup> a nearly three-fold increase from the previous version, which contained  $\sim 14\,000$  structures.<sup>248</sup>

Moreover, grand canonical Monte Carlo (GCMC) simulations of water adsorption in hydrophobic adsorbents are computationally challenging due to the long simulation times required to successfully sample the configuration space.<sup>249</sup> The use of flat histogram sampling methods have been proposed as a potential route towards reducing simulation time.<sup>250</sup> Furthermore, the hydrophilic/hydrophobic nature of porous materials reported in various databases is either unreported or unknown. To overcome this, Monte Carlo calculations of Henry's law constants (HLC) for water adsorption in MOFs have been proposed to distinguish between hydrophilic and hydrophobic MOFs.<sup>251,252</sup> HLC calculations are several orders of magnitude faster than those needed to predict the adsorption isotherm.<sup>251,252</sup> Despite these challenges, GCMC has been applied in a few high-throughput computational screening studies of MOFs for water adsorption, particularly in tandem with machine learning approaches for accelerating predictions.<sup>239,253–255</sup>

Computational screening for porous adsorbents using alcohol as the working fluid is less challenging than for water, as intermolecular interactions involving alcohols are simpler and therefore more accurately described by interatomic potentials.<sup>256</sup> Nevertheless, only a few studies on these systems have been reported.<sup>257–259</sup> Li *et al.*<sup>258</sup> predicted the  $\text{COP}_C$  for 1527 MOFs compiled from the CoRE 2014 database<sup>260</sup> for ethanol adsorption. Guidelines were provided for selecting optimal MOF-alcohol pairs based on crystallographic (pore size and specific surface area) and thermodynamic properties (HLCs and heat of adsorption).<sup>258</sup> Shi *et al.*<sup>259</sup> evaluated methanol adsorption capacities of 6013 MOFs from the CoRE 2019 database<sup>261</sup> and 137 953 hypothetical MOFs from the Northwestern database<sup>262</sup> for heating/cooling TCES systems, including heat pumps, ice making, and refrigeration applications. They identified optimal ranges for COP working capacity, volumetric surface area (VSA), isosteric heat of adsorption (IHA), largest cavity diameter (LCD), single crystal density ( $\rho$ ), and void fraction ( $\phi$ ) (Table 6). 275 COFs from the CoRE-COF 2.0 database<sup>263</sup> were evaluated using GCMC simulations by Li *et al.*<sup>264</sup> Ethanol was adopted as the working fluid and assessments were performed with respect to  $\text{COP}_C$  and  $\text{COP}_H$ . They

Table 6 Ranges of properties for MOFs from the CoRE 2019 database, *i.e.* volumetric surface area (VSA), isosteric heat of adsorption (IHA) largest cavity diameter (LCD), density, and void fraction, with a coefficient of performance (COP) and working capacity greater than the specified targets for each application. Adapted from ref. 259 with permission from the Royal Society of Chemistry, copyright 2021

Application	COP	Working capacity ( $\text{mg g}^{-1}$ )	VSA ( $\text{m}^2 \text{ cm}^{-3}$ )	IHA ( $\text{kJ mol}^{-1}$ )	LCD ( $\text{\AA}$ )	Density ( $\text{kg m}^{-3}$ )	Void fraction
Heat pump	$> 1.75$	$> 350$	1550–3000	35–50	7.1–21.7	435–880	0.67–0.89
Ice making	$> 0.70$	$> 170$	1585–2947	34–54	7.1–21.7	434–1582	0.65–0.89
Refrigeration	$> 0.80$	$> 400$	1600–3000	34–52	7.4–20.0	484–1165	0.68–0.89



found that COFs are more suitable for cooling applications compared to MOFs because COFs have weaker interactions with methanol at low temperatures. Liang *et al.*<sup>265</sup> calculated the adsorption and transport properties of 1072 MOFs from the CoRE MOF Database to evaluate their COP<sub>C</sub> and SCP. The best-performing MOF exhibited a SCP of 1359 W kg<sup>-1</sup> and a COP<sub>C</sub> of 0.64.

**Design of adsorbents for TCES.** Among the various categories adsorbents of interest for TCES systems, MOFs stand out due to their highly tunable properties. This tunability presents opportunities for tailoring the design of MOFs to optimize performance. For example, based on computational and experimental input, Cho *et al.*<sup>266</sup> designed the MOF KMF-1, and demonstrated its promising heat storage capacity. The design involved tuning of pore channels and hydrophilicity by selecting and functionalizing the 2,5-pyrroledicarboxylate (PyDC) linker. These design choices were informed by analyzing the structure and performance of two well-known MOFs:<sup>267</sup> CAU-10 and MIL-160. Similarly, Rieth *et al.*<sup>268</sup> designed two isoreticular triazolate MOFs with record-setting values for COP (1.63). They demonstrated how to control the relative humidity at which water uptake occurs by modulating the pore size. Finally, Rieth *et al.*<sup>269</sup> demonstrated an increase in the reversible water uptake of two MOFs [Ni<sub>2</sub>Cl<sub>2</sub>BTDD & Ni<sub>2</sub>Br<sub>2</sub>BTDD, where BTDD = bis(1,2,3-triazolo-[4,5-*b*],[4',5'-*i*])dibenzo-[1,4]-dioxin] by systematic anion exchange. Recent work has also demonstrated the use of mixed-linker MOFs for TCES, enabling tuning of hydrophilicity and volumetric energy density. A notable example is KMF-2, a mixed-linker Al-MOF incorporating isophthalate and pyridinedicarboxylate linkers, which exhibits a COP for cooling of 0.75 with a volumetric heat capacity of ~330 kWh m<sup>-3</sup> at regeneration temperatures <70 °C.<sup>220</sup>

**Techno-economic analysis of adsorbents.** Shi *et al.*<sup>259</sup> conducted a techno-economic analysis of real and hypothetical MOFs for use in adsorption heat pumps/chillers with methanol as the working fluid. Their analysis considered the equipment cost, cycle cost, and materials cost. The materials cost was identified as the most significant. They identified 12 MOFs with a low system-level cost of ~1 USD per kJ in heat-pump/chiller applications. Shi *et al.* validated their analysis by synthesizing a variant of Cu<sub>3</sub>BTC<sub>2</sub>,<sup>270</sup> measuring its methanol capacity and estimating costs. Emerging techno-economic analyses for porous adsorbents now consider life-cycle emissions, regeneration energy requirements, and material scalability. While most existing models focus on general adsorbents, similar scoring frameworks are being adapted to MOFs and COFs for solar-driven TCES applications.<sup>271</sup>

**Characterization and system integration of porous adsorbents.** Water adsorption/desorption characterization at multiple temperatures enables the optimization of working capacity and COP for heat pump applications, with experimental studies demonstrating that MOFs like MIL-100(Fe) achieve COP values of 0.80 and specific cooling of 569.42 kJ kg<sup>-1</sup>.<sup>272</sup> Thermal cycling stability measurements reveal that zeolite-based

composites maintain performance over hundreds of cycles, with zeolite 13X/MgCl<sub>2</sub> systems showing heat storage capacities of 686.86 kJ kg<sup>-1</sup>.<sup>273</sup> System integration approaches address thermal transport limitations of porous materials through composite design. For example, zeolite-graphene nanoplatelet composites demonstrate thermal conductivity improvements up to 127 times over pure zeolite while maintaining 43% improvement in volumetric water uptake.<sup>274</sup> These approaches leverage the high energy density of porous adsorbents while incorporating enhanced heat transfer capabilities needed for practical applications.<sup>275</sup>

**Commercial deployment and market outlook for porous adsorbents.** Zeolite–water systems have achieved commercial deployment in residential applications, with demonstrated energy densities of 150–200 kWh m<sup>-3</sup> and capabilities for seasonal heat storage with limited heat loss.<sup>276</sup> Pilot-scale demonstrations include household-scale systems with 250 L zeolite-based system achieving storage capacities of 52 kWh and maximum delivered power of 4.4 kW.<sup>277</sup> MOF-based systems continue to be researched, with MOF-ammonia working pairs showing promise due to their performance under extreme climates compared to conventional sorbent-ammonia pairs.<sup>278</sup> Improvements for industrial heat pumps have been demonstrated in MOF–water systems like aluminum fumarate, which can operate at desorption temperatures as low as 65 °C.<sup>279</sup>

#### D. Class III: sorption in liquids

Liquid sorptive TCES operates by reversibly concentrating and diluting a solute (*e.g.* LiBr) by exchanging the solvent (*e.g.*, H<sub>2</sub>O) between vapor and liquid phases.<sup>280–283</sup> Spontaneous absorption of the vapor into the liquid solution releases heat, while solute desorption/vaporization is the mechanism by which heat is stored. The solute–solvent and solvent–solvent binding interactions are primarily van der Waals in nature; they can be supplemented by hydrogen bonding for solvents such as water, alcohols, and ammonia. In the solution, the chemical potential of the solvent is reduced due to interactions with the solute. According to the Gibbs–Duhem equations, the chemical potential  $\mu$  of the solvent (*e.g.* water) decreases as the concentration of the solute increases. Thus, the vapor pressure over water solutions is lower than that for pure water:<sup>284</sup>

$$\mu(T) = \mu^0(T) + RT \ln a = \mu^0(T) + RT \ln \frac{P}{P^0} \quad (23)$$

$$\mu(T) = \mu^0(T) + RT \ln \frac{RH}{100\%} \quad (24)$$

where standard state refers to pure water,  $a$  is water activity ( $a = 1$  for pure solvent),  $P^0$  is saturated vapor pressure at temperature  $T$ , and  $RH$  is the relative humidity at temperature  $T$  for the case of water. The activity of salts in water solutions may be estimated from Debye–Hückel theory at low ionic strength of solution on the order of 10<sup>-3</sup> M. For higher concentrations, including brines, semi-empirical models such as the Pitzer–Simonson–Clegg model can succeed in predicting the activity of water.<sup>282</sup> However, the availability of parameters



for such models remain limited mainly due to their experimental origin, which makes the targeted design of solutions for absorptive applications challenging.

While there is no general theory for calculating activities for very high concentration solutions used for sorptive applications, qualitative considerations for ionic salts suggest that a higher dissolution enthalpy and a lower activity for water is observed for the case of hard ions (more polarizing, smaller radii) that form crystallohydrates with low lattice energy. The activity of water in saturated solutions corresponds to the deliquescence relative humidity and can be found in the literature.<sup>127</sup>

A typical P-T phase diagram for salt-H<sub>2</sub>O systems (Fig. 16) consists of the solution region, the region corresponding to the highest hydrate Salt-nH<sub>2</sub>O, and the area of the lower hydrates and/or the anhydrous salt. Accordingly, there are three types of sorptive cycles with various technical implementations, namely, cycles with only absorption/desorption within a (liquid) solution (cycle identified with green lines in Fig. 16), cycles involving crystallization of the highest hydrate (blue cycle) and cycles involving decomposition of the highest hydrate into lower hydrates and/or the anhydrous salt (red). Below, the energy storage densities and temperature lifts for the most popular working pairs for all three cycle types are described.

**Absorption and crystallization cycles.** Absorptive heat storage or cooling cycles typically consist of two isobars corresponding to sorption/desorption and two isosteres corresponding to strong (concentrated) and weak (diluted) solutions. The energy storage density ESD<sub>ab</sub> on the materials level can be calculated from the enthalpy difference between strong and weak solutions, or from the specific absorption enthalpy:

$$ESD_{ab} = \frac{1}{V_M} \int_{c_s}^{c_w} \overline{\Delta_{ab} H(c)} dc \quad (25)$$

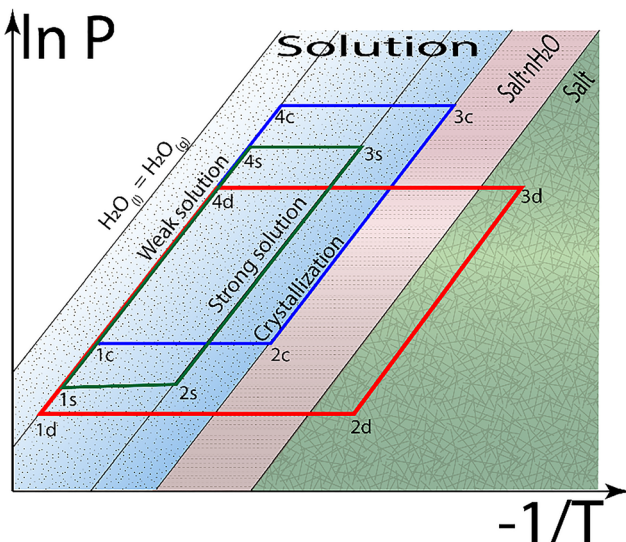


Fig. 16 Generic phase diagram for a water-salt system in van 't Hoff coordinates illustrating three types of absorptive heat storage cycles: (green) sorption in a liquid phase, 1s-2s-3s-4s; (blue) three-phase storage, 1c-2c-3c-4c; (red) storage with full decomposition, 1d-2d-3d-4d.

where  $c_s$  and  $c_w$  are concentrations of the strong and weak solution, and  $V_M$  is the molar volume of weak solution.

Due to low temperatures and concentration span, systems based on liquid sorption have relatively low temperature lift. For domestic heating, the most popular solutes are NaOH, KOH, CaCl<sub>2</sub>, LiBr, HCOOK, glycerol and ammonia.<sup>60,62</sup> For cooling applications, non-water solvents are preferred, and the list is supplemented by alcohol-based pairs such as LiBr-CH<sub>3</sub>OH and LiBr-C<sub>2</sub>H<sub>5</sub>OH.<sup>285,286</sup> Ionic liquids represent a novel alternative for which crystallization is not reached.<sup>287,288</sup>

A trade-off between energy storage density and temperature lift exists for absorptive cycles: higher energy storage densities are achieved at the expense of lower temperature lift, and *vice versa*. This approach to absorptive storage allows for low charging temperatures (< 80 °C); the largest energy storage densities for heat storage in buildings may reach 1 GJ m<sup>-3</sup> (Table 7), however the temperature lift is modest, 10–15 °C. The temperature lift can be boosted by increasing the charging temperature to access the crystalline hydrate, thus allowing access to the crystallization energy ESD<sub>cr</sub>. One drawback of this approach is that the complexity of the system design must increase to account for these 'three-phase cycles' that permit melting and solidification/crystallization of the storage medium. Three-phase thermal energy storage systems have been commercialized by ClimateWell.

**Decomposition cycles.** A further increase of energy storage density (compared to a three-phase cycle with crystallization) can be achieved by increasing the charging temperature to dehydrate the crystalline salt (red cycle in Fig. 16). In this case the energy storage density is given by:

$$ESD_d = ESD_{cr} + ESD_{ab} + \frac{1}{V_M} \Delta_{dec} H^0 \quad (26)$$

where  $\Delta_{dec} H^0$  is the specific decomposition enthalpy for the transition (or series of transitions) associated with the lower hydrates and/or complete dehydration. The most promising materials for thermal energy storage in this usage mode involve salts capable of forming hydrates with appropriate DRH = 10–40% such as LiCl, CaCl<sub>2</sub>, MgCl<sub>2</sub>, MgSO<sub>4</sub>, K<sub>2</sub>CO<sub>3</sub> (Table 8).

The practical realization of these decomposition cycles is difficult without the aid of porous media that provide efficient heat/mass transfer within the sorbent bed during cycling.<sup>289</sup> While such composites should allow high charging

Table 7 Salt-solvent working pairs for heating and cooling absorptive cycles and their characteristics. "Crystallization" indicates whether the solvates are crystalline

Working pair	Crystallization	$T_{\text{evap}}/T_{\text{release}}/T_{\text{storage}} (\text{°C})$	$ESD_{ab}, \text{GJ m}^{-3}$	Ref.
LiBr-H <sub>2</sub> O	No	7/43/80	0.40	350
LiBr-H <sub>2</sub> O	Yes	10/20/93	1.4	111
CaCl <sub>2</sub> -H <sub>2</sub> O	No	10/20/45	0.43	351
CaCl <sub>2</sub> -H <sub>2</sub> O	Yes	10/20/54	0.95	111
LiCl-H <sub>2</sub> O	Yes	10/20/66	1.4	111
LiBr-CH <sub>3</sub> OH	Yes	5/35/75	0.2	352
LiCl-CH <sub>3</sub> OH	Yes	10/35/75	0.8	352
LiBr-C <sub>2</sub> H <sub>5</sub> OH	Yes	10/30/95	0.2	353

**Table 8** Examples of “Salt in porous matrix” composites, with their corresponding specific energy, ESD per unit bed volume,  $T_{\text{evap}}/T_{\text{release}}$  for the heating cycle, and exergy storage density (ExSD)

Salt	Matrix	Specific energy (MJ kg <sup>-1</sup> )	ESD (GJ m <sup>-3</sup> )	$T_{\text{evap}}/T_{\text{release}}$ (°C)	ExSD (MJ m <sup>-3</sup> )	Ref.
CaCl <sub>2</sub>	Hollow silica	1.1	0.86	13/45	96	49
CaCl <sub>2</sub>	Ethylcellulose	2.1	0.4	10/20	14	354
CaCl <sub>2</sub>	SiO <sub>2</sub> (Grace Davisil™)	1.1	0.76	10/30	54	355
CaCl <sub>2</sub>	Silica-alumina	0.9	0.65	3/20	40	356
CaCl <sub>2</sub>	PHTS <sup>a</sup>	1.2	—	10/30	—	357
CaCl <sub>2</sub>	MIL-101(Cr)	1.6	1.0	10/30	71	358
LiCl	UiO-66	0.9	—	10/40	—	291
LiCl	Hollow silica	0.75	0.65	13/45	73	49
LiCl	Hollow silica	0.63	0.52	13/60	85	49
LiCl	MWCNT + PVA <sup>b</sup>	1.6	0.65	10/35	57	359
LiCl	Expanded vermiculite	>1.8	0.8	10/35	70	360
LiCl	SiO <sub>2</sub> (Fuji Type A)	1.1	0.6	15/40	52	361
MgCl <sub>2</sub>	Zeolite 13x	1.2	—	25/62	—	362
SrBr <sub>2</sub>	Hollow silica	0.69	0.63	18/45	59	49
SrBr <sub>2</sub>	Expanded vermiculite	1.6	0.38	20/30	13	339
SrBr <sub>2</sub>	MIL-101(Cr)	1.35	0.84	10/30	59	363
K <sub>2</sub> CO <sub>3</sub>	Expanded vermiculite	—	0.9	20/30	31	344

<sup>a</sup> Plugged hexagonal templated silicate. <sup>b</sup> MultiWall Carbon NanoTubes with polyvinyl alcohol binder.

temperatures and high relative volume change of the active storage component, the skeletal volume of the porous matrix and void space in pores necessary to accommodate for the resultant solution (to avoid leakage) decreases the effective energy storage density of the composite relative to that of the pure salt (Table 8). For this reason, the most popular porous matrices are formed from mechanically stable particles with large porosity and sub-micrometer pores capable of containing the salt solution *via* capillary forces. Popular and inexpensive options include vermiculite, attapulgite, and silica gel.<sup>290</sup> Recently, MOFs are being considered as promising matrices due to their high porosity, which yields a potentially high fraction of “useful” space to be occupied by a salt.<sup>291–293</sup> Finding a balance between energy storage density on the bed level, temperature lift, and heat/mass transfer is one important remaining challenge.<sup>49</sup>

## Suggested directions for future research

The preceding sections have introduced the primary classes of materials for low-temperature thermochemical storage and summarized their respective attributes and performance limitations. Based on those limitations, this section suggests high-priority research directions aimed at overcoming performance gaps and accelerating the adoption of TCES devices.

### Computational materials discovery

A comprehensive materials discovery effort has not been performed in the field of thermal energy storage. The absence of such an effort differs from that of related applications – *e.g.*, electrochemical energy storage, photovoltaics, CO<sub>2</sub> capture, *etc.* – in which the properties of an active material largely determine the performance of its respective device. Recent materials discovery efforts targeting these other applications have taken advantage of accurate and efficient computational methods coupled to high-performance computing.<sup>294–305</sup> These

efforts have demonstrated the capability to screen large databases of materials containing as many as 10<sup>6</sup> distinct compositions.<sup>306–308</sup>

Two of the most widely used computational methods for materials discovery are Density Functional Theory (DFT) and classical Grand Canonical Monte Carlo (GCMC). Although both techniques simulate matter at the atomic scale, they differ in their approach to describing atomic interactions (*i.e.*, bonding) and therefore exhibit distinct capabilities with respect to the size of systems that can be simulated and the properties that can be predicted. DFT is a quantum-mechanical technique that solves for the ground state electron density and total energy of a material. These quantities allow for the accurate prediction of energy densities and other macroscopic thermodynamic quantities such as enthalpies and free energies, both of which are relevant for predicting the equilibrium properties of TCES materials, such as the turning temperature.<sup>309</sup> The high accuracy of DFT calculations comes at the cost of high computational expense: if the goal is to screen thousands of compounds in a reasonable time-frame (several months), then the size of the simulation cells generally cannot exceed ~100 atoms. Fortunately, this size limitation allows calculations on a sizeable sub-set of the materials classes of interest to TCES, such as salt hydrates.<sup>87,203,205</sup>

In contrast to DFT, classical GCMC can simulate large systems. This feature makes it useful for simulating adsorption in porous hosts, such as MOFs and zeolites, where the simulation cell ranges from hundreds to thousands of atoms.<sup>249,255,310–312</sup> The greater computational efficiency of classical GCMC reflects its use of a predefined interatomic potential, which can be evaluated with low computational cost. GCMC is a statistical sampling method that predicts equilibrium properties within the grand canonical ( $\mu$ VT) ensemble.<sup>313</sup> In the context of an adsorption process, the simulation consists of a fictitious gas reservoir at constant chemical potential,  $\mu(P,T)$ , and a porous host into which the



gas molecules may adsorb. The output of the simulation is the equilibrium number of molecules adsorbed within the host at the prescribed chemical potential of the gas (which corresponds to a constant pressure and temperature). An adsorption isotherm can be predicted by calculating the number of molecules adsorbed as a function of pressure at constant temperature.<sup>313</sup> The adsorption enthalpy can also be calculated from such simulations.<sup>314</sup> As adsorption isotherms and enthalpies are also routinely measured experimentally,<sup>315,316</sup> a direct comparison between theory and experiment is possible.

The primary shortcoming of classical GCMC derives from inaccuracies in the interatomic potential. If the potential does not accurately capture the nature and strength of bonding, then the quantities derived from it – uptake capacity, shape of the isotherm – will reflect these inaccuracies.<sup>311</sup> These inaccuracies arise partly from the fact that most classical GCMC simulations assume a rigid H<sub>2</sub>O geometry. In reality, however, the H–O–H bond angle and O–H bond lengths of water molecules depend on their local environment within the MOF, which can affect the nature of their interatomic interactions.<sup>249</sup> This effect is neglected.

At present, DFT and GCMC screening have been applied only to a limited set of potential TCES materials. This includes known salt hydrates, hypothetical salt-hydrates based on halogen anions, and a small number of studies on adsorption in porous materials.<sup>87,203,205,249,250,259,317</sup> The largest study to date is that of Shi *et al.*,<sup>259</sup> who examined methanol adsorption in more than 140 000 real and hypothetical MOFs. An even larger space exists for hydrates of ‘mixed metal’ salts, where the cation sites are occupied by two or more distinct cations. In all these cases computation can be used to assess the thermodynamic stability of various hypothetical hydrate compositions, predict capacities, and estimate equilibrium turning temperatures. Subsequently, experiments should be performed to validate the synthesizability and performance of the most promising materials.

Similar discovery opportunities exist for adsorption in porous hosts. Here, the most promise arguably lies with MOFs. This promise reflects the compositional and structural tunability of MOFs – approximately a million MOF variants have been proposed<sup>318–321</sup> – but is also inspired by their crystallinity: the regularity of the pore structure in MOFs implies low tortuosity for mass transport, potentially enhancing the power density of a MOF-based thermal storage device. As with absorption in salts, care must be taken in the screening to assess stability of any new MOF composition. This is especially important in the case where water is the adsorbate, as some MOFs will undergo (irreversible) hydrolysis in humid environments.<sup>107</sup> For this reason, extending the screening to adsorbates other than water is an area also worth exploring.

**Enhancing power density.** As discussed in the preceding sections, a practical thermal storage device must store and release heat at rates that are fast enough to meet the requirements of the desired application. In turn, this system-level requirement places constraints on the underlying properties of the storage material(s), such as their thermal conductivity. In the case of TCES materials, where a chemical reaction is responsible for the uptake/release of heat, several factors

beyond thermal conductivity contribute to the achievable power density. These include intrinsic kinetic phenomena within the active storage material and larger-scale microstructural features that influence long-range heat and mass transport.<sup>131,140,322</sup>

Regarding the intrinsic kinetics of the storage material, let us consider the discharge of a salt-hydrate-based TCES device. During discharge, the anhydrous salt and water vapor react to form a salt-hydrate through absorption of the water into the solid salt. As the salt-hydrate is a distinct crystalline phase, the rate of its formation (and the accompanying rate of heat release) is governed by nucleation and growth processes, either of which may be rate-limiting.<sup>323</sup> The rate of nucleation of the hydrate is governed by a nucleation energy barrier associated with the formation of nanoscopic nuclei of the nascent hydrate phase.<sup>57</sup> Subsequent growth of these nuclei requires rearrangement of the salt’s crystalline lattice to adopt the new structure of the hydrate, and transport of water to the salt/hydrate two-phase interface.<sup>131</sup> To achieve high power density, one must ensure that both of these processes are sufficiently fast.

Similar kinetic limitations exist in hydrogen storage materials. Known strategies from the hydrogen literature for overcoming these limitations may be relevant to TCES materials that operate *via* absorption and should be investigated. One important strategy is doping. Bogdanovic *et al.*<sup>324</sup> were the first to demonstrate that doping sodium alanate, NaAlH<sub>4</sub>, with titanium significantly enhances the hydrogenation kinetics. This effect has been reported in other complex hydrides and with other dopants.<sup>323,325–328</sup> Although the exact mechanism responsible for the kinetic enhancements remains a matter of debate, it is reasonable to hypothesize that similar beneficial effects may be realized for absorption reactions of interest for TCES. Some progress in this regard has already been achieved.<sup>149,327</sup>

The second strategy that could be adopted from the field of hydrogen storage is impregnation of the active TCES material within a porous host. This approach has been used to improve the kinetics of complex hydrides,<sup>329–331</sup> and in some cases have resulted in dramatic changes to reaction behavior.<sup>332,333</sup> These improvements are hypothesized to result from reductions in particle size (which is constrained by the pore diameter) and associated diffusion lengths, and by phenomena associated with the guest/host interface. The downside to this approach is that the mass and volume of the (inactive) host decreases the system’s specific energy and ESD.

Finally, we note that the limitations associated with nucleation and growth during absorption in solids are much less severe in materials that operate *via* adsorption.<sup>334–336</sup> This behaviour provides further motivation for developing materials such as MOFs for TCES. In the field of hydrogen storage, the kinetic performance of MOFs is well-known to surpass that of materials that operate *via* absorption, such as complex hydrides.<sup>337,338</sup>

## Conclusions

Heat is a primary component of the world’s energy ecosystem. Its prevalence implies that its use and manipulation have major



implications for energy efficiency and carbon emissions. The development of systems that can store and manage heat would have a positive impact upon numerous processes throughout multiple sectors of the global economy.

This review has focused on the materials that underlie systems that store and manipulate heat, with an emphasis on those that operate *via* thermochemical reactions. Starting from an overview of general concepts, a detailed discussion of properties relevant for low-temperature (domestic) applications is subsequently presented. These applications include domestic heat storage/amplification (hot water heating), adsorptive cooling (air conditioning), and heat-moisture recuperation. Although these systems remain in an early stage of development, their commercialization will be accelerated by improving the performance of their respective thermal storage materials. This goal motivates a deep-dive into three main classes of low-temperature thermochemical storage materials: (i) absorption in solids (hydrates, ammoniates, and methanolates); (ii) sorption in porous hosts (metal-organic frameworks); and (iii) dilution in liquids. For each class the underlying storage mechanisms are introduced, benchmark materials are discussed, and a summary of advantages and limitations is provided. Although not widely discussed, the implementation of thermal energy storage also needs to consider the potential limited availability of raw materials and production constraints.

Finally, opportunities are described for research aimed at developing optimal thermochemical energy storage materials. Discovery of new storage materials and the development of strategies for increasing the rate of the heat-storing reaction – thus improving power density – are proposed as two important areas that are ripe for research and development.

## Author contributions

All authors made significant contributions to the drafting of this review.

## Conflicts of interest

There are no conflicts to declare.

## List of abbreviations

ARPA-E	Advanced Research Projects Agency - Energy
BTU	British thermal units
CAU	Christian-Albrechts-Universität
CNT	Carbon nanotube
COP	Coefficient of performance
CoRE	Computation-ready, experimental
DFT	Density functional theory
DOE	Department of Energy
DRH	Deliquescence relative humidity
ESD	Energy storage density
ETIP	European technology and innovation platform
EU	European Union

GCMC	Grand Canonical Monte Carlo
GJ	Giga-Joules
HLC	Henry's Law Constant
HTF	Heat transfer fluid
HVAC	Heating, ventilation, and air conditioning
ICSD	Inorganic crystal structure database
IHA	Isosteric heat of adsorption
IUPAC	International Union of Pure and Applied Chemistry
LCD	Largest cavity diameter
LD50	Lethal Dose 50
MIL	Materials of Institute Lavoisier
MJ	Mega-Joules
MOF	Metal-organic framework
NIST	National Institute of Standards and Technology
PCM	Phase change material
PV	Photovoltaic
RH	Relative humidity
RHC	Renewable heating and cooling
SCE	Specific cooling effect
SCP	Specific cooling power
SHE	Specific heating effect
TCES	Thermochemical energy storage
TES	Thermal energy storage
VSA	Volumetric surface area

## Data availability

No primary research results, software or code have been included and no new data were generated or analysed as part of this review.

## Acknowledgements

S. K. acknowledges support from the J. Robert Beyster Computational Innovation Graduate Fellows program. D. J. S. acknowledges the support of the Automotive Research Center (ARC), Cooperative Agreement W56HZV-19-2-0001 U.S. Army DEVCOM GVSC, the University of Michigan Graham Sustainability Institute's Carbon Neutrality Acceleration Program, and Welch Foundation grant F-2213-20240404. A. A. acknowledges support from the University of Michigan's Graham Sustainability Institute through the Carbon Neutrality Acceleration Program. H. H. and A. S. acknowledge support from the EIC Pathfinder project 4TunaTES - For Tunable Thermochemical Energy Storage (grant agreement 101130021).

## Notes and references

- 1 Lawrence Livermore National Laboratory. *Estimated U.S. Energy Consumption in 2023: 93.6 Quads*; Livermore, CA. <https://flowcharts.llnl.gov/commodities/energy> (Accessed on 16 April 2025), 2024.
- 2 C. Forman, I. K. Muritala, R. Pardemann and B. Meyer, Estimating the Global Waste Heat Potential, *Renewable Sustainable Energy Rev.*, 2016, 57, 1568–1579.



3 A. Firth, B. Zhang and A. Yang, Quantification of Global Waste Heat and Its Environmental Effects, *Appl. Energy*, 2019, **235**, 1314–1334.

4 P. Arce, M. Medrano, A. Gil, E. Oró and L. F. Cabeza, Overview of Thermal Energy Storage (TES) Potential Energy Savings and Climate Change Mitigation in Spain and Europe, *Appl. Energy*, 2011, **88**, 2764–2774.

5 N. DeForest, G. Mendes, M. Stadler, W. Feng, J. Lai and C. Marnay, Optimal Deployment of Thermal Energy Storage under Diverse Economic and Climate Conditions, *Appl. Energy*, 2014, **119**, 488–496.

6 A. Henry, R. Prasher and A. Majumdar, Five Thermal Energy Grand Challenges for Decarbonization, *Nat. Energy*, 2020, 635–637.

7 US Environmental Protection Agency (EPA). *Inventory of US Greenhouse Gas Emissions and Sinks: 1990–2009*, Washington, 2011.

8 ed. Pachauri, R. K., Meyer, L., IPCC. Climate Change 2014: Synthesis Report. Contribution of Working Groups I, II and III to the Fifth Assessment Report of the Intergovernmental Panel on Climate Change; Core Writing Team; Geneva, Switzerland, 2014.

9 P. Tatsidjodoung, N. Le Pierrès and L. Luo, A Review of Potential Materials for Thermal Energy Storage in Building Applications, *Renewable Sustainable Energy Rev.*, 2013, **18**, 327–349.

10 Y. Sun, S. Wang, F. Xiao and D. Gao, Peak Load Shifting Control Using Different Cold Thermal Energy Storage Facilities in Commercial Buildings: A Review, *Energy Convers. Manage.*, 2013, **71**, 101–114.

11 Q. Wang, R. Wu, Y. Wu and C. Y. Zhao, Parametric Analysis of Using PCM Walls for Heating Loads Reduction, *Energy Build.*, 2018, **172**, 328–336.

12 U.S. Energy Information Administration. *Annual Energy Outlook 2017*, [https://www.eia.gov/pressroom/presentations/sieminski\\_01052017.pdf](https://www.eia.gov/pressroom/presentations/sieminski_01052017.pdf), 2017.

13 U.S. Energy Information Administration. Residential Energy Consumption Survey, <https://www.eia.gov/consumption/residential/methodology/2009/pdf/techdoc-summary010413.pdf>, 2009.

14 Sonoco Thermosafe. Greenbox® Pre Qualified Shipping Box <https://www.thermosafe.com/products/pre-qualified-solutions/parcel-solutions/greenbox/> (Accessed on 16 April 2025).

15 R. K. Sharma, P. Ganesan, V. V. Tyagi, H. S. C. Metselaar and S. C. Sandaran, Developments in Organic Solid–Liquid Phase Change Materials and Their Applications in Thermal Energy Storage, *Energy Convers. Manage.*, 2015, **95**, 193–228.

16 S. Krishnan and S. V. Garimella Thermal Management of Transient Power Spikes in Electronics - Phase Change Energy Storage or Copper Heat Sinks? In *International Electronic Packaging Technical Conference and Exhibition*; Maui, Hawaii, 2003, pp. 1–12.

17 N. R. Jankowski and F. P. McCluskey, A Review of Phase Change Materials for Vehicle Component Thermal Buffering, *Appl. Energy*, 2014, **113**, 1525–1561.

18 M. Gumus, Reducing Cold-Start Emission from Internal Combustion Engines by Means of Thermal Energy Storage System, *Appl. Therm. Eng.*, 2009, **29**, 652–660.

19 J. Gao, G. Tian, A. Sorniotti, A. E. Karci and R. Di Palo, Review of Thermal Management of Catalytic Converters to Decrease Engine Emissions during Cold Start and Warm Up, *Appl. Therm. Eng.*, 2019, **147**, 177–187.

20 J. P. Putrus, S. T. Jones, B. A. Jawad, G. Kfouri, S. Arslan and P. Schihl, Solving Military Vehicle Transient Heat Load Issues Using Phase Change Materials. In *Proceedings of the ASME 2015 International Mechanical Engineering Congress and Exposition*; Houston, Texas, 2015; pp. 1–7.

21 Y. Kato, R. Takahashi, T. Sekiguchi and J. Ryu, Study on Medium-Temperature Chemical Heat Storage Using Mixed Hydroxides, *Int. J. Refrig.*, 2009, **32**, 661–666.

22 O. Myagmarjav, J. Ryu and Y. Kato, Waste Heat Recovery from Iron Production by Using Magnesium Oxide/Water Chemical Heat Pump as Thermal Energy Storage, *ISIJ Int.*, 2015, **55**, 464–472.

23 S. Brückner, S. Liu, L. Miró, M. Radspieler, L. F. Cabeza and E. Lävemann, Industrial Waste Heat Recovery Technologies: An Economic Analysis of Heat Transformation Technologies, *Appl. Energy*, 2015, **151**, 157–167.

24 H. Ishitobi, J. Ryu and Y. Kato, Combination of Thermochemical Energy Storage and Small Pressurized Water Reactor for Cogeneration System, *Energy Procedia*, 2015, **71**, 90–96.

25 A. J. Carrillo, J. González-Aguilar, M. Romero and J. M. Coronado, Solar Energy on Demand: A Review on High Temperature Thermochemical Heat Storage Systems and Materials, *Chem. Rev.*, 2019, **119**, 4777–4816.

26 L. Teng, Y. Xuan, Y. Da, X. Liu and Y. Ding, Modified Ca-Looping Materials for Directly Capturing Solar Energy and High-Temperature Storage, *Energy Storage Mater.*, 2020, **25**, 836–845.

27 A. Sharma, V. V. Tyagi, C. R. Chen and D. Buddhi, Review on Thermal Energy Storage with Phase Change Materials and Applications, *Renewable Sustainable Energy Rev.*, 2009, **13**, 318–345.

28 K. Faraj, M. Khaled, J. Faraj, F. Hachem and C. Castelain, Phase Change Material Thermal Energy Storage Systems for Cooling Applications in Buildings: A Review, *Renewable Sustainable Energy Rev.*, 2020, **119**, 109579.

29 H. U. Rammelberg, T. Schmidt and W. Ruck, Hydration and Dehydration of Salt Hydrates and Hydroxides for Thermal Energy Storage - Kinetics and Energy Release, *Energy Procedia*, 2012, **30**, 362–369.

30 K. E. N'Tsoukpoe and F. Kuznik, A Reality Check on Long-Term Thermochemical Heat Storage for Household Applications, *Renewable Sustainable Energy Rev.*, 2021, **139**, 110683.

31 P. Pardo, A. Deydier, Z. Anxionnaz-Minvielle, S. Rougé, M. Cabassud and P. Cognet, A Review on High Temperature Thermochemical Heat Energy Storage, *Renewable Sustainable Energy Rev.*, 2014, **32**, 591–610.

32 B. Zalba, J. M. Marin, L. F. Cabeza and H. Mehling, Review on Thermal Energy Storage with Phase Change: Materials,



Heat Transfer Analysis and Applications, *Appl. Therm. Eng.*, 2003, **23**, 251–283.

33 K. Pielichowska and K. Pielichowski, Phase Change Materials for Thermal Energy Storage, *Prog. Mater. Sci.*, 2014, **65**, 67–123.

34 D. Aydin, S. P. Casey and S. Riffat, The Latest Advancements on Thermochemical Heat Storage Systems, *Renewable Sustainable Energy Rev.*, 2015, **41**, 356–367.

35 U. Herrmann and D. W. Kearney, Survey of Thermal Energy Storage for Parabolic Trough Power Plants, *J. Sol. Energy Eng.*, 2002, **124**, 145–152.

36 Y. Tian and C. Y. Zhao, A Review of Solar Collectors and Thermal Energy Storage in Solar Thermal Applications, *Appl. Energy*, 2013, **104**, 538–553.

37 K. E. N'Tsoukpoe, H. Liu, N. Le Pierrès and L. Luo, A Review on Long-Term Sorption Solar Energy Storage, *Renewable Sustainable Energy Rev.*, 2009, **13**, 2385–2396.

38 V. M. van Essen, J. Cot Gores, L. P. J. Bleijendaal, H. A. Zondag, R. Schuitema, M. Bakker and W. G. J. van Helden, Characterization of Salt Hydrates for Compact Seasonal Thermochemical Storage. ASME 2009 3rd Int. Conf. Energy Sustain. 2009, **2**, 825–830.

39 K. E. N'Tsoukpoe, T. Schmidt, H. U. Rammelberg, B. A. Watts and W. K. L. Ruck, A Systematic Multi-Step Screening of Numerous Salt Hydrates for Low Temperature Thermochemical Energy Storage, *Appl. Energy*, 2014, **124**, 1–16.

40 W. E. Wentworth and E. Chen, Simple Thermal Decomposition Reactions for Storage of Solar Thermal Energy, *Sol. Energy*, 1976, **18**, 205–214.

41 Z. Jiang, F. Jiang, C. Li, G. Leng, X. Zhao, Y. Li, T. Zhang, G. Xu, Y. Jin and C. Yang, *et al.*, A Form Stable Composite Phase Change Material for Thermal Energy Storage Applications over 700 °C, *Appl. Sci.*, 2019, **9**(5), 814.

42 S. Saher, S. Johnston, R. Esther-Kelvin, J. M. Pringle, D. R. MacFarlane and K. Matuszek, Trimodal Thermal Energy Storage Material for Renewable Energy Applications, *Nature*, 2024, **636**, 622–626.

43 N. Jaziri, A. Boughamoura, J. Müller, B. Mezghani, F. Tounsi and M. Ismail, A Comprehensive Review of Thermoelectric Generators: Technologies and Common Applications, *Energy Rep.*, 2020, **6**, 264–287.

44 D. Enescu, Thermoelectric Energy Harvesting: Basic Principles and Applications, in *Green Energy Advances*, ed. D. Enescu, 2019, pp. 1–37.

45 M. Deutsch, D. Müller, C. Aumeyr, C. Jordan, C. Gierlmayer, P. Weinberger, F. Winter and A. Werner, Systematic Search Algorithm for Potential Thermochemical Energy Storage Systems, *Appl. Energy*, 2016, **183**, 113–120.

46 M. Richter, E.-M. Habermann, E. Siebecke and M. Linder, A Systematic Screening of Salt Hydrates as Materials for a Thermochemical Heat Transformer, *Thermochim. Acta*, 2018, **659**, 136–150.

47 P. A. J. Donkers, L. C. Sögütoglu, H. P. Huinink, H. R. Fischer and O. C. G. Adan, A Review of Salt Hydrates for Seasonal Heat Storage in Domestic Applications, *Appl. Energy*, 2017, **199**, 45–68.

48 N. Mazur, M. A. R. Blijlevens, R. Ruliaman, H. Fischer, P. Donkers, H. Meekes, E. Vlieg, O. Adan and H. Huinink, Revisiting Salt Hydrate Selection for Domestic Heat Storage Applications, *Renewable Energy*, 2023, **218**, 119331.

49 A. Shkatulov, R. Joosten, H. Fischer and H. Huinink, Core-Shell Encapsulation of Salt Hydrates into Mesoporous Silica Shells for Thermochemical Energy Storage, *ACS Appl. Energy Mater.*, 2020, **3**, 6860–6869.

50 B. Fumey, R. Weber, P. Gantenbein, X. Daguenet-Frick, I. Hughes and V. Dorer, Limitations Imposed on Energy Density of Sorption Materials in Seasonal Thermal Storage Systems, *Energy Procedia*, 2015, **70**, 203–208.

51 D. Nemtzow, K. Sawyer, S. Mumme and N. James, Novel Materials in Thermal Energy Storage for Buildings. *Thermal Energy Storage Webinar Series*, U.S. Department of Energy Office of Energy Efficiency & Renewable Energy, 2020.

52 The European Technology and Innovation Platform on Renewable Heating and Cooling (RHC-ETIP), Strategic Research and Innovation Agenda for Climate-Neutral Heating and Cooling in Europe, 2022. <https://www.rhc-platform.org/content/uploads/2020/10/EUREC-Brochure-RHC-SRI-06-2022-WEB.pdf> (Accessed on 21 April 2025).

53 K. E. N'Tsoukpoe and F. Kuznik, A reality check on long-term thermochemical heat storage for household applications, *Renewable Sustainable Energy Rev.*, 2021, **139**, 110683.

54 A. Crespo, C. Fernández, A. de Gracia and A. Fazzica, Solar-Driven Sorption System for Seasonal Heat Storage under Optimal Control: Study for Different Climatic Zones, *Energies*, 2022, **15**, 5604.

55 H. Liu, W. Wang and Y. Zhang, Performance gap between thermochemical energy storage systems based on salt hydrates and materials, *J. Cleaner Prod.*, 2021, **313**, 127908.

56 A. Bejan, Fundamentals of exergy analysis, entropy generation minimization, and the generation of flow architecture, *Int. J. Energy Res.*, 2002, **26**, 545–565.

57 L.-C. Sögütoglu, M. Steiger, J. Houben, D. Biemans, H. R. Fischer, P. Donkers, H. Huinink and O. C. G. Adan, Understanding the Hydration Process of Salts: The Impact of a Nucleation Barrier, *Cryst. Growth Des.*, 2019, **19**, 2279–2288.

58 D. Aydin, S. P. Casey, X. Chen and S. Riffat, Novel “Open-Sorption Pipe” Reactor for Solar Thermal Energy Storage, *Energy Convers. Manage.*, 2016, **121**, 321–334.

59 S. Afflerbach and R. Trettin, A Systematic Screening Approach for New Materials for Thermochemical Energy Storage and Conversion Based on the Strunz Mineral Classification System, *Thermochim. Acta*, 2019, **674**, 82–94.

60 M. S. Ziegler and J. E. Trancik, Re-examining rates of lithium-ion battery technology improvement and cost decline, *Energy Environ. Sci.*, 2021, **14**, 1635–1651.

61 L. G. Gordeeva; A. I. Shkatulov and Y. I. Aristov, Closed Sorption Systems, in *Reference Module in Earth Systems and Environmental Sciences*, Elsevier, 2020, DOI: [10.1016/B978-0-12-819723-3.00014-7](https://doi.org/10.1016/B978-0-12-819723-3.00014-7).

62 B. Fumey, R. Weber and L. Baldini, Sorption Based Long-Term Thermal Energy Storage – Process Classification and



Analysis of Performance Limitations: A Review, *Renewable Sustainable Energy Rev.*, 2019, **111**, 57–74.

63 J. Stengler and M. Linder, Thermal Energy Storage Combined with a Temperature Boost: An Underestimated Feature of Thermochemical Systems, *Appl. Energy*, 2020, **262**, 114530.

64 M. M. Tokarev, L. G. Gordeeva, A. D. Grekova and Y. I. Aristov, Adsorption Cycle “Heat from Cold” for Upgrading the Ambient Heat: The Testing a Lab-Scale Prototype with the Composite Sorbent  $\text{CaClBr/Silica}$ , *Appl. Energy*, 2018, **211**, 136–145.

65 Y. I. Aristov, “Heat from Cold” – A New Cycle for Upgrading the Ambient Heat: Adsorbent Optimal from the Dynamic Point of View, *Appl. Therm. Eng.*, 2017, **124**, 1189–1193.

66 Y. I. Aristov, Adsorptive Transformation of Ambient Heat: A New Cycle, *Appl. Therm. Eng.*, 2017, **124**, 521–524.

67 C. Rathgeber, E. Lävemann and A. Hauer, Economic Top-down Evaluation of the Costs of Energy Storages—A Simple Economic Truth in Two Equations, *J. Energy Storage*, 2015, **2**, 43–46.

68 R. E. Critoph, Solid Sorption Cycles: A Short History, *Int. J. Refrig.*, 2012, **35**, 490–493.

69 L. F. Cabeza, A. Solé and C. Barreneche, Review on Sorption Materials and Technologies for Heat Pumps and Thermal Energy Storage, *Renew. Energy*, 2017, **110**, 3–39.

70 Y. I. Aristov, Challenging Offers of Material Science for Adsorption Heat Transformation: A Review, *Appl. Therm. Eng.*, 2013, **50**, 1610–1618.

71 I. S. Girnik and Y. I. Aristov, Water as an Adsorptive for Adsorption Cycles Operating at a Temperature below 0 °C, *Energy*, 2020, **211**, 119037.

72 M. M. Younes, I. I. El-Sharkawy, A. E. Kabeel and B. B. Saha, A Review on Adsorbent-Adsorbate Pairs for Cooling Applications, *Appl. Therm. Eng.*, 2017, **114**, 394–414.

73 Yu. I. Aristov, Finned-Flat-Tube Heat Exchangers for Adsorptive Cooling: Review of the Current Studies, *Energy*, 2025, **316**, 134305.

74 Y. I. Aristov, A. Sapienza, D. S. Ovoshchnikov, A. Freni and G. Restuccia, Reallocation of Adsorption and Desorption Times for Optimisation of Cooling Cycles, *Int. J. Refrig.*, 2012, **35**, 525–531.

75 M. Polanyi, Section III.—Theories of the adsorption of gases. A general survey and some additional remarks. Introductory paper to section III, *Trans. Faraday Soc.*, 1932, **28**, 316–333.

76 S. M. Towsif Abtab, D. Alezi, P. M. Bhatt, A. Shkurenko, Y. Belmabkhout, H. Aggarwal, L. J. Weseliński, N. Alsadun, U. Samin and M. N. Hedhili, *et al.*, Reticular Chemistry in Action: A Hydrolytically Stable MOF Capturing Twice Its Weight in Adsorbed Water, *Chem*, 2018, **4**, 94–105.

77 D. Lenzen, P. Bendix, H. Reinsch, D. Fröhlich, H. Kummer, M. Möllers, P. P. C. Hügenell, R. Gläser, S. Henninger and N. Stock, Scalable Green Synthesis and Full-Scale Test of the Metal–Organic Framework CAU-10-H for Use in Adsorption-Driven Chillers, *Adv. Mater.*, 2018, **30**(6), 1705869.

78 E. Elsayed, R. AL-Dadah, S. Mahmoud, P. A. Anderson, A. Elsayed and P. G. Youssef, CPO-27(Ni), Aluminium Fumarate and MIL-101(Cr) MOF Materials for Adsorption Water Desalination, *Desalination*, 2017, **406**, 25–36.

79 H.-X. Fu, L.-Z. Zhang, J.-C. Xu and R.-R. Cai, A Dual-Scale Analysis of a Desiccant Wheel with a Novel Organic-Inorganic Hybrid Adsorbent for Energy Recovery, *Appl. Energy*, 2016, **163**, 167–179.

80 A. Shkatulov, L. G. Gordeeva, I. S. Girnik, H. Huinink and Y. I. Aristov, Novel Adsorption Method for Moisture and Heat Recuperation in Ventilation: Composites “LiCl/Matrix” Tailored for Cold Climate, *Energy*, 2020, **201**, 117595.

81 Z. Wang, T. Horseman, A. P. Straub, N. Y. Yip, D. Li, M. Elimelech and S. Lin, Pathways and Challenges for Efficient Solar-Thermal Desalination, *Sci. Adv.*, 2019, **5**, eaax0763.

82 Y. Tu, R. Wang, Y. Zhang and J. Wang, Progress and Expectation of Atmospheric Water Harvesting, *Joule*, 2018, **2**, 1452–1475.

83 J. Cai, X. Zheng, Q. Pan, D. Li and W. Wang, Advances in Hygroscopic Metal-Organic Frameworks for Air, Water & Energy Applications, *Appl. Energy*, 2025, **377**, 124362.

84 E. Elsayed, R. AL-Dadah, S. Mahmoud, P. Anderson and A. Elsayed, Experimental Testing of Aluminium Fumarate MOF for Adsorption Desalination, *Desalination*, 2020, **475**, 114170.

85 H. Kim, S. Yang, S. R. Rao, S. Narayanan, E. A. Kapustin, H. Furukawa, A. S. Umans, O. M. Yaghi and E. N. Wang, Water Harvesting from Air with Metal-Organic Frameworks Powered by Natural Sunlight, *Science*, 2017, **356**, 430–434.

86 L. G. Gordeeva, Y. D. Tu, Q. Pan, M. L. Palash, B. B. Saha, Y. I. Aristov and R. Z. Wang, Metal-Organic Frameworks for Energy Conversion and Water Harvesting: A Bridge between Thermal Engineering and Material Science, *Nano Energy*, 2021, **84**, 105946.

87 S. Kiyabu, J. S. Lowe, A. Ahmed and D. J. Siegel, Computational Screening of Hydration Reactions for Thermal Energy Storage: New Materials and Design Rules, *Chem. Mater.*, 2018, **30**, 2006–2017.

88 M. A. R. Blijlevens, N. Mazur, W. Kooijman, H. R. Fischer, H. P. Huinink, H. Meekes and E. Vlieg, A Study of the Hydration and Dehydration Transitions of  $\text{SrCl}_2$  Hydrates for Use in Heat Storage, *Sol. Energy Mater. Sol. Cells*, 2022, **242**, 111770.

89 B. Smeets, E. Iype, S. V. Nedea, H. A. Zondag and C. C. M. Rindt, A DFT Based Equilibrium Study on the Hydrolysis and the Dehydration Reactions of  $\text{MgCl}_2$  Hydrates, *J. Chem. Phys.*, 2013, **139**, 124312.

90 R. Cuypers, A. Anastasopol, A.-J. De Jong, H. Oversloot, L. Van Vliet, P. Bodis and C. Hoegaerts, A Novel Heat Battery to Save Energy & Reduce  $\text{CO}_2$  Production, in *International Solar Energy Society*, Palma de Mallorca, Spain, 2016, pp. 1–7.

91 D. Müller, C. Knoll, G. Gravogl, C. Jordan, E. Eitenberger, G. Friedbacher, W. Artner, J. M. Welch, A. Werner and



M. Harasek, *et al.*, Medium-Temperature Thermochemical Energy Storage with Transition Metal Ammoniates – A Systematic Material Comparison, *Appl. Energy*, 2021, **285**, 116470.

92 R. Sharma, E. Anil Kumar, P. Dutta, S. Srinivasa Murthy, Y. I. Aristov, M. M. Tokrev, T. X. Li and R. Z. Wang, Ammoniated Salt Based Solid Sorption Thermal Batteries: A Comparative Study, *Appl. Therm. Eng.*, 2021, **191**, 116875.

93 W. Y. Zhang, A. Mehari, X. J. Zhang, A. P. Roskilly and L. Jiang, Ammonia-Based Sorption Thermal Battery: Concepts, Thermal Cycles, Applications, and Perspectives, *Energy Storage Mater.*, 2023, **62**, 102930.

94 T. Yan, R. Z. Wang and T. X. Li, Experimental Investigation on Thermochemical Heat Storage Using Manganese Chloride/Ammonia, *Energy*, 2018, **143**, 562–574.

95 R. E. Critoph, Performance Limitations of Adsorption Cycles for Solar Cooling, *Sol. Energy*, 1988, **41**, 21–31.

96 K. Neumann, M. Wiegand, O. Opel and K. Korhammer, Solid Sorption Refrigeration With Calcium Chloride Methanolates on Technical Scale. *Proc. 14th Int. Renew. Energy Storage Conf. 2020 (IRES 2020)*, 2021, **6**, 142–149.

97 K. Korhammer, K. Neumann, O. Opel and W. K. L. Ruck, Thermodynamic and Kinetic Study of  $\text{CaCl}_2\text{-CH}_3\text{OH}$  Adducts for Solid Sorption Refrigeration by TGA/DSC, *Appl. Energy*, 2018, **230**, 1255–1278.

98 Y. I. Aristov, L. G. Gordeeva, Y. D. Pankratiev, L. M. Plyasova, I. V. Bikova, A. Freni and G. Restuccia, Sorption Equilibrium of Methanol on New Composite Sorbents “ $\text{CaCl}_2$ /Silica Gel”, *Adsorption*, 2007, **13**, 121–127.

99 A. Grekova, S. Strelova, L. Gordeeva and Y. Aristov, “ $\text{LiCl}/\text{Vermiculite}$  - Methanol” as Working Pair for Adsorption Heat Storage: Adsorption Equilibrium and Dynamics, *Energy*, 2019, **186**, 115775.

100 A. D. Grekova, I. S. Girnik, V. V. Nikulin, M. M. Tokarev, L. G. Gordeeva and Y. I. Aristov, New Composite Sorbents of Water and Methanol “Salt in Anodic Alumina”: Evaluation for Adsorption Heat Transformation, *Energy*, 2016, **106**, 231–239.

101 S. V. Strelova, L. G. Gordeeva, A. D. Grekova, A. N. Salanov and Y. I. Aristov, Composites “Lithium Chloride/Vermiculite” for Adsorption Thermal Batteries: Giant Acceleration of Sorption Dynamics, *Energy*, 2023, **263**, 125733.

102 J. Rouquerol, D. Avnir, C. W. Fairbridge, D. H. Everett, J. M. Haynes, N. Pernicone, J. D. F. Ramsay, K. S. W. Sing and K. K. Unger Recommendations for the Characterization of Porous Solids (Technical Report); 1994; Vol. 66.

103 S. Vasta, V. Brancato, D. La Rosa, V. Palomba, G. Restuccia, A. Sapienza and A. Fazzica, Adsorption Heat Storage: State-of-the-Art and Future Perspectives, *Nanomaterials*, 2018, **8**, 522.

104 H. Deshmukh, M. P. Maiya and S. Srinivasa Murthy, Study of Sorption Based Energy Storage System with Silica Gel for Heating Application, *Appl. Therm. Eng.*, 2017, **111**, 1640–1646.

105 S. K. Henninger, F. Jeremias, H. Kummer and C. Janiak, MOFs for Use in Adsorption Heat Pump Processes, *Eur. J. Inorg. Chem.*, 2012, 2625–2634.

106 O. M. Yaghi, M. O’Keeffe, N. W. Ockwig, H. K. Chae, M. Eddaoudi and J. Kim, Reticular Synthesis and the Design of New Materials, *Nature*, 2003, **423**(6941), 705–714.

107 N. C. Burtch, H. Jasuja and K. S. Walton, Water Stability and Adsorption in Metal–Organic Frameworks, *Chem. Rev.*, 2014, **114**, 10575–10612.

108 R. Batra, C. Chen, T. G. Evans, K. S. Walton and R. Ramprasad, Prediction of water stability of metal-organic frameworks using machine learning, *Nat. Mach. Intell.*, 2020, **2**, 704–710.

109 J. Ehrenmann, S. K. Henninger and C. Janiak, Water Adsorption Characteristics of MIL-101 for Heat-Transformation Applications of MOFs, *Eur. J. Inorg. Chem.*, 2011, 471–474.

110 T. L. Manyimo, J. Ren, H. Wang and S. Peng, Perspective on Metal-Organic Frameworks-Based Atmospheric Water Harvesting Systems towards Universal Adoption, *Coord. Chem. Rev.*, 2025, **537**, 216717.

111 N. Yu, R. Z. Wang, Z. S. Lu, L. W. Wang and T. F. Ishugah, Evaluation of a Three-Phase Sorption Cycle for Thermal Energy Storage, *Energy*, 2014, **67**, 468–478.

112 Z. Ding and W. Wu, Type II absorption thermal battery for temperature upgrading: Energy storage heat transformer, *Appl. Energy*, 2022, **324**, 119748.

113 A. Shkatulov, E. Averina, T. Raemaekers, H. Fischer, O. C. G. Adan and H. Huinink, Stabilization of reactive bed particles for thermochemical energy storage with fiber reinforcement, *J. Energy Storage*, 2024, **101**, 113764.

114 K. E. N’Tsoukpoe, T. Schmidt, H. U. Rammelberg, B. A. Watts and W. K. L. Ruck, A Systematic Multi-Step Screening of Numerous Salt Hydrates for Low Temperature Thermochemical Energy Storage, *Appl. Energy*, 2014, **124**, 1–16.

115 P. Donkers, L. Pel, M. Steiger and O. Adan, Deammoniation and Ammoniation Processes with Ammonia Complexes, *AIMS Energy*, 2016, **4**, 936–950.

116 T. Zhang, H. Miyaoka, H. Miyaoka, T. Ichikawa and Y. Kojima, Review on Ammonia Absorption Materials: Metal Hydrides, Halides, and Borohydrides, *ACS Appl. Energy Mater.*, 2018, **1**, 232–242.

117 H. D. B. Jenkins, The Thermodynamic Difference Rule (TDR) for Non-Aqueous Solvates. Part 2. Review of Methodology, Investigation and Prediction of Thermodynamic Data for Ammoniate Solvates,  $\text{M}_p\text{X}_q\cdot\text{nNH}_3$ , Routes to Expand the Database, *J. Chem. Thermodyn.*, 2019, **135**, 316–329.

118 K. Korhammer, J. Mihály, S. Bálint, L. Trif, Á. Vass, A. Tompos and E. Tálas, Reversible Formation of Alcohol Solvates and Their Potential Use for Heat Storage, *J. Therm. Anal. Calorim.*, 2019, **138**, 11–33.

119 L. Glasser, Thermodynamics of Inorganic Hydration and of Humidity Control, with an Extensive Database of Salt Hydrate Pairs, *J. Chem. Eng. Data*, 2014, **59**, 526–530.

120 K. Sugimoto, R. E. Dinnebier and J. C. Hanson, Structures of Three Dehydration Products of Bischofite from in Situ Synchrotron Powder Diffraction Data ( $\text{MgCl}_2\cdot\text{nH}_2\text{O}$ ;  $n = 1, 2, 4$ ), *Acta. Cryst.*, 2007, **B63**, 235–242.



121 H. Schmidt, E. Hennings and W. Voigt, Magnesium Chloride Tetra-Hydrate,  $MgCl_2 \cdot 4H_2O$ , *Acta Crystallogr., Sect. C: Cryst. Struct. Commun.*, 2012, **68**, i4–i6.

122 P. A. Agron and W. R. Busing, Magnesium Dichloride Hexahydrate,  $MgCl_2 \cdot 6H_2O$ , by Neutron Diffraction, *Acta Crystallogr., Sect. C: Struct. Chem.*, 1985, **41**, 8–10.

123 E. Hennings, H. Schmidt and W. Voigt, Crystal Structures of Hydrates of Simple Inorganic Salts. I. Water-Rich Magnesium Halide Hydrates  $MgCl_2 \cdot 8H_2O$ ,  $MgCl_2 \cdot 12H_2O$ ,  $MgBr_2 \cdot 6H_2O$ ,  $MgBr_2 \cdot 9H_2O$ ,  $MgI_2 \cdot 8H_2O$  and  $MgI_2 \cdot 9H_2O$ , *Acta Crystallogr., Sect. C: Cryst. Struct. Commun.*, 2013, **69**, 1292–1300.

124 K. Komatsu, A. Shinozaki, S. Machida, T. Matsubayashi, M. Watanabe, H. Kagi, A. Sano-Furukawa and T. Hattori, Crystal Structure of Magnesium Dichloride Decahydrate Determined by X-Ray and Neutron Diffraction under High Pressure, *Acta Crystallogr., Sect. B: Struct. Sci., Cryst. Eng. Mater.*, 2015, **71**, 74–80.

125 I. H. Derby and V. Yngve, The Dissociation Tensions of Certain Hydrated Chlorides and the Vapor Pressures of Their Saturated Solutions, *J. Am. Chem. Soc.*, 1916, **38**, 1439–1451.

126 R. W. Carling, Dissociation Pressures and Enthalpies of Reaction in  $MgCl_2 \cdot nH_2O$  and  $CaCl_2 \cdot nNH_3$ , *J. Chem. Thermodyn.*, 1981, **13**, 503–512.

127 L. Greenspan, Humidity Fixed Points of Binary Saturated Aqueous Solutions, *J. Res. Natl. Bur. Stand. Sect. A Phys. Chem.*, 1977, **81A**, 89.

128 R. V. Gough, V. F. Chevrier and M. A. Tolbert, Formation of liquid water at low temperatures via the deliquescence of calcium chloride: Implications for Antarctica and Mars, *Planet. Space Sci.*, 2016, **131**, 79–87.

129 H. Huinink, S. de Jong and V. Houben, Hydration fronts in packed particle beds of salt hydrates: Implications for heat storage, *J. Energy Storage*, 2023, **71**, 108158.

130 J. Romaní, J. Gasia, A. Solé, H. Takasu, Y. Kato and L. F. Cabeza, Evaluation of Energy Density as Performance Indicator for Thermal Energy Storage at Material and System Levels, *Appl. Energy*, 2019, **235**, 954–962.

131 J. Aarts, S. de Jong, M. L. Cotti, P. A. J. Donkers, H. R. Fischer, O. C. G. Adan and H. P. Huinink, Diffusion Limited Hydration Kinetics of Millimeter Sized Salt Hydrate Particles for Thermochemical Heat Storage, *J. Energy Storage*, 2022, **47**, 103554.

132 J. de Pablo, J. Andersson and M. Azoulay, Kinetic Investigation of the Sorption of Water by Lithium Hydroxide, *Thermochim. Acta*, 1987, **113**, 87–94.

133 J. Andersson, M. Azoulay and J. D. Pablo, Kinetic Investigation of the Sorption of Water by Barium Chloride Monohydrate, *Thermochim. Acta*, 1983, **70**, 291–302.

134 M. A. Stanish and D. D. Perlmutter, Kinetics of Hydration-dehydration Reactions Considered as Solid Transformations, *AIChE J.*, 1984, **30**, 557–563.

135 J. Y. Andersson, J. de Pablo and M. Azoulay, Kinetics of the Rehydration of Sodium Sulphide Dehydrated in Situ, Under Formation of its Pentahydrate, *Thermochim. Acta*, 1985, **91**, 223–234.

136 L. C. Sögütoglu, P. A. J. Donkers, H. R. Fischer, H. P. Huinink and O. C. G. Adan, In-Depth Investigation of Thermochemical Performance in a Heat Battery: Cyclic Analysis of  $K_2CO_3$ ,  $MgCl_2$  and  $Na_2S$ , *Appl. Energy*, 2018, **215**, 159–173.

137 J. Stengler, I. Bürger and M. Linder, Thermodynamic and Kinetic Investigations of the  $SrBr_2$  Hydration and Dehydration Reactions for Thermochemical Energy Storage and Heat Transformation, *Appl. Energy*, 2020, **277**, 115432.

138 S. Afflerbach and R. Trettin, A Systematic Screening Approach for New Materials for Thermochemical Energy Storage and Conversion Based on the Strunz Mineral Classification System, *Thermochim. Acta*, 2019, **674**, 82–94.

139 R. V. Gough, V. F. Chevrier, K. J. Baustian, M. E. Wise and M. A. Tolbert, Laboratory Studies of Perchlorate Phase Transitions: Support for Metastable Aqueous Perchlorate Solutions on Mars, *Earth Planet. Sci. Lett.*, 2011, **312**, 371–377.

140 K. Linnow, M. Niermann, D. Bonatz, K. Posern and M. Steiger, Experimental Studies of the Mechanism and Kinetics of Hydration Reactions, *Energy Procedia*, 2014, **48**, 394–404.

141 W. J. Dunning, Nucleation and Growth Processes in the Dehydration of Salt Crystals, in *Kinetics of reactions in ionic systems*, ed. T. J. Gray and V. D. Fréchette, Springer, New York, 1969, pp. 132–155.

142 Q. Dai, J. Hu and M. Salmeron, Adsorption of Water on  $NaCl$  (100) Surfaces: Role of Atomic Steps, *J. Phys. Chem. B*, 1997, **101**, 1994–1998.

143 S. J. Peters and G. E. Ewing, Water on Salt: An Infrared Study of Adsorbed  $H_2O$  on  $NaCl(100)$  under Ambient Conditions, *J. Phys. Chem. B*, 1997, **101**, 10880–10886.

144 M. Luna, F. Rieutord, N. A. Melman, Q. Dai and M. M. Salmeron, Adsorption of Water on Alkali Halide Surfaces Studied by Scanning Polarization Force Microscopy, *J. Phys. Chem. A*, 1998, **102**, 6793–6800.

145 P. J. Koelemeijer, C. J. Peach and C. J. Spiers, Surface Diffusivity of Cleaved  $NaCl$  Crystals as a Function of Humidity: Impedance Spectroscopy Measurements and Implications for Crack Healing in Rock Salt, *J. Geophys. Res. Solid Earth*, 2012, **117**, 1–15.

146 S. Chakraborty, The Humidity Dependent Conductance of  $Al_2(SO_4)_3 \cdot 16H_2O$ , *Smart Mater. Struct.*, 1995, **4**, 368–369.

147 P. Barboux and J. Livage, Ionic Conductivity in Fibrous  $Ce(HPO_4)_2 \cdot (3+x)H_2O$ , *Solid State Ionics*, 1989, **34**, 47–52.

148 J. Houben, J. van Biesen, H. Huinink, H. R. Fischer and O. C. G. Adan, Accelerating the hydration reaction of potassium carbonate using organic dopants, *Sol. Energy Mater. Sol. Cells*, 2023, **259**, 112410.

149 J. Houben, A. Shkatulov, H. Huinink, H. Fischer and O. Adan, Caesium doping accelerates the hydration rate of potassium carbonate in thermal energy storage, *Sol. Energy Mater. Sol. Cells*, 2023, **251**, 112116.

150 Y. Li, A. Shkatulov, M. Linder, M. Schaefer, B. Li and A. Thess, Enhancing Reactivity of  $Na_2Zn(SO_4)_2$  Hydrates by Doping for Thermochemical Energy Storage, *Sol. Energy Mater. Sol. Cells*, 2025, **292**, 113753.



151 N. Mazur, H. Huinink, H. Fischer, P. Donkers and O. Adan, Accelerating the reaction kinetics of  $K_2CO_3$  through the addition of CsF in the view of thermochemical heat storage, *Sol. Energy*, 2022, **242**, 256–266.

152 K. Linnow, M. Niermann, D. Bonatz, K. Posern and M. Steiger, Experimental Studies of the Mechanism and Kinetics of Hydration Reactions, *Energy Procedia*, 2014, **48**, 394–404.

153 R. Fisher, Y. Ding and A. Sciacovelli, Hydration Kinetics of  $K_2CO_3$ ,  $MgCl_2$  and Vermiculite-Based Composites in View of Low-Temperature Thermochemical Energy Storage, *J. Energy Storage*, 2021, **38**, 102561.

154 S. Vyazovkin, A. K. Burnham, J. M. Criado, L. A. Pérez-Maqueda, C. Popescu and N. Sbirrazzuoli, ICTAC Kinetics Committee Recommendations for Performing Kinetic Computations on Thermal Analysis Data, *Thermochim. Acta*, 2011, **520**, 1–19.

155 M. Gaeini, S. A. Shaik and C. C. M. Rindt, Characterization of Potassium Carbonate Salt Hydrate for Thermochemical Energy Storage in Buildings, *Energy Build.*, 2019, **196**, 178–193.

156 F. Birkelbach, M. Deutsch and A. Werner, The Effect of the Reaction Equilibrium on the Kinetics of Gas-Solid Reactions—A Non-Parametric Modeling Study, *Renew. Energy*, 2020, **152**, 300–307.

157 M. C. Foster and G. E. Ewing, Adsorption of Water on the  $NaCl(001)$  Surface. II. An Infrared Study at Ambient Temperatures, *J. Chem. Phys.*, 2000, **112**, 6817–6826.

158 A. Verdaguer, J. J. Segura, J. Fraxedas, H. Bluhm and M. Salmeron, Correlation between Charge State of Insulating  $NaCl$  Surfaces and Ionic Mobility Induced by Water Adsorption: A Combined Ambient Pressure X-Ray Photoelectron Spectroscopy and Scanning Force Microscopy Study, *J. Phys. Chem. C*, 2008, **112**, 16898–16901.

159 M. Reading, D. Dollimore and R. Whitehead, The Measurement of Meaningful Kinetic Parameters for Solid State Decomposition Reactions, *J. Therm. Anal.*, 1991, **37**, 2165–2188.

160 L.-C. Sögütoglu, F. Birkelbach, A. Werner, H. Fischer, H. Huinink and O. Adan, Hydration of Salts as a Two-Step Process: Water Adsorption and Hydrate Formation, *Thermochim. Acta*, 2021, **695**, 178819.

161 J. Szekely, J. W. Evans and H. Y. Sohn, Reactions of Porous Solids, *Gas-Solid Reactions*, Elsevier, 1976, pp. 108–175.

162 H. Huinink, S. de Jong and V. Houben, Hydration fronts in packed particle beds of salt hydrates: Implications for heat storage, *J. Energy Storage*, 2023, **71**, 108158.

163 H. Huinink; S. de Jong and O. Adan, Hydration Fronts in Packed Particle Beds of Salt Hydrates II: The Role of Temperature Gradients and Implications for Heat Storage. In review.

164 F. Trausel, A. J. De Jong and R. Cuyvers, A Review on the Properties of Salt Hydrates for Thermochemical Storage, *Energy Procedia*, Elsevier BV, 2014, vol. 48, pp. 447–452.

165 A.-J. De Jong, L. Van Vliet, C. Hoegaerts, M. Roelands and R. Cuyvers, Thermochemical Heat Storage - From Reaction Storage Density to System Storage Density, *Energy Procedia*, 2016, **91**, 128–137.

166 D. B. Nash, Infrared Reflectance Spectra of  $Na_2S$  with Contaminant  $Na_2CO_3$ : Effects of Adsorbed  $H_2O$  and  $CO_2$  and Relation to Studies of Io, *Icarus*, 1988, **74**, 365–368.

167 T. Kohler, T. Biedermann and K. Müller, Experimental Study of  $MgCl_2\cdot6H_2O$  as Thermochemical Energy Storage Material, *Energy Technol.*, 2018, **6**, 1935–1940.

168 J. Xu, T. Li, T. Yan, J. Chao and R. Wang, Dehydration Kinetics and Thermodynamics of Magnesium Chloride Hexahydrate for Thermal Energy Storage, *Sol. Energy Mater. Sol. Cells*, 2021, **219**, 110819.

169 H. Zhou and D. Zhang, Effect of Graphene Oxide Aerogel on Dehydration Temperature of Graphene Oxide Aerogel Stabilized  $MgCl_2\cdot6H_2O$  Composites, *Sol. Energy*, 2019, **184**, 202–208.

170 G. J. Kipouros and D. R. Sadoway, A Thermochemical Analysis of the Production of Anhydrous  $MgCl_2$ , *J. Light Met.*, 2001, **1**, 111–117.

171 Z. Zhang, X. Lu, Y. Yan and T. Wang, The Dehydration of  $MgCl_2\cdot6H_2O$  by Inhibition of Hydrolysis and Conversion of Hydrolysate, *J. Anal. Appl. Pyrolysis*, 2019, **138**, 114–119.

172 A. K. Galwey and G. M. Laverty, The Thermal Decomposition of Magnesium Chloride Dihydrate, *Thermochim. Acta*, 1989, **138**, 115–127.

173 M. S. Ferrandon, M. A. Lewis, D. F. Tatterson, A. Gross, D. Doizi, L. Croizé, V. Dauvois, J. L. Roujou, Y. Zanella and P. Carles, Hydrogen Production by the Cu-Cl Thermochemical Cycle: Investigation of the Key Step of Hydrolysing  $CuCl_2$  to  $Cu_2OCl_2$  and  $HCl$  Using a Spray Reactor, *Int. J. Hydrogen Energy*, 2010, **35**, 992–1000.

174 A. Farsi, I. Dincer and G. F. Naterer, Second Law Analysis of  $CuCl_2$  Hydrolysis Reaction in the Cu-Cl Thermochemical Cycle of Hydrogen Production, *Energy*, 2020, **202**, 117721.

175 S. Shoval, S. Yariv and Y. Kirsh, The Study of Thermal Dehydration and Hydrolysis of  $MgBr_2\cdot6H_2O$  by DTA and TG, *Thermochim. Acta*, 1988, **133**, 263–273.

176 R. Hamze, I. Nevoigt, U. Sazama, M. Fröba and M. Steiger, Carnallite Double Salt for Thermochemical Heat Storage, *J. Energy Storage*, 2024, **86**, 111404.

177 A. Gutierrez, S. Ushak and M. Linder, High Carnallite-Bearing Material for Thermochemical Energy Storage: Thermophysical Characterization, *ACS Sustainable Chem. Eng.*, 2018, **6**, 6135–6145.

178 K. Korhammer, M.-M. Druske, A. Fopah-Lele, H. U. Rammelberg, N. Wegscheider, O. Opel, T. Osterland and W. Ruck, Sorption and Thermal Characterization of Composite Materials Based on Chlorides for Thermal Energy Storage, *Appl. Energy*, 2016, **162**, 1462–1472.

179 H. U. Rammelberg, M. Myrau, T. Schmidt and W. K. L. Ruck, An Optimization of Salt Hydrates for Thermochemical Heat Storage. In *International Symposium on Innovative Materials for Processes in Energy Systems 2013 Fukuoka, Japan*; 2013; pp. IMPRES2013-117.

180 M. A. J. M. Beving, A. J. H. Frijns, C. C. M. Rindt and D. M. J. Smeulders, Effect of cycle-induced crack formation on



the hydration behaviour of  $K_2CO_3$  particles: Experiments and modelling, *Thermochim. Acta*, 2020, **692**, 178752.

181 H. D. B. Jenkins and L. Glasser, Difference Rule - A New Thermodynamic Principle: Prediction of Standard Thermodynamic Data for Inorganic Solvates, *J. Am. Chem. Soc.*, 2004, **126**, 15809–15817.

182 J. Aarts, H. Fischer, O. Adan and H. Huinink, Impact of cycling on the performance of mm-sized salt hydrate particles, *J. Energy Storage*, 2024, **76**, 109806.

183 A. Arya, M. Beving, A. Mahmoudi, P. A. J. Donkers, G. Brem and M. Shahi, Quantifying volume variation and agglomeration in thermochemical materials: An in-situ measurement methodology, *J. Energy Storage*, 2025, **124**, 116877.

184 J. Aarts, H. Fischer, O. Adan and H. Huinink, Towards stable performance of salt hydrates in thermochemical energy storage: A review, *J. Energy Storage*, 2025, **114**, 115726.

185 W. Kooijman, D. J. Kok, M. A. R. Blijlevens, H. Meekes and E. Vlieg, Screening double salt sulfate hydrates for application in thermochemical heat storage, *J. Energy Storage*, 2022, **55**, 105459.

186 J. Smith, P. Weinberger and A. Werner, Dehydration performance of a novel solid solution library of mixed Tutton salts as thermochemical heat storage materials, *J. Energy Storage*, 2024, **78**, 110003.

187 J. G. de Oliveira Neto, L. F. L. da Silva, T. K. C. Alves, A. Neumann, F. F. de Sousa, A. P. Ayala and A. O. dos Santos, Mixed tutton salts  $K_2Mn_{0.15}Co_{0.85}(SO_4)_2(H_2O)_6$  and  $K_2Mn_{0.16}Zn_{0.84}(SO_4)_2(H_2O)_6$  for applications in thermochemical devices: experimental physicochemical properties combined with first-principles calculations, *J. Mater. Sci.*, 2024, **59**, 14445–14464.

188 A. Fopah Lele, K. E. N'Tsoukpoe, T. Osterland, F. Kuznik and W. K. L. Ruck, Thermal Conductivity Measurement of Thermochemical Storage Materials, *Appl. Therm. Eng.*, 2015, **89**, 916–926.

189 F. Kleiner, K. Posern and A. Osburg, Thermal Conductivity of Selected Salt Hydrates for Thermochemical Solar Heat Storage Applications Measured by the Light Flash Method, *Appl. Therm. Eng.*, 2017, **113**, 1189–1193.

190 B. K. Purohit and V. S. Sistla, Inorganic Salt Hydrate for Thermal Energy Storage Application: A Review, *Energy Storage*, 2021, **3**, e212.

191 A. D. Pathak, K. Heijmans, S. Nedea, A. C. T. van Duin, H. Zondag, C. Rindt and D. Smeulders, Mass Diffusivity and Thermal Conductivity Estimation of Chloride-Based Salt Hydrates for Thermo-Chemical Heat Storage: A Molecular Dynamics Study Using the Reactive Force Field, *Int. J. Heat Mass Transfer*, 2020, **149**, 119090.

192 W. Li, J. J. Klemeš, Q. Wang and M. Zeng, Development and Characteristics Analysis of Salt-Hydrate Based Composite Sorbent for Low-Grade Thermochemical Energy Storage, *Renew. Energy*, 2020, **157**, 920–940.

193 Q. Miao, Y. Zhang, X. Jia, Z. Li, L. Tan and Y. Ding,  $MgSO_4$ -Expanded Graphite Composites for Mass and Heat Transfer Enhancement of Thermochemical Energy Storage, *Sol. Energy*, 2021, **220**, 432–439.

194 Eurostat. *First Population Estimates - EU Population up to Nearly 513 Million on 1 January 2019 - More Deaths than Births*, 2019.

195 Eurostat. *Housing in Europe - Statistics Visualized/2020 Edition*, 2020.

196 International Energy Agency (IEA). *The Role of Critical Minerals in Clean Energy Transitions*; 2021.

197 U.S. Geological Survey. *Mineral Commodity Summaries 2025*, 2025, <https://pubs.usgs.gov/periodicals/mcs2025/mcs2025.pdf>.

198 P. E. Marín, Y. Milian, S. Ushak, L. F. Cabeza, M. Grágeda and G. S. F. Shire, Lithium Compounds for Thermochemical Energy Storage: A State-of-the-Art Review and Future Trends, *Renewable Sustainable Energy Rev.*, 2021, **149**, 111381.

199 J. Xiao, X. Cao, B. Gridley, W. Golden, Y. Ji, S. Johnson, D. Lu, F. Lin, J. Liu, Y. Liu, Z. Liu, H. N. Ramesh, F. Shi, J. Schrooten, M. J. Sims, S. Sun, Y. Shao, A. Vaisman, J. Yang and M. S. Whittingham, From Mining to Manufacturing: Scientific Challenges and Opportunities behind Battery Production, *Chem. Rev.*, 2025, **125**(13), 6397–6431, DOI: [10.1021/acs.chemrev.4c00980](https://doi.org/10.1021/acs.chemrev.4c00980).

200 K. Shizume, N. Hatada, K. Toyoura and T. Uda, Characteristic Microstructure Underlying the Fast Hydration-Dehydration Reaction of  $\beta$ - $La_2(SO_4)_3$ : “Fine Platy Joints” with “Loose Grain Boundaries”, *J. Mater. Chem. A*, 2018, **6**, 24956–24964.

201 K. Shizume, N. Hatada and T. Uda, Experimental Study of Hydration/Dehydration Behaviors of Metal Sulfates  $M_2(SO_4)_3$  ( $M = Sc, Yb, Y, Dy, Al, Ga, Fe, In$ ) in Search of New Low-Temperature Thermochemical Heat Storage Materials, *ACS Omega*, 2020, **5**, 13521–13527.

202 W. Li, H. Guo, M. Zeng and Q. Wang, Performance of  $SrBr_2 \bullet 6H_2O$  Based Seasonal Thermochemical Heat Storage in a Novel Multilayered Sieve Reactor, *Energy Convers. Manage.*, 2019, **198**, 111843.

203 M. Richter, E.-M. Habermann, E. Siebecke and M. Linder, A Systematic Screening of Salt Hydrates as Materials for a Thermochemical Heat Transformer, *Thermochim. Acta*, 2018, **659**, 136–150.

204 S. Kiyabu, P. Girard and D. J. Siegel, Discovery of Salt Hydrates for Thermal Energy Storage, *J. Am. Chem. Soc.*, 2022, **144**, 21617.

205 S. Kiyabu and D. J. Siegel, Computational Discovery of Thermochemical Heat Storage Materials Based on Chalcogenide and Complex Anion Salt Hydrates, *ACS Appl. Eng. Mater.*, 2023, **1**, 2614–2625.

206 A.-J. De Jong, F. Trausel, C. Finck, L. Van Vliet and R. Cuypers, Thermochemical Heat Storage - System Design Issues, *Energy Procedia*, 2014, **48**, 309–319.

207 S. Thakur and A. Giri, Supramolecular reinforcement drastically enhances thermal conductivity of interpenetrated covalent organic frameworks, *J. Mater. Chem. A*, 2023, **11**, 18660–18667.

208 H. Kim, J. H. Choe, H. Yun, J. F. Kurisigal, S. Yu, Y. H. Lee and C. S. Hong, High ammonia storage capacity in  $LiCl$  nanoparticle-embedded metal-organic framework composites, *Chem. Eng. J.*, 2024, **489**, 151319.



209 M. F. De Lange, K. J. F. M. Verouden, T. J. H. Vlugt, J. Gascon and F. Kapteijn, Adsorption-Driven Heat Pumps: The Potential of Metal-Organic Frameworks, *Chem. Rev.*, 2015, **115**, 12205–12250.

210 Mitsubishi Plastics, Inc. Low Temperature Heat Use. <https://www.aaasaveenergy.com/products/001/temperature/>, (Accessed on 16 April 25).

211 R. M. Madero-Castro, A. Luna-Triguero, C. González-Galán, J. M. Vicent-Luna and S. Calero, Alcohol-based adsorption heat pumps using hydrophobic metal-organic frameworks, *J. Mater. Chem. A*, 2023, **12**, 3434–3448.

212 Z. Lu, Comprehensive Investigation of Cooling, Heating, and Power Generation Performance in Adsorption Systems Using Compound Adsorbents: Experimental and Computational Analysis, *Sustainability*, 2023, **15**, 15202.

213 Z. Wang, X. K. Xu, T. Yan, H. Zhang, L. W. Wang and W. G. Pan, Preparation and thermal properties of zeolite 13X/MgSO<sub>4</sub>-LiCl binary-salt composite material for sorption heat storage, *Appl. Therm. Eng.*, 2024, **245**, 122905.

214 C. Weckerle, M. Dörr, M. Linder and I. Bürger, A Compact Thermally Driven Cooling System Based on Metal Hydrides, *Energies*, 2020, **13**(10), 2482.

215 F. Shabir, M. Sultan, T. Miyazaki, B. B. Saha, A. Askalany, I. Ali, Y. Zhou, R. Ahmad and R. R. Shamshiri, Recent Updates on the Adsorption Capacities of Adsorbent-Adsorbate Pairs for Heat Transformation Applications, *Renewable Sustainable Energy Rev.*, 2020, **119**, 109630.

216 M. Thommes, K. Kaneko, A. V. Neimark, J. P. Olivier, F. Rodriguez-Reinoso, J. Rouquerol and K. S. W. Sing, Physisorption of Gases, with Special Reference to the Evaluation of Surface Area and Pore Size Distribution (IUPAC Technical Report), *Pure Appl. Chem.*, 2015, **87**, 1051–1069.

217 I. S. Glaznev, D. S. Ovoshchnikov and Y. I. Aristov, Kinetics of Water Adsorption/Desorption under Isobaric Stages of Adsorption Heat Transformers: The Effect of Isobar Shape, *Int. J. Heat Mass Transfer*, 2009, **52**, 1774–1777.

218 B. N. Okuney, A. P. Gromov and Y. I. Aristov, Modelling of Isobaric Stages of Adsorption Cooling Cycle: An Optimal Shape of Adsorption Isobar, *Appl. Therm. Eng.*, 2013, **53**, 89–95.

219 S. Kayal, S. Baichuan and B. B. Saha, Adsorption characteristics of AQSOA zeolites and water for adsorption chillers, *Int. J. Heat Mass Transfer*, 2016, **92**, 1120–1127.

220 B. N. Truong, D. D. Borges, J. Park, J. S. Lee, D. Jo, J.-S. Chang, S. J. Cho, G. Maurin, K. H. Cho and U.-H. Lee, Tuning Hydrophilicity of Aluminum MOFs by a Mixed-Linker Strategy for Enhanced Performance in Water Adsorption-Driven Heat Allocation Application, *Adv. Sci.*, 2023, **10**, 2301311.

221 Abdullah, X. Q. Duong, N. A. Shah and J. D. Chung, Comparative study of various adsorbents for adsorption-based thermal energy storage, *J. Energy Storage*, 2024, **80**, 110332.

222 S. Builes, S. I. Sandler and R. Xiong, Isosteric Heats of Gas and Liquid Adsorption, *Langmuir*, 2013, **29**, 10416–10422.

223 A. Nuhnen and C. Janiak, A Practical Guide to Calculate the Isosteric Heat/Enthalpy of Adsorption via Adsorption Isotherms in Metal-Organic Frameworks, MOFs, *Dalton Trans.*, 2020, **49**, 10295–10307.

224 K. H. Cho, D. D. Borges, U.-H. Lee, J. S. Lee, J. W. Yoon, S. J. Cho, J. Park, W. Lombardo, D. Moon, A. Sapienza, G. Maurin and J.-S. Chang, Rational design of a robust aluminum metal-organic framework for multi-purpose water-sorption-driven heat allocations, *Nat. Commun.*, 2020, **11**, 5112.

225 W. Wongsuwan, S. Kumar, P. Neveu and F. Meunier, A Review of Chemical Heat Pump Technology and Applications, *Appl. Therm. Eng.*, 2001, **21**, 1489–1519.

226 S. Narayanan, S. Yang, H. Kim and E. N. Wang, Optimization of Adsorption Processes for Climate Control and Thermal Energy Storage, *Int. J. Heat Mass Transfer*, 2014, **77**, 288–300.

227 J. Crank, *The Mathematics of Diffusion*, Clarendon Press, Oxford, 2nd edn, 1979.

228 S. Narayanan, H. Kim, A. Umans, S. Yang, X. Li, S. N. Schiffres, S. R. Rao, I. S. McKay, E. N. Wang and C. A. Rios Perez, *et al.*, A Thermophysical Battery for Storage-Based Climate Control, *Appl. Energy*, 2017, **189**, 31–43.

229 A. LaPotin, H. Kim, S. R. Rao and E. N. Wang, Adsorption-Based Atmospheric Water Harvesting: Impact of Material and Component Properties on System-Level Performance, *Acc. Chem. Res.*, 2019, **52**, 1588–1597.

230 M. Alonso, E. Sainz, F. A. Lopez and K. Shinohara, Void-Size Probability Distribution in Random Packings of Equal-Sized Spheres, *Chem. Eng. Sci.*, 1995, **50**, 1983–1988.

231 B. L. Huang, Z. Ni, A. Millward, A. J. H. McGaughey, C. Uher, M. Kaviani and O. Yaghi, Thermal conductivity of a metal-organic framework (MOF-5): Part II. Measurement, *Int. J. Heat Mass Transfer*, 2007, **50**, 405–411.

232 K. J. Erickson, F. Léonard, V. Stavila, M. E. Foster, C. D. Spataru, R. E. Jones, B. M. Foley, P. E. Hopkins, M. D. Allendorf and A. A. Talin, Thin Film Thermoelectric Metal-Organic Framework with High Seebeck Coefficient and Low Thermal Conductivity, *Adv. Mater.*, 2015, **27**, 3453–3459.

233 W. D. C. B. Gunatilleke, K. Wei, Z. Niu, L. Wojtas, G. Nolas and S. Ma, Thermal conductivity of a perovskite-type metal-organic framework crystal, *Dalton Trans.*, 2017, **46**, 13342–13344.

234 A. Hoe, A. Tamraparni, C. Zhang, A. Elwany, J. R. Felts and P. J. Shamberger, Design of Radially Variant Phase-Change Material Composites, *Adv. Eng. Mater.*, 2022, **25**, 2200841.

235 P. J. Shamberger and T. S. Fisher, Cooling power and characteristic times of composite heatsinks and insulants, *Int. J. Heat Mass Transfer*, 2018, **117**, 1205–1215.

236 A. Tamraparni, A. Hoe, M. Deckard, C. Zhang, A. Elwany, P. J. Shamberger and J. R. Felts, Design and Optimization of Lamellar Phase Change Composites for Thermal Energy Storage, *Adv. Eng. Mater.*, 2021, **23**, 2001052.

237 H. Ma, Z. Aamer and Z. Tian, Ultrahigh thermal conductivity in three-dimensional covalent organic frameworks, *Mater. Today Phys.*, 2021, **21**, 100536.



238 S. K. S. Freitas, R. S. Borges, C. Merlini, G. M. O. Barra and P. M. Esteves, Thermal Conductivity of Covalent Organic Frameworks as a Function of Their Pore Size, *J. Phys. Chem. C*, 2017, **121**, 27247–27252.

239 D. B. Boman, D. C. Hoysall, D. G. Pahinkar, M. J. Ponkala and S. Garimella, Screening of Working Pairs for Adsorption Heat Pumps Based on Thermodynamic and Transport Characteristics, *Appl. Therm. Eng.*, 2017, **123**, 422–434.

240 N. Makhanya, B. Oboirien, J. Ren, N. Musyoka and A. Sciacovelli, Recent Advances on Thermal Energy Storage Using Metal-Organic Frameworks (MOFs), *J. Energy Storage*, 2021, **34**, 102179.

241 Z. Liu, W. Li, P. Z. Moghadam and S. Li, Screening Adsorbent-Water Adsorption Heat Pumps Based on an Experimental Water Adsorption Isotherm Database. *Sustain. Energy Fuels*, 2021, **5**, 1075–1084.

242 National Institute of Standards and Technology. NIST/ARPA-E Database of Novel and Emerging Adsorbent Materials. <https://adsorption.nist.gov/isodb/index.php> (Accessed on 17 April 2025).

243 X. Peng, L.-C. Lin, W. Sun and B. Smit, Water Adsorption in Metal-Organic Frameworks with Open-Metal Sites, *AIChE J.*, 2015, **61**, 677–687.

244 S. Hamad, S. R. G. Balestra, R. Bueno-Perez, S. Calero and A. R. Ruiz-Salvador, Atomic Charges for Modeling Metal-Organic Frameworks: Why and How, *J. Solid State Chem.*, 2015, **223**, 144–151.

245 D. Nazarian, J. S. Camp and D. S. Sholl, A Comprehensive Set of High-Quality Point Charges for Simulations of Metal-Organic Frameworks, *Chem. Mater.*, 2016, **28**, 785–793.

246 M. Islamov, H. Babaei, R. Anderson, K. B. Sezginel, J. R. Long, A. J. H. McGaughey, D. A. Gomez-Gualdrón and C. E. Wilmer, High-throughput screening of hypothetical metal-organic frameworks for thermal conductivity, *npj Comput. Mater.*, 2023, **9**, 11.

247 G. Zhao, L. M. Brabson, S. Chheda, J. Huang, H. Kim, K. Liu, K. Mochida, T. D. Pham, Prerna, G. G. Terrones, S. Yoon, L. Zoubritzky, F.-X. Coudert, M. Haranczyk, H. J. Kulik, S. M. Moosavi, D. S. Sholl, J. I. Siepmann, R. Q. Snurr and Y. G. Chung, CoRE MOF DB: A curated experimental metal-organic framework database with machine-learned properties for integrated material-process screening, *Matter*, 2025, **8**, 102140.

248 Y. G. Chung, E. Haldoupis, B. J. Bucior, M. Haranczyk, S. Lee, H. Zhang, K. D. Vogiatzis, M. Milisavljevic, S. Ling, J. S. Camp, B. Slater, J. I. Siepmann, D. S. Sholl and R. Q. Snurr, Advances, Updates, and Analytics for the Computation-Ready, Experimental Metal-Organic Framework Database: CoRE MOF 2019, *J. Chem. Eng. Data*, 2019, **64**, 5985–5998.

249 H. Zhang and R. Q. Snurr, Computational Study of Water Adsorption in the Hydrophobic Metal-Organic Framework ZIF-8: Adsorption Mechanism and Acceleration of the Simulations, *J. Phys. Chem. C*, 2017, **121**, 24000–24010.

250 A. Datar, M. Witman and L.-C. Lin, Improving Computational Assessment of Porous Materials for Water Adsorption Applications via Flat Histogram Methods, *J. Phys. Chem. C*, 2021, **125**, 4253–4266.

251 S. Li, Y. G. Chung and R. Q. Snurr, High-Throughput Screening of Metal-Organic Frameworks for CO<sub>2</sub> Capture in the Presence of Water, *Langmuir*, 2016, **32**, 10368–10376.

252 Z. Qiao, Q. Xu and J. Jiang, Materials for Energy and Sustainability Computational Screening of Hydrophobic Metal-Organic Frameworks for the Separation of H<sub>2</sub>S and CO<sub>2</sub> from Natural Gas, *J. Mater. Chem. A*, 2018, **6**, 18898.

253 R. Long, X. Xia, Y. Zhao, S. Li, Z. Liu and W. Liu, Screening Metal-Organic Frameworks for Adsorption-Driven Osmotic Heat Engines via Grand Canonical Monte Carlo Simulations and Machine Learning, *iScience*, 2021, **24**, 101914.

254 C. Altintas, O. F. Altundal, S. Keskin and R. Yildirim, Machine Learning Meets with Metal Organic Frameworks for Gas Storage and Separation, *J. Chem. Inf. Model.*, 2021, **61**, 2131–2146.

255 H. Daglar and S. Keskin, Combining Machine Learning and Molecular Simulations to Unlock Gas Separation Potentials of MOF Membranes and MOF/Polymer MMMs, *ACS Appl. Mater. Interfaces*, 2022, **14**, 32134–32148.

256 S. Izadi, R. Anandakrishnan and A. V. Onufriev, Building Water Models: A Different Approach, *J. Phys. Chem. Lett.*, 2014, **5**, 3863–3871.

257 M. Erdős, M. F. De Lange, F. Kapteijn, O. A. Moulton and T. J. H. Vlugt, In Silico Screening of Metal-Organic Frameworks for Adsorption-Driven Heat Pumps and Chillers, *ACS Appl. Mater. Interfaces*, 2018, **10**, 27074–27087.

258 W. Li, X. Xia, M. Cao and S. Li, Structure-Property Relationship of Metal-Organic Frameworks for Alcohol-Based Adsorption-Driven Heat Pumps via High-Throughput Computational Screening, *J. Mater. Chem. A*, 2019, **7**, 7470–7479.

259 Z. Shi, X. Yuan, Y. Yan, Y. Tang, J. Li, H. Liang, L. Tong and Z. Qiao, Techno-Economic Analysis of Metal-Organic Frameworks for Adsorption Heat Pumps/Chillers: From Directional Computational Screening, Machine Learning to Experiment, *J. Mater. Chem. A*, 2021, **9**, 7656–7666.

260 Y. G. Chung, J. Camp, M. Haranczyk, B. J. Sikora, V. Krungleviciute, T. Yildirim, O. K. Farha, D. S. Sholl and R. Q. Snurr, Computation-Ready, Experimental Metal-Organic Frameworks: A Tool To Enable High-Throughput Screening of Nanoporous Crystals.

261 Y. G. Chung, E. Haldoupis, B. J. Bucior, M. Haranczyk, S. Lee, K. D. Vogiatzis, S. Ling, M. Milisavljevic, H. Zhang, J. S. Camp, *et al.*, Computation-Ready Experimental Metal-Organic Framework (CoRE MOF) 2019 Dataset. 2019.

262 C. E. Wilmer, M. Leaf, C. Y. Lee, O. K. Farha, B. G. Hauser, J. T. Hupp and R. Q. Snurr, Large-Scale Screening of Hypothetical Metal-Organic Frameworks, *Nat. Chem.*, 2011, **4**, 83–89.

263 M. Tong, Y. Lan, Z. Qin and C. Zhong, Computation-Ready, Experimental Covalent Organic Framework for Methane Delivery: Screening and Material Design, *J. Phys. Chem. C*, 2018, **122**, 13009–13016.

264 W. Li, X. Xia and S. Li, Screening of Covalent-Organic Frameworks for Adsorption Heat Pumps, *ACS Appl. Mater. Interfaces*, 2019, **12**, 3265–3273.



265 T. Liang, W. Li, S. Li, Z. Cai, Y. Lin and W. Wu, Performance Evaluation of Metal–Organic Frameworks in Adsorption Heat Pumps via Multiscale Modeling, *ACS Sustainable Chem. Eng.*, 2024, **12**, 2825–2840.

266 K. H. Cho, D. D. Borges, U.-H. Lee, J. S. Lee, J. W. Yoon, S. J. Cho, J. Park, W. Lombardo, D. Moon and A. Sapienza, *et al.*, Rational Design of a Robust Aluminum Metal–Organic Framework for Multi-Purpose Water-Sorption-Driven Heat Allocations, *Nat. Commun.*, 2020, **11**, 1–8.

267 A. Cadiau, J. S. Lee, D. D. Borges, P. Fabry, T. Devic, M. T. Wharmby, C. Martineau, D. Foucher, F. Taulelle and C.-H. Jun, *et al.*, Design of Hydrophilic Metal Organic Framework Water Adsorbents for Heat Reallocation, *Adv. Mater.*, 2015, **27**, 4775–4780.

268 A. J. Rieth, A. M. Wright, S. Rao, H. Kim, A. D. LaPotin, E. N. Wang and M. Dincă, Tunable Metal–Organic Frameworks Enable High-Efficiency Cascaded Adsorption Heat Pumps, *J. Am. Chem. Soc.*, 2018, **140**, 17591–17596.

269 A. J. Rieth, A. M. Wright, G. Skorupskii, J. L. Mancuso, C. H. Hendon and M. Dincă, Record-Setting Sorbents for Reversible Water Uptake by Systematic Anion Exchanges in Metal–Organic Frameworks, *J. Am. Chem. Soc.*, 2019, **141**, 13858–13866.

270 Y. Wu, A. Kobayashi, G. J. Halder, V. K. Peterson, K. W. Chapman, N. Lock, P. D. Southon and C. J. Kepert, Negative Thermal Expansion in the Metal–Organic Framework Material  $\text{Cu}_3(1,3,5\text{-Benzene tricarboxylate})_2$ , *Angew. Chem., Int. Ed.*, 2008, **47**, 8929–8932.

271 J. Zhang, Z. Cao, S. Huang, X. Huang, Y. Han, C. Wen, J. H. Walther and Y. Yang, Solidification performance improvement of phase change materials for latent heat thermal energy storage using novel branch-structured fins and nanoparticles, *Appl. Energy*, 2023, **342**, 121158.

272 T. H. Rupam, F. J. Tuli, I. Jahan, M. L. Palash, A. Chakraborty and B. B. Saha, Isotherms and kinetics of water sorption onto MOFs for adsorption cooling applications, *Therm. Sci. Eng. Prog.*, 2022, **34**, 101436.

273 J. Chao, J. Xu, Z. Bai, P. Wang, R. Wang and T. Li, Integrated heat and cold storage enabled by high-energy-density sorption thermal battery based on zeolite/MgCl<sub>2</sub> composite sorbent, *J. Energy Storage*, 2023, **64**, 107155.

274 K. A. Rocky, A. Pal, T. H. Rupam, N. Nasruddin and B. B. Saha, Zeolite-graphene composite adsorbents for next generation adsorption heat pumps, *Microporous Mesoporous Mater.*, 2021, **313**, 110839.

275 S. Chaemchuen, X. Xiao, N. Klomkliang, M. S. Yusubov and F. Verpoort, Tunable Metal–Organic Frameworks for Heat Transformation Applications, *Nanomaterials*, 2018, **8**, 661.

276 S. Rönsch, B. Auer, M. Kinateder and K. Gleichmann, Zeolite Heat Storage: Key Parameters from Experimental Results with Binder-Free NaY, *Chem. Eng. Technol.*, 2020, **43**, 2530–2537.

277 R. van Alebeek, L. Scapino, M. A. J. M. Beving, M. Gaeini, C. C. M. Rindt and H. A. Zondag, Investigation of a household-scale open sorption energy storage system based on the zeolite 13X/water reacting pair, *Appl. Therm. Eng.*, 2018, **139**, 325–333.

278 S.-F. Wu, B.-Z. Yuan and L.-W. Wang, MOF-ammonia working pairs in thermal energy conversion and storage, *Nat. Rev. Mater.*, 2023, **8**, 636–638.

279 R. AL-Dadah, S. Mahmoud, E. Elsayed, P. Youssef and F. Al-Mousawi, Metal-organic framework materials for adsorption heat pumps, *Energy*, 2020, **190**, 116356.

280 Y. Zhang and R. Wang, Sorption thermal energy storage: Concept, process, applications and perspectives, *Energy Storage Mater.*, 2020, **27**, 352–369.

281 H. Ayaz, V. Chinnasamy, J. Yong and H. Cho, Review of Technologies and Recent Advances in Low-Temperature Sorption Thermal Storage Systems, *Energies*, 2021, **14**, 6052.

282 D. Li, D. Zeng, H. Han, L. Guo, X. Yin and Y. Yao, Phase Diagrams and Thermochemical Modeling of Salt Lake Brine Systems. I. LiCl + H<sub>2</sub>O System, *Calphad*, 2015, **51**, 1–12.

283 T. Brünig, M. Maurer and R. Pietschnig, Sorbent Properties of Halide-Free Ionic Liquids for Water and CO<sub>2</sub> Perfusion, *ACS Sustainable Chem. Eng.*, 2017, **5**, 7228–7239.

284 P. W. Atkins and J. De Paula, *Physical Chemistry*, W.H. Freeman and Co., New York, 2010.

285 T. X. Li, R. Z. Wang, J. K. Kiplagat and L. W. Wang, Performance Study of a Consolidated Manganese Chloride–Expanded Graphite Compound for Sorption Deep-Freezing Processes, *Appl. Energy*, 2009, **86**, 1201–1209.

286 J. V. Veselovskaya, M. M. Tokarev and Y. I. Aristov, Novel Ammonia Sorbents “Porous Matrix Modified by Active Salt” for Adsorptive Heat Transformation. 1. Barium Chloride in Various Matrices, *Appl. Therm. Eng.*, 2010, **30**, 584–589.

287 W. Wu, Low-Temperature Compression-Assisted Adsorption Thermal Energy Storage Using Ionic Liquids, *Energy Built Environ.*, 2020, **1**, 139–148.

288 Y. J. Kim and M. Gonzalez, Exergy Analysis of an Ionic-Liquid Adsorption Refrigeration System Utilizing Waste-Heat from Datacenters, *Int. J. Refrig.*, 2014, **48**, 26–37.

289 Y. Y. Tanashev, A. V. Krainov and Y. I. Aristov, Thermal Conductivity of Composite Sorbents “Salt in Porous Matrix” for Heat Storage and Transformation, *Appl. Therm. Eng.*, 2013, **61**, 401–407.

290 F. Wang, J. Zhang, S. Jia, X. Chen and Z. Cheng, A Review of Modification Strategies and Applications for Hydrated Salts: Insights from Energy Storage Materials Encapsulation Technology, *Renewable Sustainable Energy Rev.*, 2025, **223**, 115998.

291 Y. Sun, A. Spieß, C. Jansen, A. Nuhnen, S. Gökpinar, R. Wiedey, S.-J. Ernst and C. Janiak, Tunable LiCl@UiO-66 Composites for Water Sorption-Based Heat Transformation Applications, *J. Mater. Chem. A*, 2020, **8**, 13364–13375.

292 B. Tan, Y. Luo, X. Liang, S. Wang, X. Gao, Z. Zhang and Y. Fang, Composite Salt in MIL-101(Cr) with High Water Uptake and Fast Adsorption Kinetics for Adsorption Heat Pumps, *Microporous Mesoporous Mater.*, 2019, **286**, 141–148.



293 A. U. Rehman, T. Zhao, S. Yun, Q. Xiao, W. Zhu and F. Zhang,  $\text{MgCl}_2\cdot6\text{H}_2\text{O}$  Supported on an  $\text{NH}_2\text{-MIL-88(Fe)}/\text{MXene}$  Hybrid Substrate to Enhance Thermochemical Heat Storage Performance, *J. Energy Storage*, 2025, **109**, 115186.

294 X. Qu, A. Jain, N. N. Rajput, L. Cheng, Y. Zhang, S. P. Ong, M. Brafman, E. Maginn, L. A. Curtiss and K. A. Persson, The Electrolyte Genome project: A big data approach in battery materials discovery, *Comput. Mater. Sci.*, 2015, **103**, 56–67.

295 R. Sewak, V. Sudarsanan and H. Kumar, Accelerating discovery and design of high-performance solid-state electrolytes: a machine learning approach, *Phys. Chem. Chem. Phys.*, 2025, **27**, 3834–3843.

296 A. O. Boev, S. S. Fedotov, K. J. Stevenson and D. A. Aksyonov, High-throughput computational screening of cathode materials for  $\text{Li-O}_2$  battery, *Comput. Mater. Sci.*, 2021, **197**, 110592.

297 Z. Lu, B. Zhu, B. W. B. Shires, D. O. Scanlon and C. J. Pickard, Ab initio random structure searching for battery cathode materials, *J. Chem. Phys.*, 2021, **154**, 174111.

298 A. H. Farmahini, S. Krishnamurthy, D. Friedrich, S. Brandani and L. Sarkisov, Performance-Based Screening of Porous Materials for Carbon Capture, *Chem. Rev.*, 2021, **121**, 10666–10741.

299 J. Liu, L. Liang, B. Su, D. Wu, Y. Zhang, J. Wu and C. Fu, Transformative strategies in photocatalyst design: merging computational methods and deep learning, *J. Mater. Inf.*, 2024, **4**, 33.

300 G. S. Priyanga, G. Pransu, H. Krishna and T. Thomas, Discovery of Novel Photocatalysts Using Machine Learning Approach. in *Machine Learning for Advanced Functional Materials*, ed. N. Joshi, V. Kushvaha and P. Madhushri, Springer, Singapore, 2023.

301 S. Luo, T. Li, X. Wang, M. Faizan and L. Zhang, High-throughput computational materials screening and discovery of optoelectronic semiconductors, *WIREs Comput. Mol. Sci.*, 2021, **11**, e1489.

302 F. Dinic, I. Neporozhnii and O. Voznyy, Machine learning models for the discovery of direct band gap materials for light emission and photovoltaics, *Comput. Mater. Sci.*, 2024, **231**, 112580.

303 A. Pulido, L. Chen, T. Kaczorowski, D. Holden, M. A. Little, S. Y. Chong, B. J. Slater, D. P. McMahon, B. Bonillo, C. J. Stackhouse, A. Stephenson, C. M. Kane, R. Clowes, T. Hasell, A. I. Cooper and G. M. Day, Functional materials discovery using energy-structure-function maps, *Nature*, 2017, **543**, 657–664.

304 X. Yin and C. E. Gounaris, Computational discovery of Metal–Organic Frameworks for sustainable energy systems: Open challenges, *Comput. Chem. Eng.*, 2022, **167**, 108022.

305 H. Daglar and S. Keskin, Computational Screening of Metal–Organic Frameworks for Membrane-Based  $\text{CO}_2/\text{N}_2/\text{H}_2\text{O}$  Separations: Best Materials for Flue Gas Separation, *J. Phys. Chem. C*, 2018, **122**, 17347–17357.

306 J. Kim, D. H. Mok, H. Kim and S. Back, Accelerating the Search for New Solid Electrolytes: Exploring Vast Chemical Space with Machine Learning-Enabled Computational Calculations, *ACS Appl. Mater. Interfaces*, 2023, **15**, 52427–52435.

307 C. Chen, D. T. Nguyen, S. J. Lee, N. A. Baker, A. S. Karakoti, L. Lauw, C. Owen, K. T. Mueller, B. A. Bilodeau, V. Murugesan and M. Troyer, Accelerating Computational Materials Discovery with Machine Learning and Cloud High-Performance Computing: from Large-Scale Screening to Experimental Validation, *J. Am. Chem. Soc.*, 2024, **146**, 20009–20018.

308 A. Merchant, S. Batzner, S. S. Schoenholz, M. Aykol, G. Cheon and E. D. Cubuk, Scaling deep learning for materials discovery, *Nature*, 2023, **624**, 80–85.

309 R. Cai, H. Bektas, X. Wang, K. McClintock, L. Teague, K. Yang and F. Li, Accelerated Perovskite Oxide Development for Thermochemical Energy Storage by a High-Throughput Combinatorial Approach, *Adv. Energy Mater.*, 2023, **13**, 2203833.

310 L. Li, Z. Shi, H. Liang, J. Liu and Z. Qiao, Machine Learning-Assisted Computational Screening of Metal–Organic Frameworks for Atmospheric Water Harvesting, *Nanomaterials*, 2022, **12**, 159.

311 S. Kancharlapalli, A. Gopalan, M. Haranczyk and R. Q. Snurr, Fast and Accurate Machine Learning Strategy for Calculating Partial Atomic Charges in Metal–Organic Frameworks, *J. Chem. Theory Comput.*, 2021, **17**, 3052–3064.

312 E. J. Garcia, D. Bahamon and L. F. Vega, Systematic Search of Suitable Metal–Organic Frameworks for Thermal Energy-Storage Applications with Low Global Warming Potential Refrigerants, *ACS Sustainable Chem. Eng.*, 2021, **9**, 3157–3171.

313 D. Dubbeldam, A. Torres-Knoop and K. S. Walton, On the inner workings of Monte Carlo codes, *Mol. Simul.*, 2013, **39**, 1253–1292.

314 A. L. Myers, Thermodynamics of adsorption in porous materials, *Thermodynamics*, 2004, **48**, 145–160.

315 H. Furukawa, F. Gándara, Y.-B. Zhang, J. Jiang, W. L. Queen, M. L. Hudson and O. M. Yaghi, Water Adsorption in Porous Metal–Organic Frameworks and Related Materials, *J. Am. Chem. Soc.*, 2014, **136**, 4369–4381.

316 F. Jeremias, V. Lozan, S. K. Henninger and C. Janiak, Programming MOFs for water sorption: amino-functionalized MIL-125 and UiO-66 for heat transformation and heat storage applications, *Dalton Trans.*, 2013, **42**, 15967–15973.

317 Z. Liu, W. Li and S. Li, High-efficiency prediction of water adsorption performance of porous adsorbents by lattice grand canonical Monte Carlo molecular simulation, *RSC Appl. Interfaces*, 2025, **2**, 230–242.

318 P. G. Boyd, Y. Lee and B. Smit, Computational development of the nanoporous materials genome, *Nat. Rev. Mater.*, 2017, **2**, 17037.

319 P. G. Boyd, A. Chidambaram, E. Garcia-Diez, C. P. Ireland, T. D. Daff, R. Bounds, A. Gladysiak, P. Schouwink, S. M. Moosavi, M. M. Maroto-Valer, J. A. Reimer, J. A. R. Navarro, T. K. Woo, S. Garcia, K. C. Stylianou and B. Smit, Data-driven design of metal–organic frameworks for wet flue gas  $\text{CO}_2$  capture, *Nature*, 2019, **576**, 253–256.



320 D. A. Gomez-Gualdrón, Y. J. Colon, X. Zhang, T. C. Wang, Y.-S. Chen, J. T. Hupp, T. Yildirim, O. K. Farha, J. Zhang and R. Q. Snurr, Evaluating topologically diverse metal-organic frameworks for cryo-adsorbed hydrogen storage, *Energy Environ. Sci.*, 2016, 3279–3289.

321 C. E. Wilmer, M. Leaf, C. Y. Lee, O. K. Farha, B. G. Hauser, J. T. Hupp and R. Q. Snurr, Large-scale screening of hypothetical metal-organic frameworks, *Nat. Chem.*, 2012, 83–89.

322 Z. Ye, H. Liu, W. Wang, H. Liu, J. Lv and F. Yang, Reaction/sorption kinetics of salt hydrates for thermal energy storage, *J. Energy Storage*, 2022, 56, 106122.

323 N. Koga, M. Hotta and L. Favergéon, Hydration Kinetics in Inorganic Salt-Water Vapor Systems: A Case of Lithium Sulfate, *J. Phys. Chem. C*, 2024, 128, 15487–15504.

324 B. Bogdanovic, M. Felderhoff, S. Kaskel, A. Pommerin, K. Schlichte and F. Schüth, Improved Hydrogen Storage Properties of Ti-Doped Sodium Alanate Using Titanium Nanoparticles as Doping Agents, *Adv. Mater.*, 2003, 15, 1012–1015.

325 L. Xie, Y. Liu, Y. T. Wang, J. Zheng and X. G. Li, Superior hydrogen storage kinetics of MgH<sub>2</sub> nanoparticles doped with TiF<sub>3</sub>, *Acta Mater.*, 2007, 55, 4585–4591.

326 E. German and R. Gebauer, Improvement of Hydrogen Vacancy Diffusion Kinetics in MgH<sub>2</sub> by Niobium- and Zirconium-Doping for Hydrogen Storage Applications, *J. Phys. Chem. C*, 2016, 120, 4806–4812.

327 A. Shkatulov, H. Miura, S. T. Kim, M. Zamengo, T. Harada, H. Takasu, Y. Kato and Y. Aristov, Thermochemical Storage of Medium-Temperature Heat Using MgO Promoted with Eutectic Ternary Mixture LiNO<sub>3</sub>-NaNO<sub>3</sub>-KNO<sub>3</sub>, *J. Energy Storage*, 2022, 51, 104409.

328 H. Hu, C. Ma and Q. Chen, Improved hydrogen storage properties of Ti<sub>2</sub>CrV alloy by Mo substitutional doping, *Int. J. Hydrogen Energy*, 2022, 47, 11929–11937.

329 Y. Luo, Q. Wang, J. Li, F. Xu, L. Sun, Y. Zou, H. Chu, B. Li and K. Zhang, Enhanced hydrogen storage/sensing of metal hydrides by nanomodification, *Mater. Today Nano*, 2020, 9, 100071.

330 Y. Cho, H. Cho and E. S. Cho, Nanointerface Engineering of Metal Hydrides for Advanced Hydrogen Storage, *Chem. Mater.*, 2023, 35, 366–385.

331 Z. Chen, R. C. Muduli, Z. Xu, F. Guo, A. Jain, S. Isobe, Y. Wang, H. Miyaoka, T. Ichikawa and P. Kale, Exploring the cycling solid-state hydrogen storage performance in lithium Hydride-Porous silicon composite, *Chem. Eng. J.*, 2025, 512, 162492.

332 Y. Cho, S. Li, J. L. Snider, M. A. T. Marple, N. A. Strange, J. D. Sugar, F. El Gabaly, A. Schneemann, S. Kang, M.-H. Kang, H. Park, J. Park, L. F. Wan, H. E. Mason, M. D. Allendorf, B. C. Wood, E. S. Cho and V. Stavila, Reversing the Irreversible: Thermodynamic Stabilization of LiAlH<sub>4</sub> Nanoconfined Within a Nitrogen-Doped Carbon Host, *ACS Nano*, 2021, 15, 10163–10174.

333 V. Stavila, S. Li, C. Dun, M. A. T. Marple, H. E. Mason, J. L. Snider, J. E. Reynolds, F. El Gabaly, J. D. Sugar, C. D. Spataru, X. Zhou, B. Dizdar, E. H. Majzoub, R. Chatterjee, J. Yano, H. Schlamberg, B. V. Lotsch, J. J. Urban, B. C. Wood and M. D. Allendorf, *Angew. Chem., Int. Ed.*, 2021, 60, 25815–25824.

334 A. E. Abu EL-Maaty, M. A. Abdalla, M. Essalhi, M. M. Abdelnaby, M. M. Mahmoud, M. A. Habib, M. Antar and R. Ben-Mansour, Kinetics of Water Adsorption in Metal-Organic Framework(MOF-303) for Adsorption Cooling Application, *Energy Convers. Manage.*, 2024, 24, 100694.

335 A. Fuchs, F. Knechtel, H. Wang, Z. Ji, S. Wuttke, O. M. Yaghi and E. Ploetz, Water Harvesting at the Single-Crystal Level, *J. Am. Chem. Soc.*, 2023, 145, 14324–14334.

336 L. Shi, K. O. Kirlikovali, Z. Chen and O. K. Farha, Metal-organic frameworks for water vapor adsorption, *Chem.*, 2024, 10, 484–502.

337 D. Saha, Z. Wei and S. Deng, Equilibrium, kinetics and enthalpy of hydrogen adsorption in MOF-177, *Int. J. Hydrogen Energy*, 2008, 33, 7479–7488.

338 V. Zelenák and I. Saldan, Factors Affecting Hydrogen Adsorption in Metal-Organic Frameworks: A Short Review, *Nanomaterials*, 2021, 11(7), 1638.

339 H. Zondag, B. Kikkert, S. Smeling, R. de Boer and M. Bakker, Prototype Thermochemical Heat Storage with Open Reactor System, *Appl. Energy*, 2013, 109, 360–365.

340 L. Houben, L. Sögütoglu, P. Donkers, H. Huinink and O. Adan, K<sub>2</sub>CO<sub>3</sub> in closed heat storage systems, *Renewable Energy*, 2020, 166, 35–44.

341 Y. N. Zhang, R. Z. Wang, Y. J. Zhao, T. X. Li, S. B. Riffat and N. M. Wajid, Development and Thermochemical Characterizations of Vermiculite/SrBr<sub>2</sub> Composite Sorbents for Low-Temperature Heat Storage, *Energy*, 2016, 115, 120–128.

342 V. Brancato, L. G. Gordeeva, A. Sapienza, V. Palomba, S. Vasta, A. D. Grekova, A. Frazzica and Y. I. Aristov, Experimental Characterization of the LiCl/Vermiculite Composite for Sorption Heat Storage Applications, *Int. J. Refrig.*, 2019, 105, 92–100.

343 E. Courbon, P. D'Ans, O. Skrylnyk and M. Frère, New Prominent Lithium Bromide-Based Composites for Thermal Energy Storage, *J. Energy Storage*, 2020, 32, 101699.

344 A. I. Shkatulov, J. Houben, H. Fischer and H. P. Huinink, Stabilization of K<sub>2</sub>CO<sub>3</sub> in Vermiculite for Thermochemical Energy Storage, *Renew. Energy*, 2020, 150, 990–1000.

345 Y. I. Aristov, G. Restuccia, G. Cacciola and V. N. Parmon, A Family of New Working Materials for Solid Sorption Air Conditioning Systems, *Appl. Therm. Eng.*, 2002, 22, 191–204.

346 K. C. Chan, C. Y. H. Chao and C. L. Wu, Measurement of Properties and Performance Prediction of the New MWCNT-Embedded Zeolite 13X/CaCl<sub>2</sub> Composite Adsorbents, *Int. J. Heat Mass Transfer*, 2015, 89, 308–319.

347 J. V. Veselovskaya, R. E. Critoph, R. N. Thorpe, S. Metcalf, M. M. Tokarev and Y. I. Aristov, Novel Ammonia Sorbents “Porous Matrix Modified by Active Salt” for Adsorptive Heat Transformation: 3. Testing of “BaCl<sub>2</sub>/Vermiculite” Composite in a Lab-Scale Adsorption Chiller, *Appl. Therm. Eng.*, 2010, 30, 1188–1192.



348 L. G. Gordeeva, A. D. Grekova, T. A. Krieger and Y. I. Aristov, Adsorption Properties of Composite Materials (LiCl + LiBr)/Silica, *Microporous Mesoporous Mater.*, 2009, **126**, 262–267.

349 K. Johannes, F. Kuznik, J.-L. Hubert, F. Durier and C. Obrecht, Design and Characterisation of a High Powered Energy Dense Zeolite Thermal Energy Storage System for Buildings, *Appl. Energy*, 2015, **159**, 80–86.

350 X. Zhang, M. Li, W. Shi, B. Wang and X. Li, Experimental Investigation on Charging and Discharging Performance of Absorption Thermal Energy Storage System, *Energy Convers. Manage.*, 2014, **85**, 425–434.

351 N. Yu, R. Z. Wang and L. W. Wang, Sorption Thermal Storage for Solar Energy, *Prog. Energy Combust. Sci.*, 2013, **39**, 489–514.

352 A. Grekova, L. Gordeeva and Y. Aristov, Composite sorbents “Li/Ca halogenides inside Multi-wall Carbon Nanotubes” for Thermal Energy Storage, *Sol. Energy Mater. Sol. Cells*, 2016, **155**, 176–183.

353 L. Gordeeva, A. Fazzica, A. Sapienza, Y. Aristov and A. Freni, Adsorption cooling utilizing the “LiBr/silica – ethanol” working pair: Dynamic optimization of the adsorber/heat exchanger unit, *Energy*, 2014, **75**, 390–399.

354 M. Gaeini, A. L. Rouws, J. W. O. Salari, H. A. Zondag and C. C. M. Rindt, Characterization of Microencapsulated and Impregnated Porous Host Materials Based on Calcium Chloride for Thermochemical Energy Storage, *Appl. Energy*, 2018, **212**, 1165–1177.

355 E. Courbon, P. D'Ans, A. Permyakova, O. Skrylnyk, N. Steunou, M. Degrez and M. Frère, Further Improvement of the Synthesis of Silica Gel and CaCl<sub>2</sub> Composites: Enhancement of Energy Storage Density and Stability over Cycles for Solar Heat Storage Coupled with Space Heating Applications, *Sol. Energy*, 2017, **157**, 532–541.

356 A. Jabbari-Hichri, S. Bennici and A. Auroux, Enhancing the Heat Storage Density of Silica-Alumina by Addition of Hygroscopic Salts (CaCl<sub>2</sub>, Ba(OH)<sub>2</sub>, and LiNO<sub>3</sub>), *Sol. Energy Mater. Sol. Cells*, 2015, **140**, 351–360.

357 A. Ristić and N. Zabukovec Logar, New Composite Water Sorbents CaCl<sub>2</sub>-PHTS for Low-Temperature Sorption Heat Storage: Determination of Structural Properties, *Nanomaterials*, 2019, **9**, 27.

358 A. Permyakova, S. Wang, E. Courbon, F. Nouar, N. Heymans, P. D'Ans, N. Barrier, P. Billemont, G. De Weireld and N. Steunou, *et al.*, Design of Salt-Metal Organic Framework Composites for Seasonal Heat Storage Applications, *J. Mater. Chem. A*, 2017, **5**, 12889–12898.

359 V. Brancato, L. G. Gordeeva, A. D. Grekova, A. Sapienza, S. Vasta, A. Fazzica and Y. I. Aristov, Water Adsorption Equilibrium and Dynamics of LiCl/MWCNT/PVA Composite for Adsorptive Heat Storage, *Sol. Energy Mater. Sol. Cells*, 2019, **193**, 133–140.

360 A. D. Grekova, L. G. Gordeeva and Y. I. Aristov, Composite “LiCl/Vermiculite” as Advanced Water Sorbent for Thermal Energy Storage, *Appl. Therm. Eng.*, 2017, **124**, 1401–1408.

361 N. Yu, R. Z. Wang, Z. S. Lu and L. W. Wang, Development and Characterization of Silica Gel-LiCl Composite Sorbents for Thermal Energy Storage, *Chem. Eng. Sci.*, 2014, **111**, 73–84.

362 G. T. Whiting, D. Grondin, D. Stosic, S. Bennici and A. Auroux, Zeolite–MgCl<sub>2</sub> Composites as Potential Long-Term Heat Storage Materials: Influence of Zeolite Properties on Heats of Water Sorption, *Sol. Energy Mater. Sol. Cells*, 2014, **128**, 289–295.

363 P. D'Ans, E. Courbon, A. Permyakova, F. Nouar, C. Simonnet-Jégat, F. Bourdrex, L. Malet, C. Serre, M. Frère and N. Steunou, A New Strontium Bromide MOF Composite with Improved Performance for Solar Energy Storage Application, *J. Energy Storage*, 2019, **25**, 100881.

